Alma Mater Studiorum – Università di Bologna

DOTTORATO DI RICERCA IN

Oncologia, Ematologia e Patologia

Ciclo XXXII

Settore Concorsuale: 06/D3

Settore Scientifico Disciplinare: MED15

Exploring novel targeted therapeutic strategies against Acute Myeloid Leukemia cells based on inhibition of bromodomain proteins and CDC20 activity

Presentata da: *Dott.ssa Samantha Bruno*

Coordinatore Dottorato **Supervisore**

Prof. Pier Luigi Lollini *Dott.ssa Simona Soverini*

Esame finale anno 2020

ABSTRACT

Acute myeloid leukemia (AML) is a haematological malignancies arising from the accumulation of undifferentiated myeloid progenitors with an uncontrolled proliferation. The genomic landscape of AML revealed that the disease is characterized by high level of heterogeneity and is subjected to clonal evolution driven by selective pressure of chemotherapy. In this study, we investigated the therapeutic effects of the inhibition of BRD4 and CDC20 *in vitro* and *ex vivo*.

We demonstrated that inhibition of BRD4 with GSK1215101A in AML cell lines was effective under hypoxia. It induced the activation of antioxidant response both, at transcriptomic and metabolomic levels, driven by enrichment of NRF2 pathway under normoxic and hypoxic condition. Moreover, the combined treatment with Omaveloxolone, a drug inducing NRF2 activation and NF-κB inhibition, potentiated the effects on apoptosis and colony forming capacity of stem progenitor cells. Lastly, gene expression profiling data revealed that combination treatment induced major changes in genes related to cell cycle, together with enrichment of cell differentiation pathways and negative regulation of WNT, in normoxia and hypoxia.

Regarding CDC20, we observed its up-regulation in AML patients. Treatment with two different inhibitors, Apcin and proTAME, was effective in primary AML cells and in AML cell lines, through induction of apoptosis and mitotic arrest. The lack of correlation between proliferation markers and CDC20 levels in AML cell subpopulations supports the idea of alternative CDC20 functions, independent from its essential role during mitosis. CDC20-KD experiments conducted in AML cell lines revealed a mild effect on apoptosis induction, but no significant change in cell cycle progression.

In summary, these results allowed the identification of a new strategy combination to improve the effects of BRD4 inhibition on LSC residing in the BM hypoxic niche, and provide some new evidence regarding the potential role of CDC20 as a new target for AML treatment.

Tables of contents

1. Introduction

1.1 Acute myeloid leukemia

Acute myeloid leukemia (AML) is a haematological disorder caused by defects in the programs regulating the differentiation potential and self-renewing capacity of hematopoietic stem cells (HSC). The resulting clonal expansion of un-differentiated myeloblasts is responsible of bone marrow (BM) failure with accumulation of myeloid precursors in the BM and in the peripheral blood (PB). Etiologically, AML is classified in three categories, which include "*de novo*" or primary AML that arises in patients which are not exposed to risk factors; AML secondary to leukemogenic agent exposure, namely "therapy-related" AML; and AML secondary to myeloproliferative disorders, as myelodisplastic syndrome (MDS). AML is a relatively rare cancer, affecting 1% of world population approximately, with an incidence of 3.7 per 100.000 persons[1]. The mean age at diagnosis is 68 years and the disease incidence increases sharply with age. AML is a highly heterogeneous disorder caused by a complex and dynamic interaction between somatically acquired *driver* mutations, responsible of leukemic transformation of HSC, and *passenger* mutations, which play a role in progressive adaptive mechanisms involved on disease progression and treatments failure. Historically, the classification of AML in different subtype is based on two different models:
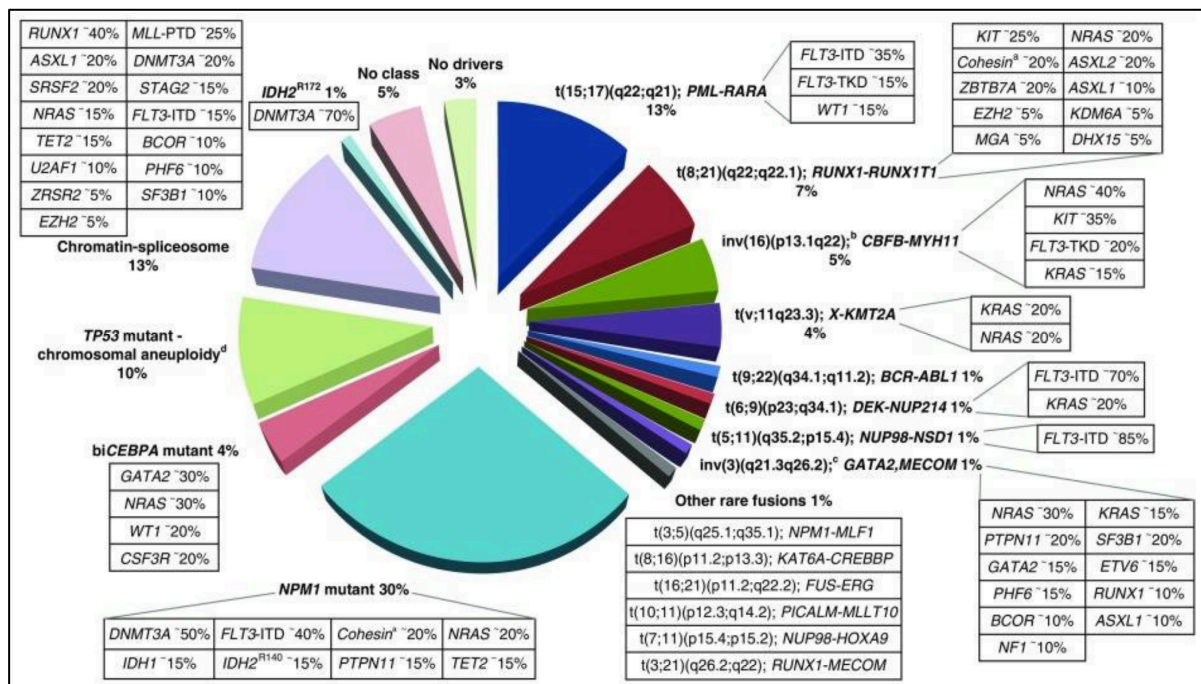
- French-American-British (FAB) classification: was proposed in 1976 and divides AML into eight subtypes, from M0 to M7, based on cell morphology defined by cytogenetic and cytochemical analysis.

- World Health Organization (WHO): provide a classification system incorporating morphology, cytogenetic, molecular genetics and

immunological markers; it was updated in 2016 incorporating the new *somatic* driver mutations described in AML.

Although a good proportion of patients responds to induction chemotherapy, AML refractory cases are still common and long-term disease-free survival is achieved in less the 50% of cases[2]. Systematic studies based on Next Generation Sequencing (NGS) technologies have provided a genetic landscape of AML identifying the landscape of *driver* alterations[3] (Fig.1) and the impact on clinical outcome of their cooperativity and mutual exclusivity patterns[4,5,6]. Indeed, Papaemmanuil and colleagues have recently proposed a new classification in 13 AML subgroups including *NPM1* mutated, chromatin-spliceosome, *TP53*-aneuploidy, inv(16), *CEBPA*[biallelic], t(15;17), t(8;21), *MLL* fusion, inv(3), *IDH2*[R172], t(6;9) and two classes which identify cases not belonging to the previous one or lacking any drivers mutations[7].
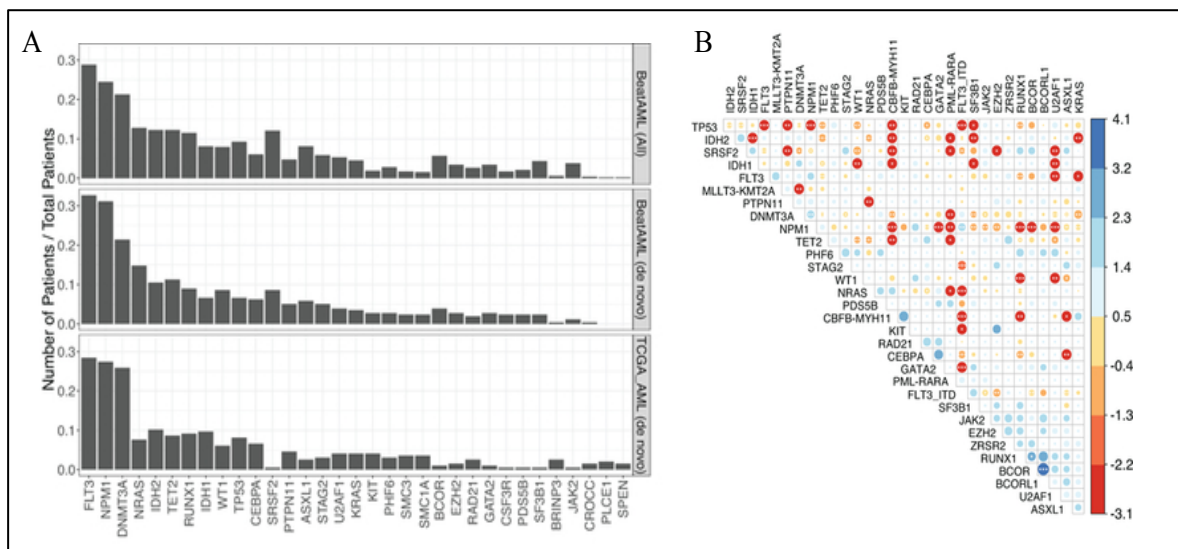
Figure 1. Genomic landscape of AML *driver* mutations[3] **.** A) Frequency of mutational events most frequent in 531 patients from Beat AML cohort (full cohort in the top row and only *de novo* cases in the middle bar) and in 200 patients from TCGA database. *FLT3*-ITD mutations were excluded from graph. B) Co-occurrence (blue) or exclusivity (red) study of the most recurrent mutations in the full cohort of Beat AML. The circle size and the asterisks indicate the FDR-corrected statistical significance.

Figure 2 content (circos plot labels):

Chromatin-spliceosome box:
RUNX1 ˜40%	MLL-PTD ˜25%
ASXL1 ˜20%	DNMT3A ˜20%
SRSF2 ˜20%	STAG2 ˜15%
NRAS ˜15%	FLT3-ITD ˜15%
TET2 ˜15%	BCOR ˜10%
U2AF1 ˜10%	PHF6 ˜10%
ZRSR2 ˜5%	SF3B1 ˜10%
EZH2 ˜5%	

Chromatin-spliceosome 13%

IDH2^R172 1%
DNMT3A ˜70%

No class 5%
No drivers 3%

t(15;17)(q22;q21); PML-RARA 13%
FLT3-ITD ˜35%	
FLT3-TKD ˜15%	
WT1 ˜15%	

t(8;21)(q22;q22.1); RUNX1-RUNX1T1 7%
KIT ˜25%	NRAS ˜20%
Cohesin^a ˜20%	ASXL2 ˜20%
ZBTB7A ˜20%	ASXL1 ˜10%
EZH2 ˜5%	KDM6A ˜5%
MGA ˜5%	DHX15 ˜5%

inv(16)(p13.1q22);^b CBFB-MYH11 5%
NRAS ˜40%
KIT ˜35%
FLT3-TKD ˜20%
KRAS ˜15%

t(v;11q23.3); X-KMT2A 4%
KRAS ˜20%	
NRAS ˜20%	

t(9;22)(q34.1;q11.2); BCR-ABL1 1%
FLT3-ITD ˜70%
KRAS ˜20%

t(6;9)(p23;q34.1); DEK-NUP214 1%
FLT3-ITD ˜85%

t(5;11)(q35.2;p15.4); NUP98-NSD1 1%

inv(3)(q21.3q26.2);^c GATA2,MECOM 1%
NRAS ˜30%	KRAS ˜15%
PTPN11 ˜20%	SF3B1 ˜20%
GATA2 ˜15%	ETV6 ˜15%
PHF6 ˜15%	RUNX1 ˜10%
BCOR ˜10%	ASXL1 ˜10%
NF1 ˜10%	

Other rare fusions 1%
t(3;5)(q25.1;q35.1); NPM1-MLF1
t(8;16)(p11.2;p13.3); KAT6A-CREBBP
t(16;21)(p11.2;q22.2); FUS-ERG
t(10;11)(p12.3;q14.2); PICALM-MLLT10
t(7;11)(p15.4;p15.2); NUP98-HOXA9
t(3;21)(q26.2;q22); RUNX1-MECOM

TP53 mutant - chromosomal aneuploidy^d 10%

biCEBPA mutant 4%
GATA2 ˜30%
NRAS ˜30%
WT1 ˜20%
CSF3R ˜20%

NPM1 mutant 30%
DNMT3A ˜50%	FLT3-ITD ˜40%	Cohesin^a ˜20%	NRAS ˜20%
IDH1 ˜15%	IDH2^R140 ˜15%	PTPN11 ˜15%	TET2 ˜15%

Figure 2. Molecular classes of AML according to ELN 2017[6]. The circos plot show the frequency of each molecular subgroup and their co-occurring mutations are shown in the relative boxes.

The increasing understanding about the genomic landscape of AML provides new knowledge also about the impact of co-occurring mutations and their temporal evolution during the adaptive response to selective pressure of therapeutic treatments[7]. For example, the study showed that the deleterious effect of $FLT3^{ITD}$ was most clinically relevant in patients with co-occurrence of *NPM1* and *DNMT3A* mutations compared to those with either *NPM1* or *DNMT3A* or with neither of two genes[7]. Also concomitant mutations of $FLT3^{TKD}$ and MLL^{PTD}, or *DNMT3A* and $IDH2^{R140}$ confer a significantly poorer prognosis in mutated patients[7]. On the contrary, they found a benign prognosis in patients carrying $NPM1\text{-}DNMT3A\text{-}NRAS^{G12/13}$ genotype[7]. According with these new evidences the 2017 European LeukemiaNet (ELN) provided an updated classification of AML patients (Fig. 2) to re-define the diagnosis procedures and the management of patients[6]. Moreover, during the last decade, the discovery of somatic driver mutations has leading to the identification of

new potential targets for AML treatment, which has prompted the development of several targeted therapies, which have been approved or are under clinical investigation (Tab. 1). This new approach, based on a deep characterization of leukemic clones, might be useful to hit specific lesions in order to improve the outcome of high-risk patients and to tailor a personalized therapy based on the genetic background of leukemic stem cells (LSC).

New therapies in AML	
Protein kinase inhibitors	• FLT3 inhibitors (midostaurin, quizartinib, gilteritinib, crenolanib) • KIT inhibitors • PI3K/AKT/mTOR inhibitors • Aurora and PLK inhibitors, CDK4/6 inhibitors, CHK1, WEE1, and MPS inhibitors • SRC and HCK inhibitors • RAS inhibitors
Epigenetic modulators	• DNA methyltransferase inhibitors (SGI-110) • HDAC inhibitors • IDH1 and IDH2 inhibitors • DOT1L inhibitors • BET-bromodimain inhibitors
Chemotherapeutic agents	• CPX-351 • Vosaroxin • Nucleoside analogs
Mitochondrial inhibitors	• Bcl-2, Bcl-xL, and Mcl-1 inhibitors • Caseinolytic protease inhibitors
Therapies targeting oncogenic proteins	• Fusion transcript targeting • EVI1 targeting • NPM1 targeting • Hedgehog inhibitors
Antibodies and immunotherapies	• Monoclonal antibodies agains CD33, CD44, CD47, CD123, CLEC12A • Immunoconjugates (eg. GO, SGN33A) • BiTEs and DARTs • CAR T cells or genetically engineered TCR T cells • Immune checkpoint inhibitors (PD-1/PD-L1, CTLA-4) • Anti-KIR antibody • Vaccines (eg, WT1)
Therapies targeting AML environment	• CXCR4 and CXCL12 antagonists • Antiangiogenic therapies

Table 1. Novel therapies available for clinical trial in AML, (adjusted from ELN 2017[6]).
Legend: BiTE, bispecific T-cell engager; CAR, chimeric antigen receptor; DART, dual-affinity retargeting molecule; HDAC, histone deacetylase; KIR, killer-cell immunoglobulin-like receptor; mTOR, mechanistic target of rapamycin; PD-1, programmed cell death protein 1; PD-L1, programmed death ligand 1; PI3K, phosphatidylinositol 3-kinase; TCR, T-cell receptor.

1.2 The eukaryotic cell cycle

The cell-division cycle is among the most important processes of cellular life, which includes a series of events that ensure the formation of two genetically identical daughter cells. In eukaryotic cells, the complete cell-division cycle is composed of three major phases: interphase, mitosis and cytokinesis. All of them are organized in a series of steps that ensure the proper DNA replication and its equal distribution in daughter cells (Fig.3). This process is of great importance and both, prokaryotic and eukaryotic cells developed a sophisticated control mechanism based on sequential checkpoints in order to avoid errors during cell cycle.

Interphase

The interphase is considered a preparatory phase which lasts for about 90% of the total time necessary for the complete cell cycle. It consists in a series of changes organized in three different phases:

- G_1 phase (gap1): corresponds to the time between the end of previous mitosis and the beginning of DNA replication. The duration of G1 phase is highly variable among different cell type and it depends on microenvironmental stimuli. During G1 phase the cell is metabolically active in order to supply the necessity of proteins and organelles, such as ribosomes and mitochondria, essential to support the progression in S phase. Alternatively to cell cycle progression, the cell can enter in a phase of quiescence defined G_0 phase (gap0) and become arrested until it receives the signals to start again the cell cycle or to start the differentiation process.

- S phase: during this phase the cell synthesizes a new copy of DNA and duplicates the centrosomes, thus the amount of DNA in the cell will be doubled (4n).
- G_2 phase (gap2): represents a brief period after DNA replication, during which the cell grows and synthesizes proteins to sustain the cellular mitosis. Moreover, microtubules begin to reorganize to form the two spindles pole.

Mitosis

Mitosis or M phase consists of five sequentially different steps that are highly regulated to ensure the correct nuclear division of daughter cells. The M phase is relatively brief and it is followed by division of daughter cells, through a process called cytokinesis. The mitosis is composed of the following phases:

- Prophase: the cell starts condensing its chromosomes and initiates the formation of mitotic spindle and the disintegration of nucleolus.
- Prometaphase: the nuclear membrane breaks down to form small membrane vesicles and microtubules start to capture the kinetochore of chromosomes.
- Metaphase: all the chromosomes are aligned along the equatorial plane of cell and the two kinetochores of each chromosome will be attached to microtubules from opposite spindle poles.
- Anaphase: the sister chromatids are divided and the microtubules tension pulls the newly formed daughters chromosomes to the opposite poles of the cell in a process called chromosomes segregation.
- Telophase: the cell starts restoring its normal structure, with the decondensation of the chromosomes, the disassembling of the mitotic spindle and the reassembly of the nuclear membrane and nucleoli.

<u>Cytokinesis</u>

Cytokinesis is the last phase of the cell cycle, which consists in the division of nuclei, cytoplasm, organelles and cell membrane to form two separated and identical cells. It might start during late mitosis and finish shortly after the telophase.
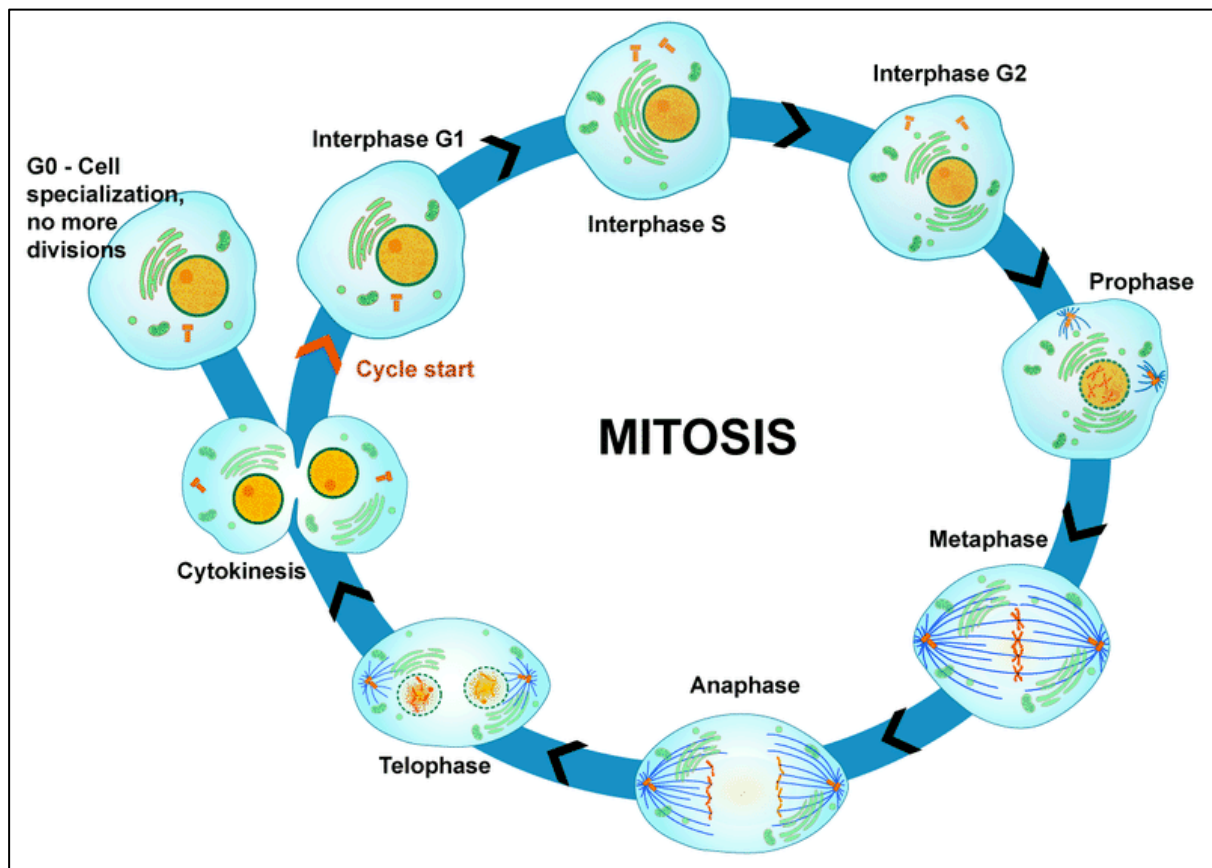
Figure 3. Phases of eukaryotic cell division cycle.

1.3 Regulation of cell cycle

The cell cycle is a process of great importance for cell life and it is highly regulated in order to ensure the formation of daughter cells with such a low level of genetic errors. Furthermore, during the last years lots of evidences have showed the relationship between cancer development and deregulation of those genes involved in the cell cycle[8], enough to make this class of genes a new potential therapeutic target[9]. In particular we previously reported that, in aneuploid AML patients, the deregulation of cell cycle genes is among the most represented classes[10]. Many studies are clarifying the complex network of regulatory proteins involved in cell cycle control and progression. So far it is evident that eukaryotic cells developed a sophisticated system to provide the transition through each phase of the cell cycle only in the absence of errors. For example, among the players involved in the control of G_1 phase the transcription factor BRD4 was identified as regulator of several early G_1 genes, including *Aurora B*, *MYC* and *FOS*. The conclusive proof of BRD4 role came from *in vitro* models lacking BRD4, which showed an arrests of cell cycle in G_1 phase [11,12,13], accompanied with an increase of apoptosis or senescence[14]. Moreover it was demonstrated that BRD4 depletion leads to aberrant mitosis, with high frequency of lagging chromosomes, micronuclei formation and bridging chromosomes, responsible of cytokinesis failure and formation of multilobulated nuclei[15,16]. In addition to its role during G_1 phase, it has been reported that BRD4 regulates also the transition from G_2 to M phase through its interaction with SPA-1, which relieves the block to cell-cycle progression[17].

In addition to network involved in the regulation of expression of protein necessary for cell cycle induction and progression, the cells dispose of different checkpoints, which ensure that the previous phase of cell cycle has been completed correctly. A snug example of this control mechanism is represented from anaphase-promoting complex/cyclosome (APC/C) and its co-activator

CDC20. They play a crucial role during M phase to signal the correct association of sister chromatids to microtubule from the opposite pole of cells. Several evidences support the involvement of CDC20 deregulation in generation of aneuploid cells[18].

1.4 Structure and functions of BRD4 protein

Bromodomain-containing protein 4 (BRD4) (Fig. 4) is a member of the bromodomain and extraterminal motif (BET) protein family, that also includes BRD2, BRD3, BRD4 and BRDt[19]. BET proteins are defining "reader" proteins thanks to the ability to recognize and bind acetylated lysine of histone proteins [20]. The interaction of BRD4 with chromatin is mediated by the N-terminal domain, which contains two tandem bromodomain motifs (BD1 and BD2) that mediate the binding of BRD4 to acetylated lysine on histone H3 and H4[21]. Moreover, BRD4 functions as protein scaffold through its C-terminal domain. The C-terminal domain includes two conserved motifs named A (aa 280-299) and B (aa 502-547), that allows the interaction between BRD4 and nucleosomal DNA[22], and an N-terminal cluster of phosphorylation sites (NPS; aa 485-504), involved in a phosphoswitch mechanism that regulates the function of BRD4[23]. Furthermore, BRD4 displays an extra-terminal (ET) domain (aa 600-678), that consist of 3 α-helices and it is probably involved in protein-protein interaction[24]; the SEED domain (aa 695-720), enriched in serine residues together with glutamic and aspartic acid residues, that are phosphorylation sites for CK2, which triggers the regulatory conformational changes of BRD4[23]. In conclusion, the CTM region (aa 1325-1362) mediates the interaction of BRD4 with the transcription elongation factor PTEFb [25].
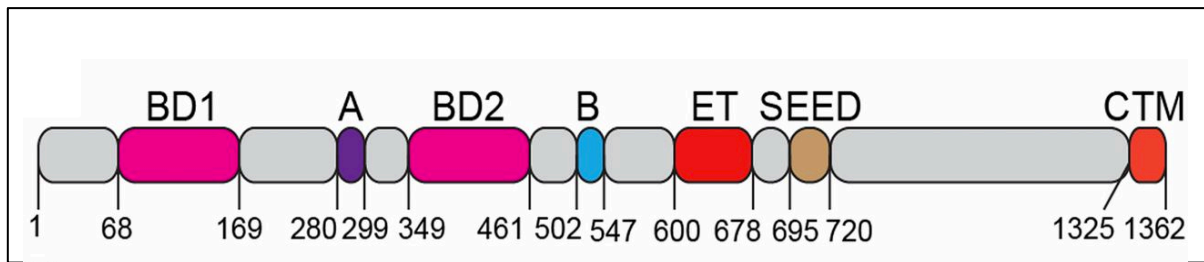
Figure 4. Functional domain of human BRD4, *adapted from Crowe et al, PNAS 2016.*

1.4.1 *Transcription role of BRD4*

BRD4 plays several regulatory roles as scaffold for transcriptional regulators, chromatin modulators and chromatin-modifying enzymes. Moreover, it can be also classified as transcriptional co-activator. Indeed it can directly or indirectly bind transcription factors (TFs), in order to promote the activation of RNA polymerase II (Pol II)[26] (Fig. 5). As a passive scaffold, BRD4 recruits several TFs at the transcription start sites. Among the TFs regulated by BRD4, the best characterized one is PTEFb, which enables, during telophase, the transcription elongation of early G1 genes, involved in cell cycle progression[11]. Devaiah and colleagues showed that BRD4 has also an active role in transcription, indeed performing Fast Protein Liquid Chromatography (FPLC) on nuclear extract from HeLa cells, they demonstrate that BRD4 is able to phosphorylates Ser2 of RNA Pol II CTD, that is a modification necessary for the transition from initiation to elongation phase and for the recruitment of RNA splicing factors[27]. Moreover, in colorectal cancer cells, phosphorylation of Ser2 of RNA Pol II, mediated by BRD4, results in the activation of Top I, which controls transcription by unwinding the DNA supercoils to allow the progression of Pol II[28]. In addition to these functions at promoters, it has been demonstrated that in primary human CD4+ T cells BRD4 is also enriched at super-enhancers, where it controls their activity[29]. Comparing the binding of BRD4 in T cells and in human embryonic stem cells, Zhang and colleagues observed that the super-

enhancer sites recognized by BRD4, play an important role in regulating lineage-specific gene transcription[29]. This is relevant since many super-enhancers are enriched at oncogenes and are cell type specific[30]. Finally, in HeLa cells BRD4 was found to be associated to specific subunits of the Mediator complex[21,31], a component of the pre-initiation complex that combine TFs to Pol II.
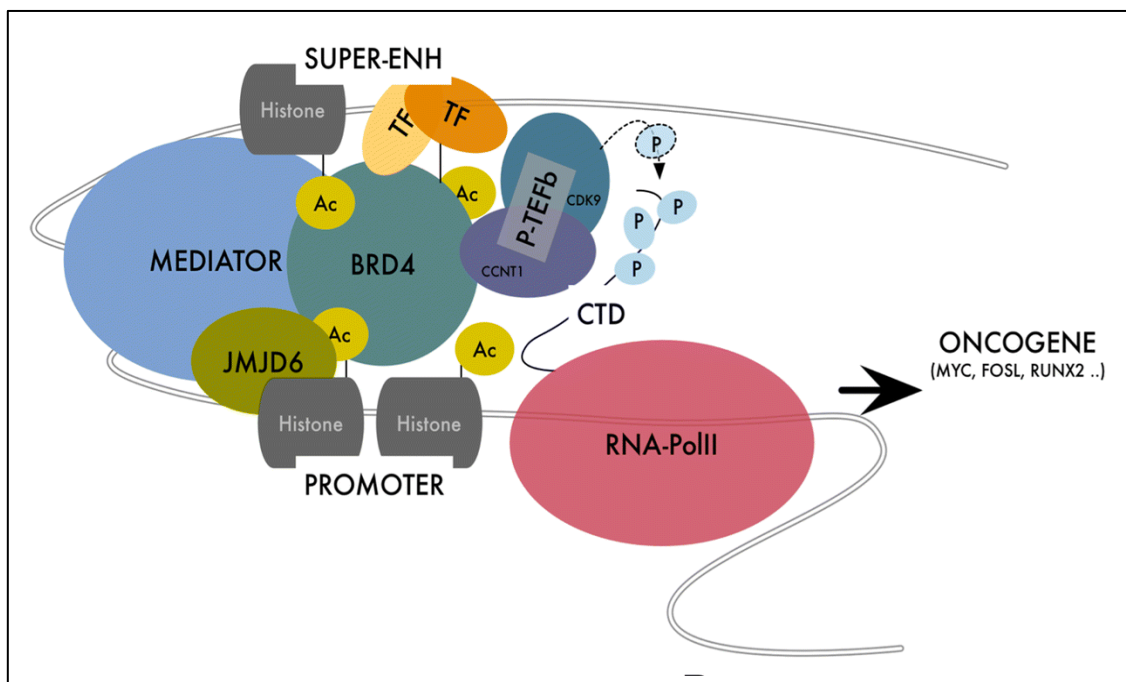
Figure 5. Transcriptional role of BRD4 at promoter and super-enhancer of target genes. Adapted from *Donati et al, Mol. Cancer 2018*.

1.4.2 *BRD4 in chromatin structure*

In addition to its scaffold functions, it has been shown that BRD4 also plays a role in regulating chromatin condensation. Indeed, the resulting effect on chromatin structure is based on the various isoforms of expressed BRD4. In particular, *in vitro* studies performed on different cancer cell lines (HeLa, U2OS, DLD1, MCF7 and NIH3T3 cell lines) demonstrated that the full-length

isoform of BRD4 mediates chromatin decondensation via its intrinsic HAT activity, which is necessary for normal chromatin structure maintenance[32]. On the contrary, experiments performed in O2OS cell lines using the different isoforms of BRD4 showed that the alternatively spliced short isoform of BRD4 (aa 1-794), that does not contain HAT domain, is involved in recruitment of condensin II chromatin remodelling complex to chromatin, which in turn leads to compacted chromatin and insulation from DNA damage[33]. The mechanism that regulates the alternative splicing of BRD4 is still unknown.

1.4.3 *BRD4 in cell differentiation and development*

Several studies showed that BRD4 plays an important role in controlling cellular differentiation and development. Indeed, thanks to its ability to selectively bind super-enhancer, the transcriptional activation mediated by BRD4 regulates genes that define the cellular differentiation status type[33]. Germline deletion of BRD4 is embryonically lethal in mice and results in failure of ESCs differentiation[34], whereas heterozygous deletion of BRD4 is sufficient to allow ESC differentiation, but it is not sufficient for total mice development. Indeed, BRD4$^{+/-}$ heterozygous embryos can develop, but only half of them survive after birth, and adult mice display morphologic abnormalities in the skin, liver, brain, testis, and eye[34]. Bolden and colleagues showed that adult transgenic mice depleted of BRD4, display several developmental defects, including epidermal hyperplasia, alopecia, decreased cellular diversity, depletion of stem cell in small intestine, and depletion of differentiated CD4+ and CD8+ T lymphoid cells[35]. In addition, *in vitro* studies of BRD4-depleted human ESC, cultured on OP9 cells, demonstrated that the absence of BRD4 do not generate any differentiation of ESC in hematopoietic progenitors or mature blood cells[36]. Regarding the differentiation of specific cell types, it has been shown that the inflammatory status observed in atherogenic inflammatory

response is dependent to the increased expression of NF-κB induced by BRD4 super-enhancer activations, which is responsible of U937 cell line differentiation to produce monocytes, and of acute inflammatory activation of HUVEC endothelial cells[30,37,38].

1.4.4 BRD4 in hematological malignancies

During the last years, BRD4 received more and more attention as new therapeutic target, particularly in hematopoietic cancer thanks to its ability to regulate the transcription of different genes that supports the proliferation and differentiation of malignant cells. The best-known BRD4 target is the oncogene c-*MYC*. Targeting *MYC* expression has always represented an important goal for several hematopoietic and solid tumors, which are driven by its over-expression. The relevance of BRD4 as a new target for cancer treatment was already demonstrated in AML, mixed-lineage leukemia fusion–driven leukemia, diffuse large B cell lymphoma (DLBCL) and Burkitt lymphoma[34,39–41]. In AML models it was shown that inhibition of BRD4 by small-molecule inhibitors, such as JQ1 or iBET, is able to reduce *MYC* expression and to induce cell cycle arrest of AML cells in G_0/G_1 phase as well as a myeloid differentiation[42,43]. These effects are accompanied with a global reduction of histone acetylation and a closed chromatin configuration, probably related to the absence of HAT activity of BRD4[32]. Additionally, *in vivo* transplantation of AML cells depleted of BRD4 delay leukemia progression in recipient mice[43]. In other models it has been demonstrated that BRD4 plays also a MYC-independent role. For example, it has been observed that in mouse models BET inhibitors specifically target genetic lesions in AML including IDH2[44], NPM1[45] and MLL-fusion[46]; besides *in vitro* models showed that BET inhibition results activated in Kasumi-1 cell lines carrying the translocation t(8;21)[47]. Moreover, in DLBCL, the decreased

proliferation induced by BRD4 inhibition is related to the reduction of *OCA-B* expression, involved in B cell development and maturation and in germinal center formation[40]. Whereas in mixed-lineage leukemia fusion leukemia, BRD4 inhibition influences the expression of BCL2 and CDK6[46]. Taken together, the available evidence indicates that BRD4 plays a critical role in regulating gene expression, based on the cell-type identity.

1.5 Role of *MYC* in cancer, metabolism and hypoxia

The proto-oncogene *c-MYC* is located on chromosome 8 (8q24.21) and it is a member of the MYC family, which also includes *N-MYC* and *L-MYC*. Since it was first discovered, several studies have been showing that *c-MYC* is among the most frequently deregulated oncogenes in cancers[48]. In particular in AML, the over-expression of *c-MYC* is mainly associated with trisomy of chromosome 8, which is the most common aneuploidy, occurring as a sole abnormality in about 6% of AML and coexists with other cytogenetic aberrations in 16% of AML cases [49].

Evidences suggest that *MYC* plays a central role in different processes to promote cell growth and proliferation[50] and because of its oncogenic potential it is tightly regulated in normal cells both, at transcriptional and post transcriptional levels[51]. To play its functions, MYC dimerizes with MAX and together they can bind with high affinity to a consensus sequence named E-boxes (5'-CACGTG-3'), or nonconsensus sites with lower affinity[52]. The sequences recognized by MYC are proximal to the promoter regions and their association with MYC-MAX heterodimer promotes the activation of RNA polymerases to catalyzes transcriptional elongation of target genes[53]. Based on this observation, it has been proposed that MYC enforces the expression of genes that are already expressed at basal levels in the cell[54]. In particular, MYC

regulates genes related with translation and metabolic processes as glycolysis, glutaminolysis and lipid synthesis[52]. It was demonstrated that *c-MYC* overexpression represents an important strategy adopted by cancer cells to change their metabolism and sustain proliferation. MYC deregulation breaks the physiological feedback loop that aims to inhibit MYC expression in conditions of low availability of growth factors or nutrients. For example, MYC-overexpressing cells have increased glucose and glutamine utilization, accompanied with increased an enhanced expression of several glycolytic and glutaminolytic key enzymes[55–57], in order to allow the cellular proliferation regardless of nutrients availability. In particular, cancer cells overexpressing MYC are usually addicted to glutamine, which is a major source of energy to drive TCA cycle in cancer cells, for example its deprivation induces a MYC-dependent apoptosis[58]. This glutamine dependency is related to the ability of MYC to regulate glutamine metabolism inducing transcription of genes involved in this metabolic pathway[59]. MYC directly up-regulates those enzymes involved in glutamine catabolism, such as glutaminase (GLS) and in this way it provides a source of nitrogens and carbons to sustain proliferation of cancer cells[60]. Furthermore, mouse models that overexpresses MYC in kidney or liver develop tumor with high levels of GLS, and the inhibition of GLS reduces tumor progression[61,62]. Moreover, it is known that the regulation of MYC is also influenced by the hypoxic microenvironment. Indeed, it was shown that HIF1α is able to down-regulate MYC through two different mechanisms: on one side HIF-1α binds in a competitive manner the cofactor MAX, inhibiting the function of MYC[63], on the other side it promotes activation of *MXI-1* expression that is an antagonist of MYC[64]. However, the cross-talk between c-MYC and HIF1α is altered in cancer cells, where the over-expression of c-MYC can cooperate with HIF1α to "fine tune" the metabolic changes necessary for adaptive response of tumor cells to hypoxic microenvironment[65].

1.6 Hypoxic microenvironment in AML

The microenvironment plays a crucial role in tumor development and progression and the behaviour of cancer cells is modulated by interactions with and signals from the other components of the microenvironment. HSC and LSC physiologically reside in two different niches, defined endosteal and vascular niches[66–68] (Fig. 6). These are characterized by the presence of different components including osteoblasts and osteoclasts, mesenchymal stem cells (MSCs), sinusoidal endothelium and perivascular stromal cells, and immune cells[69]. In particular, the endosteal HSC niche is mainly composed of osteoblasts that supports hematopoiesis[66,70] and *in vivo* imaging studies demonstrated that HSCs are close to endostium which supports HSC expansion in response to damage signals[71,72]. Moreover, HSCs in endosteal niche are protect from immune attack by regulatory T cells (Treg)[73]. Regarding the HSC vascular niche, it contains mainly sinusoidal endothelial cells[67], which supports HSCs growth[74–76]. Although the BM is highly vascularized, it is among the organs characterized by low pO_2 levels, a condition known as hypoxia[77]. In particular, it was shown that O_2 levels in BM are ranging from 1% to 4% [78,77], decreasing from vessels to the endostium, hence the term "hypoxic niche". The increasing interest on the hypoxic niche arises from both *in vivo* studies, which confirmed that HSCs resides in hypoxic BM areas with diminished blood perfusion[79–82], and from *in vitro* hypoxic culture (1%-3% O_2) that elucidated the role of hypoxia in promoting quiescence and self-renewal of HSCs[83,84], as well as differentiation in erythroid, megakaryocytic, and granulocytic-monocytic progenitors[84–87]. So far these studies suggest that the hypoxic niche is essential to maintaining the stemness of HSCs.

The increasing interest on BM microenvironment is related to its potential role in the initiation and propagation of leukemia. Several evidences demonstrated that the hematopoietic niches sustain survival, proliferation and differentiation

of LSC[66,67,70,83,98,99]. Indeed, in a recent study it has been illustrated that engraftment and proliferation of CD34+ LSC in BM induced alterations in the stromal microenvironment, creating a "malignant niche" inhospitable to normal HSC[100]. Moreover, several evidences have demonstrated that alterations in the BM niche can contribute to hematologic tumor development. For example, it was reported that the activation of β-catenin and FOXO1 in osteoblasts can lead to the development of AML[101,102]. In addition, Wei J. and colleagues showed that the microenvironment could determine the lineage commitment of acute leukemia. They transplanted human CD34+ cord blood cells in different recipient mice, transformed with the *MLL-AF9* oncogene, and observed that NOD/SCID/β2microglobulin null mice developed ALL or biphenotypic leukemia, whereas NOD/SCID mice transgenic for SCF, GM-CSF, and IL-3 developed AML[103]. However, the role of hypoxic microenvironment in the proliferation of LSC and its impact on therapy success remains to be clarified.

The major adaptive response to hypoxia is mediated by HIFs proteins, through the induction of several genes mainly involved in metabolic processes. HIFs family includes two O_2-sensitive α-subunits, HIF1α and HIF2α and one stable β-subunit, HIF1β. They work as heterodimer through the interaction between α and β subunits. Briefly, in normal O_2 conditions, the two α-subunits are hydroxylated and degraded by the interaction with PHDs (prolyl hydroxylases) located on VHL (von Hippel-Lindau)-associated E3-ubiquitin ligase, to ensure a rapid turnover. However, under hypoxic conditions, the PHDs are inactive because they require molecular oxygen as a cofactor, thus the binding of HIF-α subunit to VHL is inhibited. The final consequence is the stabilization of HIF-α and its translocation into the nucleus where it can dimerizes with HIF1β. This heterodimer in turn interacts with the transcriptional co-activators CBP (p300/CREB-binding protein) to recognized the hypoxia responsive elements (HREs), leading the adaptive response to hypoxia[88] through the expression of downstream genes with roles in angiogenesis, metabolism, proliferation and

survival, autophagy, proteolysis, and pH regulation[89–91]. Among genes regulated by HIF-1α several important players for HSC function are included such as: VEGF, ADM, SDF1, SCF, Ang2, Angptls, IGF-2, IGFBPs, p16, p19, p21, FOXOs[89–93]. Furthermore, it was demonstrated that HIF-1α activates the transcription of glucose transporters, glycolytic enzymes and glycolytic inducing factors[94,95]. HSCs show an enrichment of HIF-1α levels as consequence of hypoxic microenvironment[96,92], and its deletion results in loss of quiescence and reduction of repopulation activity of HSCs[92]. As mentioned before, a number of genes regulated by hypoxia are involved in the cellular metabolism. Furthermore, hypoxic conditions induce a reorganization of energy production from mitochondrial oxidative phosphorylation (OXPHOS) to glycolysis, which becomes the main source for energy production, in order to reduce the oxidative damage related to OXPHOS function in conditions with low O_2 levels. Indeed, conditional deletion of HIF-1α in HSC results in a metabolic shift to oxidative metabolism, with increased oxidative stress[97].

Although the importance of hypoxic microenvironment in solid tumor was deeply understood, its role in haematological malignancies is not yet clear. HIF1α is up-regulated in CD34+CD38- human AML primary cells, furthermore HIF1α KD or inhibition by echinomycin induced apoptosis of LSC and impair their ability to reconstitute AML into xenotransplanted mice[104]. Recently HIF1α has been shown to induce the expression of IL-8 in AML cell lines and in primary AML blasts, which in turn supports survival and proliferation of AML cells[105]. Lodi and colleagues described the metabolic effects induced by hypoxia in two different cell lines, K562 and KG-1. They showed that although the two cell lines have different metabolic profile in normoxia, when they are cultured under hypoxia (1% O), the metabolic changes were strikingly similar, suggesting that both cell lines adopt a common adaptive response to hypoxia[106]. In particular, this study described that hypoxia induces an increased concentration of amino acids and several metabolites involved in phospholipids

biosynthesis and catabolism, and an enrichment of glycolytic pathway without altering metabolites within the TCA cycle[106]. Consequently, the current studies demonstrate that the crosstalk between LSC and BM niche plays a dual role being involved in both leukemia-induced microenvironment reprogramming and microenvironment-induced leukemogenesis mechanisms. These evidences indicate that the comprehension of the crosstalk between LSC and BM niche is essential to better understand the leukemogenic process and some therapy resistance/evasion mechanisms adopted by LSC, providing the rationale to develop novel therapeutic approaches to target the cytoprotective mechanism derived from "malignant niche".
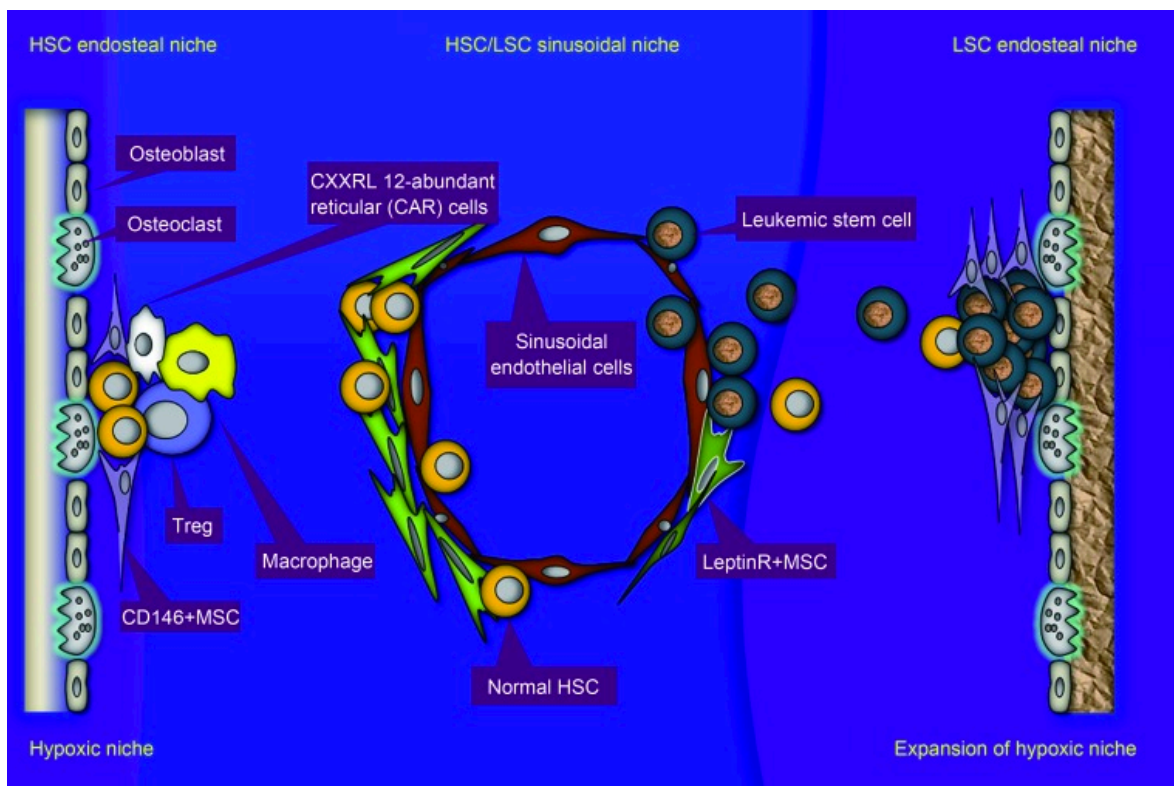
Figure 6. Organization of HSC and LSC BM niches[107]. HSC and LSC niches are represented with their cellular populations. The oxygen gradient decreases from vessels to the endostium and the expansion of hypoxic niche in LSC microenvironment is here illustrated

1.7 BRD4 as a therapeutic target in AML

As mentioned in the previous sections, BRD4 plays a role in several tumors where it is a key regulator of MYC expression. This characteristic makes it a potential therapeutic target for cancer treatment. For these reasons in the last years several small molecule inhibitors of BET proteins have been developed and some of them are currently used in clinical trials[108]. In AML, BRD4 is expressed by myeloblasts, leukemic stem- and progenitor-cells[109] and its chromatin occupancy associates with the hematopoietic transcription factors (TFs) PU.1, FLI1, ERG, C/EBPa, C/EBPb, and MYB at promoter and enhancer regions[42]. BET inhibition was able to suppress leukemogenic transcriptional programs and proved efficacy across diverse disease subtypes, including MLL-[43,46] or EVI1-driven[110] leukemia, NPM1[45] or IDH[44] mutant AML, t(8;21) AML[111], MLL3-suppressed and 7/del(7q) AML[112]. Moreover, *ex vivo* studies showed that treatment with the small-molecule inhibitor of BRD4 was effective in primary AML blasts, inducing apoptosis on stem- and progenitor-cells CD34+/CD38+ as well as CD34+/CD38- populations derived from AML patients at diverse disease stages, including refractory and relapsed AML without relevant differences within FAB or WHO subtype[109]. Additionally, the study showed that BET inhibition synergized with ARA-C in inducing anti-leukemic effects[109]. The relevance of BRD4 in AML progression was confirmed by *in vivo* experiments performed in mice transplanted with MLL-AF9/N-RAS^{G12D} leukemia cells containing *BRD4* shRNA or control; after the disease onset, the silencing of BRD4 resulted in a delay of leukemia progression and survival advantage of mice[43]. Morphologic analysis of MLL-AF9/N-RAS^{G12D} leukemia cells treated with a small-molecule inhibitor of BRD4 revealed that the treatment induces a macrophage-like phenotype of blast cells, with an increased expression of myeloid differentiation markers and a reduced expression of KIT[43]. As expected, consistent with the described transcriptional

role of BRD4, BET inhibition induced the down-regulation of key genes involved in cell cycle progression, such as *MYC*, *CDK6* and *E2F*[40,43,46,113], LSC maintenance (e.g. *KIT*)[43,111], apoptosis control (e.g. *BCL2*), and metabolism (e.g. oxidative phosphorylation, RNA transport, ribosome biogenesis)[111]. The alterations of gene expression programs induced by BET inhibition results in suppression of self-renewal capacity accompanied with a significant reduction of cell growth, highlighted by cell cycle arrest at G0/G1 phase, and induction of the myeloid differentiation, as well as an increase of leukemic cell death[43,46].

The promising results obtained in cellular and mouse models, prompted the development of Phase 1 and Phase 1/Phase 2 clinical trials investigating the efficacy of BET inhibition in human AML, among other hematological malignancies (NCT01713582, NCT02158858, and NCT02308761, NCT02543879, NCT01943851, NCT02391480, NCT02431260, NCT02698189, http://clinicaltrials.gov/) (Tab 2). According to the available results/data, the disease reduction was achieved in five out of 36 AML patients, including complete remission with or without complete recovery of platelet and partial blast clearance[114].

In parallel, drug resistance mechanisms have been identified after long-term treatment with BET inhibitor associated with the restoration of the expression of MYC and its target driven by a focal enhancer formed during acquisition of resistance[115]. Moreover, it was demonstrated that in human and mouse leukemia cells, the resistance to BET inhibitors is related to the activation of WNT/β-catenin signaling, which in turn can drive *MYC* transcription[115,116]. Gene set enrichment analysis (GSEA) identified alterations in five signaling pathways in resistant cells, which include WNT, TGFβ, HIPPO, VEGF, and CAMP pathways[115]. This data indicate that resistance mechanisms observed after long-term treatments with BET inhibitor are mostly related to changes in the enhancer landscape, and that the activation of WNT pathway could be a potential predictive biomarker of BET inhibitor response in AML[117].

Taken together these findings indicate that BRD4 plays a critical role in LSC maintenance, thus BET inhibition represents a promising therapeutic approach for AML treatment.

BET Inhibitor	Indication	Clinical Status	Reference
CPI-0610	Leukemia; Lymphoma; Multiple myeloma; Myelodysplastic syndromes; Myeloproliferative disorders	Phase I	NCT02158858
OTX 015	Acute Myeloid Leukemia; Diffuse Large B-cell Lymphoma; Acute Lymphoblastic Leukemia; Multiple Myeloma	Phase I	NCT01713582; NCT02698189
RO 6870810; TEN 010	AML; myelodysplastic syndrome	Phase I	NCT02308761
INCB-054329	Advanced malignancies	Phase I/II	NCT02431260
ABBV-075	Advanced malignancies	Phase I	NCT02391480
FT 1101	Hematological malignancies	Phase I	NCT02543879
GSK525762; I-BET-762	Relapsed, refractory hematological malignancies, solid tumors	Phase I/II	NCT01943851
PLX-51107	AML, myelodysplasia, solid tumors	Phase I	NCT02683395

Table 2. Overview of clinical trial based on BRD4 inhibitors in hematological malignancies. Are listed the BET inhibitor used, the indication for treatment, the phase of study and the corresponding clinical trial.

1.8 Spindle assembly checkpoint

The spindle assembly checkpoint (SAC) system acts during transition from metaphase to anaphase, playing an important role during mitosis to ensure the equal segregation of sister chromatids in daughter cells. It prevents the anaphase entry until each doubled kinetochore is properly attached with microtubules from the opposite poles of cell. Intrakinetochore tension is one of the mechanism used by SAC components to verify the correct alignment of chromosomes in the equator of cell and the correct attachments of chromatids to kinetochore[118].

When the kinetochore lacks spindle attachment, Aurora B protein kinase phosphorylates kinetochore substrates[119,120] and contributes to the recruitment of MPS1 kinase by the kinetochore Knl1 complex–Mis12 complex–Ndc80 complex (KMN network)[121,122]. Mps1 in turn phosphorylates the kinetochore KNL1 complex at multiple sites (Fig. 7A)[123–125]. This event promotes binding of the SAC proteins (BUB3, BUB1, BUBR1, MAD1, MAD2 and CDC20) to the kinetochore[126], in order to organize the mitotic checkpoint complex (MCC). Phosphorylated KNL1 recruits BUB3-BUB1 protein complex[127,128], which is also phosphorylated by MPS1, enabling the interaction with the heterotetrameric MAD1-MAD2 complex[129]. This is involved in the conversion of inactive cytosolic MAD2 into an active conformation[130], a process requiring MPS1 activity[131,132]. Active MAD2 forms heterodimers with inactive MAD2 molecules in the nucleus, in order to recruit them to the kinetochore[130]. This network organizes the MCC, which sequesters CDC20 from binding and activating the anaphase-promoting complex/cyclosome (APC/C). PLK1 cooperates to the process by phosphorylating CDC20[133,134]. Moreover, BUB1 provides docking sites for CDC20, and BUBR1 can also bind CDC20, once recruited by BUB1[135]. Finally, the MCC can repress APC/C activation by interacting with CDC20 molecules that are already complexed to APC/C (Fig.

7B).

When the kinetochore is properly attached, KNL1 is dephosphorylated and SAC proteins are released[136,137]. CDC20 binds and activate APC/C, an E3 ubiquitin ligase, involved in ubiquitination of several target proteins containing a D-Box domain[138,139], TEK[140] or the newly identified ABBA[135] motifs. APC/C in turn polyubiquitinates cyclin B1 and securin, CDK1 and separase partners, respectively (Fig. 7C). Cyclin B1 is degradated through the proteasome, leading to a rapid decline of CDK1 activity. Securin is released from separase, thus activating the degradation of the cohesion complex at and near sister chromatid kinetochores. These events lead to faithful chromosome segregation into daughter cells.
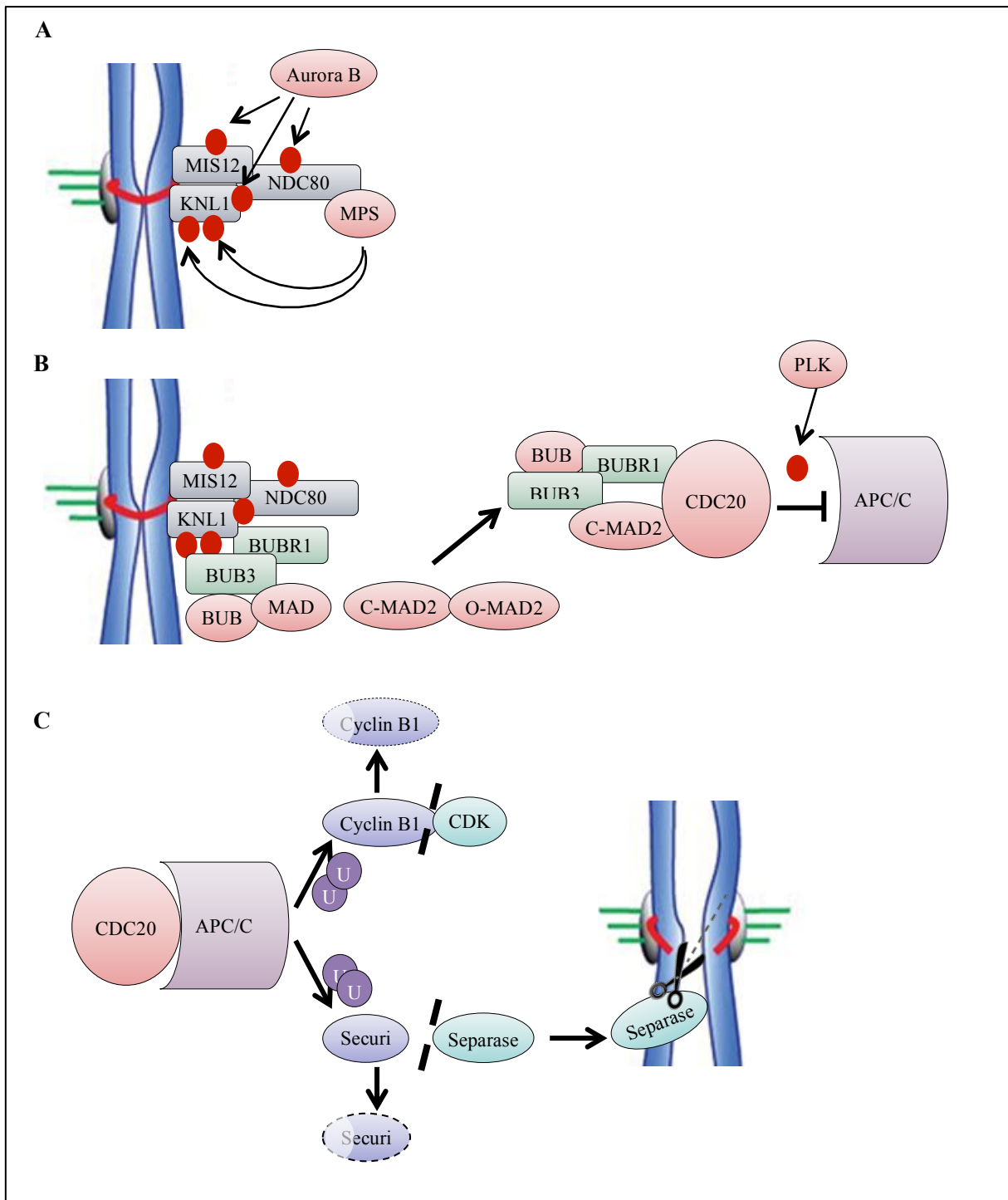
Figure 7. The SAC and MCC activity. (**A**) The KMN network undergoes post-translational modifications at unattached kinetochores, leading to recruitment of SAC proteins (**B**) and conformational changes of MAD2. This leads to the formation of the MCC, that binds CDC20, thus inhibiting activation of the APC/C. When the kinetochore is properly attached, CDC20 is released and activates APC/C (**C**), that orchestrates cyclin B1 and securin degradation. Separase in turn degrades the cohesion complex at and near sister chromatid kinetochores. These events are needed for a faithful chromosome segregation.

1.9 Structure and biological functions of CDC20

CDC20 was discovered by Lee Hartwell in 1970. Using CDC20 mutated yeasts, Hartwell's group showed that in absence of CDC20 the yeasts failed to initiate anaphase and chromosome segregation[141]. So far, it has become clear that CDC20 is one of the components of the SAC involved in anaphase onset, ensuring correct chromatid separation during mitosis. The first identified role of CDC20 was related to cell cycle progression. Indeed many substrates of APC^{CDC20} were critical cell cycle regulators, including Securin[142], Cyclin B1[143], Cyclin A[144], Nek2A[145], Cenp-F[146] and p21[147]. Proteasome degradation of these proteins, promoted by APC/C^{CDC20} allows the progression through the cell cycle, by inducing the onset of anaphase. To exert its biological functions, CDC20 is structurally composed of several domain, including the C box and IR motif implicated in binding to APC8 and APC3 subunits of APC/C complex, the MAD2-interacting motif (MIM), the WD40 repeats involved in binding of D-Box domain on substrate, KEN and CRY box responsible of auto degradation signal after phosphorylation induced by Plk1.

It was demonstrated that in mice, loss of CDC20 caused embryonic lethality and condensed chromosomes due to securin stabilization and aberrant metaphases arrest[148,149,150]. During the last years it was showed also that CDC20 exerts a pivotal role in other biological processes including ciliary disassembly[151], brain development[152], DNA damage repair[153], suppression of necrosis in neural stem cells under catastrophic cellular stresses[154], Wnt/β-catenin signaling[155], tissue homeostasis and stem cell fate in human keratinocytes[156], proliferation, invasiveness and self-renewal of glioblastoma stem-like cells[157] and apoptosis[158,159].

Regarding the regulation of apoptosis, it was observed that depletion of endogenous CDC20 or pharmacological inhibition of APC/C^{CDC20} led to mitotic arrest followed by cell death[160]. It has been reported that CDC20 could regulate

apoptosis through controlling the stability of MCL-1[158] and Bim[159]. Both of them are members of the BCL-2 family proteins, which are classified into anti-apoptotic and pro-apoptotic members[161]. The anti-apoptotic members are BCL-2, BCL-xL, BCL-W and MCL-1, while BAX, BAK, and BIM are the pro-apoptotic members[162]. Wan and colleague recently confirmed that CDC20 interacts through its WD40 repeats motifs with two evolutionary D boxes conserved on BIM. Furthermore they showed that CDC20 depletion allows a significant up-regulation of BIM and that BIM is physiologically reduced during mitosis, when APC^CDC20 is active[159]. Lastly, another study suggested that CDC20 induces apoptosis in hepatocellular carcinoma cells through the degradation of PC-PLC (phosphatidylcholine specific phospholipase C)[163].

1.9.1 *Upstream regulators of CDC20*

To fully understand the CDC20 regulatory network system, recent studies have defined the upstream regulators of CDC20. We have already described the role of SAC proteins like Mad2, Bub1 and Bub3 in APC^CDC20 inhibition. Additionally, F-box protein Emi 1 (early mitotic inhibitor1) is a pseudo substrate of CDC20 that binds APC/C^CDC20 and inhibits its E3 ligase activity[164,165]. Moreover, USP44 (ubiquitin specific protease 44) stabilizes the APC/C inhibitory Mad2-CDC20 complex through CDC20 deubiquitination to block premature activation of APC/C[166]. Another inhibitor of APC/C^CDC20 is the tumor suppressor RASSF1A, that blocks degradation of Cyclins A and B at the spindle poles[167]. Interestingly, Kidokoro and colleague showed that p53 exerts its anti-tumor activity by regulating CDC20 expression. Indeed they reported that the overexpression of p53 inhibits CDC20, whereas depletion of p53 increases CDC20 expression[168]. Strikingly, another study showed that p53 induced by DNA damage binds the CDC20 promoter leading its down-regulation along with chromatin remodelling[169]. Lastly, it was discovered that

also some microRNA, including miR-449 and miR-494are, involved in regulation of CDC20 mRNA levels[170,171].

1.10 Role of CDC20 in human cancers

During the last years, the role of CDC20 is gaining more and more interest because of its association with clinical pathological parameters in various human cancers[18]. Increasing evidence has revealed the oncogenic role of CDC20 in human tumorigenesis, including both tumor progression and prognosis.

1.10.1 CDC20 in solid tumors

Several studies showed that abnormal levels or dysfunction of CDC20 could play an important role in carcinogenesis and cancer progression. Overexpression of CDC20 has been shown in pancreatic cancer patient, where Li et al. observed that pancreatic tumor tissue showed higher CDC20 levels compared to normal adjacent tissues[172], and high expression of CDC20 was associated with a lower 5-year recurrence-free survival rate[173]. Moreover, mRNA and protein levels of CDC20 have been observed to up-regulate in high-grade primary breast cancer tissues[174] and that this high expression is correlated to an extremely poor outcome of breast cancer patients[175]. Additionally, the regulation of CDC20 is related to the APC/C inhibitor Daxx in prostate cancer. Daxx is know to interactwith CDC20 to avoid the ubiquitination and degradation of APC/C^{CDC20} substrates[176]. Two different studies suggest that inhibition of LATs (L-type amino acids transporter) protein[177] or COX-2[178] inhibit the tumor growth and the cell cycle progression suppressing several M-phase cell cycle genes including CDC20. In colorectal cancer, CDC20 is up-

regulated by more than five-fold in 77% of primary tissues[168] and this over-expression was associated with clinical stage, metastasis and shorter overall survival[179]. Strikingly, the same condition was found in hepatocellular carcinoma tissues[180] and gastric cancer[181], where the high levels of CDC20 correlate with the tumor differentiation, with the TNM stage and metastasis. Furthermore, CDC20 up-regulation has been reported in glioblastoma[182], urothelial carcinoma[183], oral and cervical cancer[184,185] and in head and neck tumors[186]. Altogether, these findings suggest that CDC20 could represent an independent prognostic biomarker and a potential therapeutic target for solid human cancer.

1.10.2 CDC20 in hematological malignancies

Alterations of CDC20 expression levels have been observed also in several hematological malignancies. For example Multiple Myeloma (MM) patients with high CDC20 levels had a significant inferior overall survival[187,188]. Moreover, MM cells isolated from patients with high CDC20 expression showed a significant increase of enrichment in genes associated with proliferation, confirmed by PI analysis[188]. The inhibition of CDC20 is able to induce apoptosis and G2/M arrest[189] in MM cell lines and primary cells. In MDS patients, high CDC20 expression was associated with high risk patients which suffer of thrombocytopenia, cytopenias, dysplasia, lower platelets count and complex karyotype[190,191]. Moreover, we observed a significant up-regulation of CDC20 expression in AML patients with aneuploid karyotype compared with the euploid ones[10]. In particular, a 3-genes signature including high CDC20 and PLK1 and low RAD50 expression was able to discriminate aneuploid from euploid cases. Recently, CDC20-mediated ubiquitination of MEIS1 and p21 have been discovered to be involved in the the regulation of quiescence in HSC and leukemia initiating cells (LIC) in AML[192]. Analysis of

high-throughput data obtained from DLBCL patients showed that up-regulated genes were enriched for those involved in mitosis, cell cycle checkpoints, APC/CDC20-mediated degradation of Nek2A. Furthermore, high CDC20 expression correlates with promoter hypo-methylation and is significantly associated with poor OS[193]. Moreover, expression of the viral trans-activator oncoprotein Tax, which is involved in pathogenesis of adult T cell leukemia/lymphoma (ATL), perturbs mitotic entry and G2/M arrest in S. cerevisiae, rodent, and human cells[194]. The mitotic defects caused by Tax are associated with a premature and drastic reduction in Securin and Cyclin B1 levels mediated by APC/C^{CDC20}. This evidence supports the idea that Tax promotes aberrant activation of APC/C^{CDC20} to avoid the block of mitotic entry and progression of aneuploid cells, highly represented in ATL[195].

1.11 CDC20 inhibitors

Considering the oncogenic role of CDC20 in tumorigenesis and its over-expression in several human tumors, pharmacological inhibition of CDC20 activity could represent a novel strategy for the treatment of human cancers.

The fact that APC/C^{CDC20} can be involved in the proliferation capacity of cancer cells provides new opportunities for an exploration of its therapeutic potential. Accordingly, the efficacy of several CDC20 inhibitors has recently been reported to induce cell cycle arrest and apoptosis of cancer cell lines and primary cells. Multiple molecules showed an inhibitor activity on CDC20 function including: TAME and pro-TAME, Apcin, Withaferin A, N-alkylated amino acid-derived sulfonamide hydroxamate (NAHA), Ganodermanontriol (GDNT), and Genistein[196–198].

1.11.1 TAME and pro-TAME

TAME (tosyl-L-arginine methyl ester) is a small molecule that mimes the IR motif of CDC20 involved in its recruitment to the APC/C. Since TAME is not cell permeable, it was synthesized a TAME prodrug (pro-TAME), which can be processed by intracellular esterases to yield the active form TAME. Pro-TAME binds in a competitive manner the APC/C core complex and prevents its association with CDC20 and CDH1 inhibiting APC/C activation. This leads to the inhibition of the degradation of both, APC^{CDC20} and APC^{CDH1} substrates[199]. Moreover, pro-TAME is able to induce mitotic arrest [200] through stabilization of Cyclin B1.

1.11.2 APCIN

Apcin (APC inhibitor) is a small compound that prevents substrate recognition by CDC20[199]. This molecule blocks the recognition of CDC20 substrates that interacts with APC/C through the D-box motif, including Cyclin B1 and Securin, which are stabilized during treatment with Apcin. Compared with TAME, Apcin specifically acts on the APC/C^{CDC20} complex without interfere on the activity of APC^{CDH1}.

2. AIMS

The development of new targeted therapies is the current challenge to improve AML treatment, with the aim of selectively eradicate leukemia initiating cells while sparing normal cells or, at least reducing the hematological toxicity. As mentioned, during the last decade several of news drugs were develop to target specific mutations or altered pathway (eg. *FLT3* inhibitors, checkpoint inhibitors), providing a new chance for some subgroups of AML.

Based on preliminary data from our group and others, this study aims to investigate the molecular mechanisms associated with the inhibitions of a new potential target and to investigate the effect of a novel therapeutic combinations. To this propose we used *in vitro* models of AML reflecting different genomic background. In particular, the specific aims were:

- **Analysis of genomic and metabolic alterations induced by bromodomain inhibitor GSK1215101A.** BET inhibitor showed to be promising therapeutics in preclinical model, while limited efficacy was observed in patients as single agent. We aimed to evaluate the role of the hypoxic BM microenvironment on AML cell lines treated with GSK1215101A, in order to understand whether LSC can be targeted by the drug under physiological conditions. Moreover, since c-MYC was described among the final targets of BRD4 inhibition, and together with hypoxic microenvironment is a master regulator of several genes related to metabolism, we wanted to elucidate the molecular mechanism and metabolic changes associated with BETi activity, in order to identify a novel potential combination treatment.

- **Investigation of the potential role of CDC20 as a new target in AML treatment.** We previously showed that CDC20 is highly expressed in aneuploid AML, therefore representing a novel potential target. We aimed to investigate the effect of inhibition of CDC20 activity in aneuploid and near-euploid AML models, in order to assess its role in the proliferation and survival capacity of leukemic cells.

3. Materials and Methods

3.1 Cell-biological methods

Cell lines and drugs

Human AML cell lines (Tab. 3) were cultured at 37°C and 5% CO_2 in RPMI-1640 (Invitrogen) or α-MEM (Lonza) with 1% l-glutamine (Sigma-Aldrich), penicillin (100 U/ml, Gibco) and streptomycin (100 U/ml, Gibco) supplemented with 10% or 20% fetal bovine serum (FBS, Gibco). For experiment under hypoxic conditions AML cell lines were incubated in hypoxic chamber set at 37°C, 1% O_2 and 5% CO_2. Drugs used in this study were listed in table 4.

Cell line	Cytogenetics
HL-60	human flat-moded hypotetraploid karyotype with hypodiploid sideline and 1.5% polyploidy,c-myc amplicons present in der(1) and in both markers
OCI-AML3	human hyperdiploid karyotype , hemizygous for RB1, *NPM1* and *DNMT3A* mutated
Kasumi-1	human hypodiploid karyotype, t(8;21)(q22;22))
NOMO-1	human hyperdiploid karyotype with 8% polyploidy, t(9;11)(p22;q23) with rearrangement of KMT2A (MLL) -
MOLM-13	human hyperdiploid karyotype with 4% polyploidy , ins(11;9)(q23;p22p23)
KG-1	human hypodiploid karyotype with 4.5% polyploidy
HT-93A	human near-diploid karyotype; carries complex t(1;12) and t(15;17) rearrangements effecting ETV6-ABL2 (ETV6-ARG) and PML-RARA rearrangements, respectively
MV-4-11	48, XY, t(4;11)(q21;q23), +8, +19

Table 3. List of AML cell lines and cytogenetic characteristics obtained from DSMZ catalogue.

Chemical compound	Catalogue n°	Conc. Stock solution	Company
GSK1215101A	????	10mM	GlaxoSmithKline
RTA-408	17854 ?	10mM	Reata Pharmaceuticals
Apcin	AG.CR1-3603	40mM	LifeScience
proTAME	AG-CS10100	20mM	LifeScience

Table 4. List of drugs used in the study. All diluted stock solution were stored at -20°C and diluted at desired concentrations in culture media immediately before use.

Patients and primary AML cells

Primary samples were obtained from AML patients after informed consent as approved by the Institutional Ethical Committee (protocol 112/2014/U/Tess of Policlinico Sant'Orsola-Malpighi) in accordance with the Declaration of Helsinki. BM mononuclear cells were isolated by Ficoll density-gradient (Amersham Biosciences), and after counting, about 20×10^6 cells were lysed in guanidine-thiocyanate–containing lysis buffer (RLT, Qiagen, Ltd) whereas the remaining cells were cryopreserved with 90% FBS and 10% DMSO and stored in liquid nitrogen. DNA, RNA and protein from primary mononuclear cells stored with RLT buffer were extracted using AllPrep DNA/RNA/Protein Mini Kit (Qiagen, Ltd) according to the manufacturer's instructions.

Immunophenotypic analysis

Primary AML cell after isolation were washed with cold PBS, then fixed using 70% ethanol and stored at -20°C for 24 h. Ethanol was removed and cells were washed once with PBS with 0.5 % (v/v) Tween 20 (Bio Rad) and once with PBS 0.1% Bovine Serum Albumin (BSA, Sigma), then the cells were incubated for intracellular staining with anti-Ki67 BV421 (#562899, BD Biosciences) and

anti-CDC20 PE (#562899, NovusBio) for 1 h at 4°C in the dark. After incubation cells were washed twice with PBS and incubated for 15 minutes at 4°C in the dark with anti-CD45 PerCP-CyTM5.5 (#564106, BD Biosciences), anti-CD34 PE-CyTM7 (8G12, #348811, BD Biosciences), anti-CD-38 FITC (#555459, BD Biosciences). After washing cells were analyzed by FACS. The expression levels of CD34, CD38 and CDC20 are relative to CD34-positive cell populations and were obtained by FlowJo software.

Drug treatments

AML cell lines were incubated with the selected doses of drugs: GSK1215101A (250 and 500 nM), omaveloxolone (400 nM and 600 nM), Apcin (50 and 100μM) and proTAME (5 and 10 μM) for 24 and 48 h at 37°C and 5% CO_2. Primary cells: AML BM cells were thawed in IMDM medium with 10% FBS and DNAse I (10 U/mL, Roche) and incubated at 37°C and 5% CO_2 for 1 hours. Then, cells were centrifuged at 400g for 5 minutes and washed with 10 mL of complete medium in order to remove dead cells. CD34+ cells were isolated by immunomagnetic separation (Miltenyi Biotec) and seeded at $2-3x10^6$ cells/ml in SFEM-II medium (Stem Cell Technologies) containing L-glutamine (2 mM), rhIL-3 (20 ng/mL), rhIL-6 (20 ng/mL), rhSCF (20 ng/mL), rhG-CSF (20 ng/mL) (Miltenyi Biotec) and incubated for 24 hours at 37°C and 5% CO_2 before to start drug treatments. In particular primary cell isolated from four patients at diagnosis were treated for 48 hours with GSK1215101A (250 nM and 500 nM) and omaveloxolone (RTA-408, 400nM and 600 nM) as single agents and in combination. Moreover, the effects of CDC20 inhibition were tested on primary cells isolated from 5 AML patients using Apcin (10 and, 50 μM).

Cell viability assay

In order to monitor cell viability, AML cell lines were incubated with Cell Titer Glo or RealTime-Glo™MT Cell Viability Assay (Promega) during treatment with increasing concentration of the tested drugs, as single agents: GSK1215101A from 0 to 1000 nM, omaveloxolone from 0 to 1500 nM, Apcin from 0 to 1000 μM, and proTAME from 0 to 32 μM. The cell viability was evaluated at 24, 48 and 72h using Tecan Infinite M200 Microplate Reader. The IC50 was calculated by GraphPad Prism v6.01.

Colony forming unit (CFU) assay

To evaluate the effects of drug treatments on clonogenicity capacity, 7.5×10^5 primary BM cells were isolated, washed with PBS and resuspended in IMDM media with 2% FBS. Successively cells were were added to 1.3 ml of methylcellulose medium (StemMACS™) previously prepared with desired doses of drugs: 0.5 and 1 μM for GSK1215101A, 0.6 and 1.2 μM for Omaveloxolone, as single agents and in combination, and 10 and 50 μM for Apcin. After vortexing and incubation of about 15-30 minutes to remove air bubbles, cells were gently seeded in a 6 well plate and incubated for 14 days at 37°C and 5% CO_2. AML cell colonies were counted under an inverted microscope.

Apoptosis and cell cycle analysis

Apoptosis analyses were performed using Annexin V/Propidium Iodide (PI) staining according to the manufacturer's instructions (4830-250-K, Trevigen). Then, cells were washed and analyzed by BD Accuri C6 flow cytometer. The apoptosis levels were expressed as percent of Annexin V/PI-positive cells

determined by assaying 10,000 cells. The mean percentage of Annexin V-PI-positive cells and standard error measurements were calculated from at least three independent experiments. Cell cycle analyses were performed using the PI staining mix (BD). After incubation cells were harvested and washed with cold PBS, then fixed using 70% ethanol and stored at -20°C for 24 h. Ethanol was removed by PBS wash and the cells were incubated for 30 minutes at room temperature (RT) with the PI staining mix, then they were analyzed by FACSDivaTM (BD). Quantitative analyses were performed using Flowing software (Cell Imaging Core, Turku Centre for Biotechnology, Turku, Finland).

Western blot analysis

After treatments cells were harvested and incubated with cell lysis RIPA buffer (9806S Cell Signaling) for 30 minutes at 4°C, then they were centrifuged at 13000 rpm for 30 minutes at 4°C. Protein extracts were separated by Sodium Dodecyl Sulphate-PolyAcrylamide Gel Electrophoresis (SDS-PAGE, Bio-Rad) and transferred onto nitrocellulose membranes. After transfer membranes were blocked for 1h at RT in PBS with 0.1% (v/v) Tween 20 (PBS-T) and 5% milk (w/v), and then were incubated over night (ON) at 4°C with primary antibody diluted 1:1000 in PBS-T with 5% milk or BSA (Tab. 5). The day after membranes were washed 2 times with PBS-T and were incubated with horseradish peroxidase (HRP)-conjugated anti-rabbit Immunoglobulin (Ig)G (GE Healthcare), anti-mouse IgG (GE Healthcare) and anti-goat IgG (Santa Cruz) secondary antibody for 1-2h at RT. Finally, membranes were washed 3 times with PBS-T and the antibodies signal was detected using the enhanced chemiluminescence ECL (GE) reagent and the ChemiDoc XRS+ System (Bio Rad). Signal quantification was performed using Image J software.

Antibody	Company
Anti-BRD4	Cell signalling
Anti-cMYC	Cell signalling
Anti-p21	Cell signalling
Anti-HIF1α	Cell signalling
Anti-H4pan acetyl	Millipore
Anti-H4	Cell signalling
Anti-H3K14	Cell signalling
Anti-H3	Cell signalling
Anti-Lamin	Cell signalling
Anti-Tubulin	Cell signalling
Anti-Cyclin A	Cell signalling
Anti-CDC20	Cell signalling
Anti-Cyclin B1	Cell signalling
Anti-BIM	Invitrogen
Anti-CDK1	
Anti-BCL2	Life technologies
Anti-p53	Cell signalling
Anti-CDH1	Sigma
Anti-Securin	Thermo Fisher

Table 5. List of primary antibodies used.

Cell Cycle synchronizations

Serum Starvation: In order to block cell cycle in G_0/G_1 phase cells were plated at 0.5×10^6 and were cultured at 37°C and 5% CO_2 in RPMI-1640 without neither, FBS and L-glutamine. After 72h cells were harvested, washed with PBS, centrifuged at 3000 rpm for 5 minutes and the derived pellets were stored at -80°C.

Double thymidine block: To achieve a synchronization in S phase cells were plated at $0.5x10^6$ in complete medium with thymidine (3mM) and were incubated for 16 h at 37°C and 5% CO_2. Then, the cells were washed with PBS and incubated for 8h with complete medium to release the thymidine block and finally they were incubated again with thymidine (3 mM) for 24h at 37°C and 5% CO_2. After the second block cells were washed with PBS and incubated with complete medium for 2 h to reach the higher amount of cells in S phase, therefore they were harvested, washed with PBS, centrifuged at 3000 rpm for 5 minutes and stored at -80°C.

Inhibition of microtubules formation: With the aim to obtain G_2/M synchronization cells were plated at $0.5x10^6$ in complete medium with thymidine (1 mM) and were incubated for 24 h at 37°C and 5% CO_2. Later cells were washed with PBS and incubated in complete medium with nocodazole (50 ng/ml) for 24h, at the end of which the cells were harvested, washed with PBS, centrifuged at 3000 rpm for 5 minutes and stored at -80°C.

Metabolomic profiling

In order to perform the analysis of intracellular metabolites $20x10^6$ cells were treated with GSK1215101A for 4+20h under hypoxic and normoxic conditions. Then, cells were harvested, washed with PBS, centrifuged at 3000 rpm for 5 minutes at 4°C, and stored at -80°C. The Ultralight Performance Liquid Chromatography-Tandem Mass Spectroscopy was performed by Metabolon, which provided to give back a complete profile of metabolic alterations identified comparing treated cells versus controls (vehicle, DMSO).
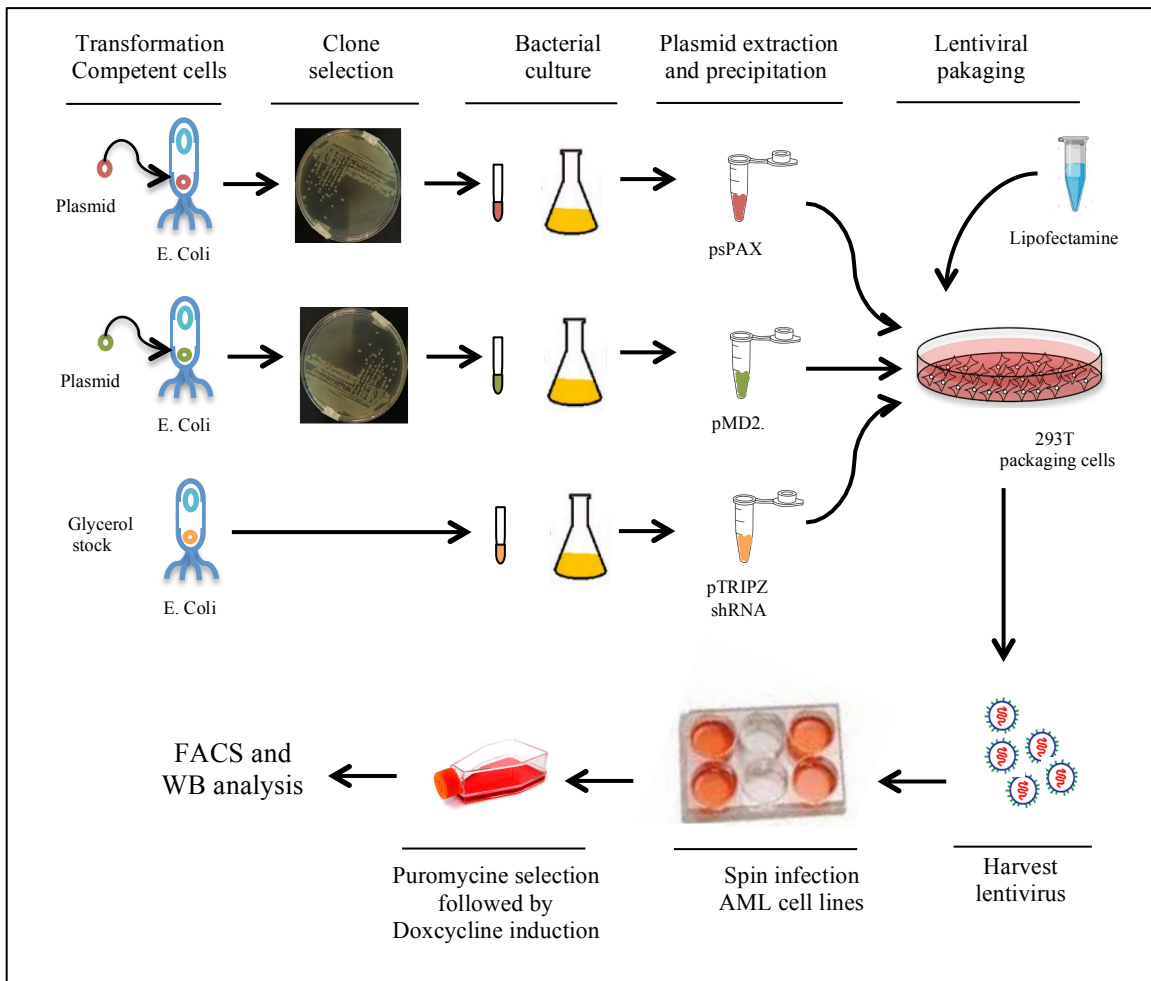
Lentiviral shRNA production, infection and screening

Knock down of CDC20 was performed through lentiviral shRNA, which allow to silence the gene expression in a stable manner inducing the degradation of mRNA target. The main steps of this protocol are illustrated in figure 8 and are described below.

- Transformation of competent cells: DH5α (Thermo Fisher) competent cells were used in order to produces packaging plasmid psPAX and envelope plasmid pMD2.G. Briefly, bacterial cells were thawed on ice and were incubated with 10-20 ng of plasmid for 30 minutes on ice. After 45 seconds of heat shock at 42°C followed by 2 minutes on ice cells were diluted with 250 µl of SOC medium, and incubated for 1 h at 37°C 225 rpm. Then, cells were selectively growth onto 10 cm^2 dish previously prepared with 10 ml of LB Broth with agar (Lennox, Sigma) and 100 µg/ml ampicillin (Sigma), as consequence only cells that contain the plasmid will be able to grow and form colonies. After 16-18 h of incubation at 32°C a single colony has been picked and expanded for 8 h at 37°C 225 rpm into 3 ml of LB Broth (Sigma) supplemented with glucose (1 g/l) and with ampicillin (100 µg/ml), and later 100-200 µl of bacterial suspension were transferred into 250 ml of LB Agar with ampicillin (100 µg/ml) and incubated 16-18 h at 37°C 225 rpm. The ON transformed DH5α culture was harvested by centrifugation and plasmid DNA was recovered using GeneEluteTM HP Plasmid Maxiprep Kit (Sigma). The pTRIPZ (Carlo Erba) vector carrying shRNA or scrambled was bought as glycerol stock and was expanded as described for DH5α transformed with psPAX2 and pMD2.G starting from 3 ml of LB agar.
- Lentiviral production: 293T packaging cells were seeded in 10 cm plates at $3x10^6$ cells per plate in DMEM supplemented with 10% FBS, penicillin (100 U/ml, Gibco) and streptomycin (100 U/ml, Gibco) and were

incubated about 24 h at 37°C 5% CO_2. Transfection of 293T cells was performed with Lipofectamine 200 Transfection Reagent (Thermo Fisher). For each dish were prepared 270 μl of Optimem with 30 μl of Lipofectamine, and in a separate tubes, the plasmid mix with psPAX2 (3 μg), pMD2.G (6 μg) and pTRIPZ carrying shRNA or scrambled (6 μg). After 5 minutes of incubation at RT the plasmid mix was added into tube with lipofectamine, incubated for 20 minutes RT, and added drop wise to 293T cells, plated in 5.4 ml of complete media, and later incubated at 32°C 5% CO_2 for 16-18 h. Then, medium was replaced with 8 ml of complete fresh medium and the virus was harvested at 48 and 72 h post transfection.

- Virus concentrations and infections: virus particle produced from 5 dishes of 10 cm were used in order to successfully transduce $2x10^6$ AML cell lines. After 48 and 72 h of incubation viral supernatant was harvested, filtered through a 0.45 μm PVDF filter (Merck Millipore) and incubated with Lenti-X Concentrator (Clontech) at 4°C for 6 h. Then the mixture was centrifuged at 1500 g for 45 minutes at 4°C and the pellet was gently resuspended with 1 ml of RPMI supplemented with 20% of FBS. Then, the concentrated virus has been used to infect $2x10^6$ AML cell lines by adding polybrine (8 μg/μl) and spin infection at 2000 rpm for 60 minutes at 32°C.

- Selection and screening: infected AML cell lines were incubated with complete RPMI medium for 48 h at 37°C 5% CO_2 before to start selection of efficiently transduced cells by puromycin (1 μg/ml). The expression of plasmid carrying shRNA or scrambled was induced by doxycycline (1 μg/ml), and was monitored by FACS through GFP signal.

Figure 8. Workflow of KD production by lentiviral shRNA.

3.2 Molecular biology methods

RNA extraction and isolation of Polysomal mRNA

Sucrose gradient were obtained by stratifying in ultracentrifuge tube two low salt buffer solutions with different concentration of sucrose: 15% (w/v) sucrose stratified above 55% sucrose. Lysates were stratified on sucrose gradient by 2h ultracentrifugation at 36000 rpm. The Teledyne Isco Fractionator was used to perform isolation of polysomal fractions based on molecular weight as followed: small ribosomal subunit (40s), large ribosomal subunit (60s), ribosomes (80s), and mRNA associated with ribosomes (monosomes, disomes etc). Samples were precipitated in Isopropanol and lysed in TriZol (sigma).

RNA was extracted using chloroform, precipitated with 70% ethanol and finally was dissolved in DEPC-nuclease free water. For gene expression profiling we discarded the first 3 fractions, representative of ribosomes, and mixed together the other obtained fractions in order to analyse the actively translated mRNA.

Gene expression profiling (GEP)

Total mRNA and polysomal mRNA were hybridized to GeneChip[TM] Human Transcriptome Array (HTA) 2.0 (Thermo Fisher Scientific) to detect the levels of all known transcript isoforms produced by human genes. RNA samples were processed to obtain fragmented and labeled single-stranded cDNA as illustrated in figure 9. The cDNA fragments were hybridized on cartridge array using the GeneChip[TM] Hybridization Oven 645 set ON at 60 rpm and 45°C. The hybridized microarray were washed with Fluidics Station (protocol FS450_0001) and the scanning were performed with GeneChip[TM] Scanner 3000 System. The fluorescent signals relative to hybridized probes were obtained as DAT files and were converted into CEL digital signal by Affymetrix GeneChip Command Console (AGCC) software. Next, Expression Console (EC) through the algorithm signal space transformation Robust Multiple-array Average (sst-RMA) carried out normalization and quality control analysis of CEL files. Transcriptome Analysis Console (TAC, Thermo Fisher Scientific) was used to analyze differentially expressed genes comparing treated versus control, with a minimum of 1.5 fold change and $p \leq 0.05$. Finally, pathway enrichment analysis was performed by Gene Set Enrichment Analysis (GSEA) and EnrichR.
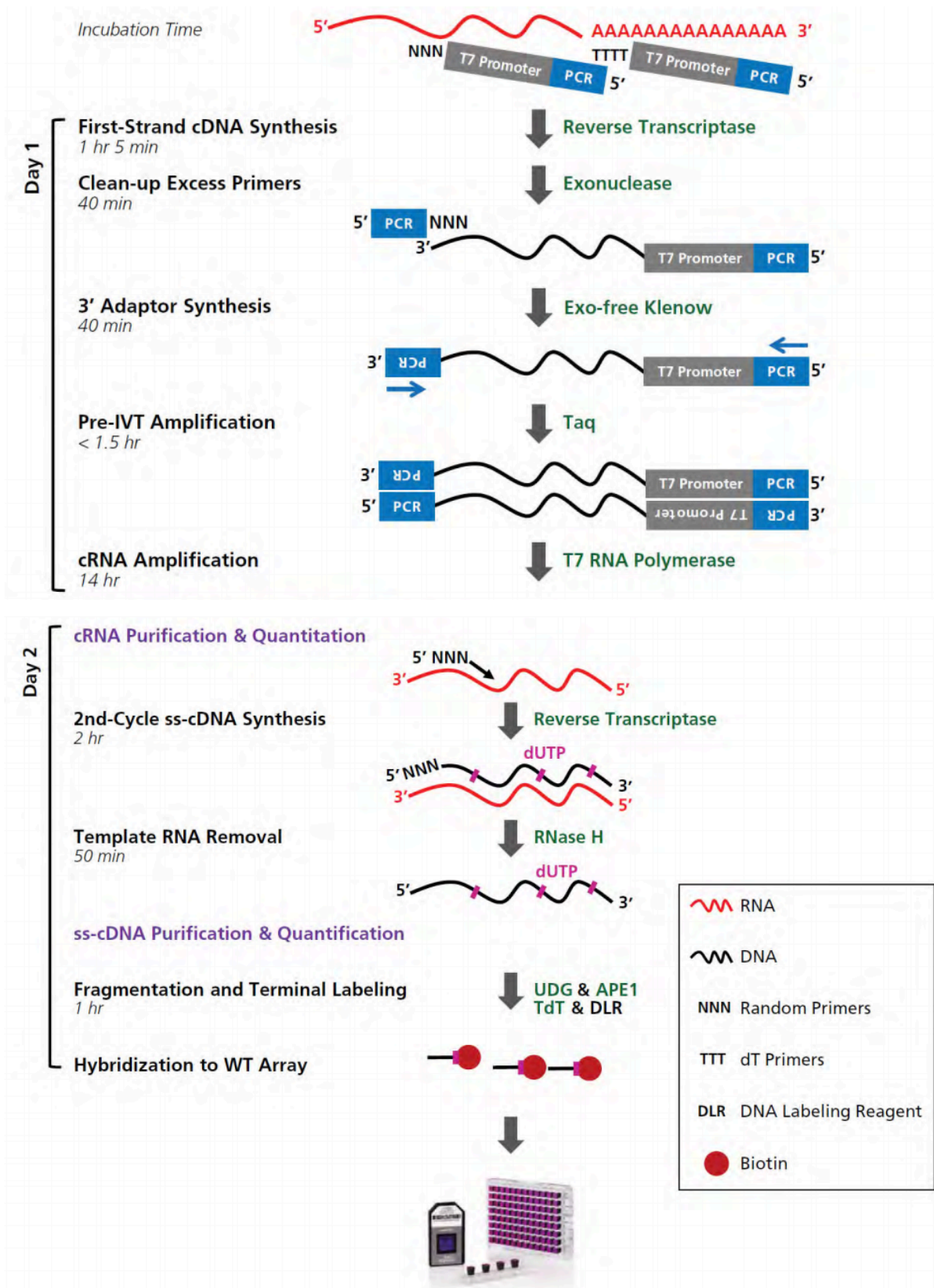
Figure 9. Workflow of GEP.

4. Results

4.1 BET inhibition is effective on AML cells under hyopoxic conditions and its activity is potentiated by Omaveloxolone

GSK1215101A kills leukemic cells under hypoxia

We performed *in vitro* experiments on AML cell lines, in order to evaluate the effect of bromodomain inhibitor GSK1215101A on cellular viability and proliferation under hypoxic conditions (1% O_2) to reproduce the effects observed in the hypoxic BM niche, where physiologically LSC resides. To this aim, we selected six AML cell lines representative of different genetic background: MOLM-13 and NOMO-1 are MLL-driven, OCI-AML3 carries *NPM1* and DNMT3A mutations, Kasumi-1 with translocation t(8;21), HL-60 shows c-MYC-amplification and KG-1 with complex karyotype and 7q deletion. First of all, we confirmed by western blot analysis that 24h of treatment with 250 nM of BET inhibitor is sufficient to reduce the protein levels of c-MYC in AML (Fig. 10). Additionally, we evaluated the effect of hypoxia on expression of the target, BRD4 and of its binding sites, namely acetylated histone residues in selected cell lines by western blot analysis of nuclear and cytoplasmic protein fractions (Fig. 11). BRD4 expression was not altered by culture under hypoxic conditions and the level of acetylated histone residues (H3K14 and H4K5-8-12-16) are not negatively affected. Furthermore, we confirmed that 20h of culture under hypoxic condition are sufficient to induce HIF1 stabilization and c-MYC down-regulation (in OCI-AML3).
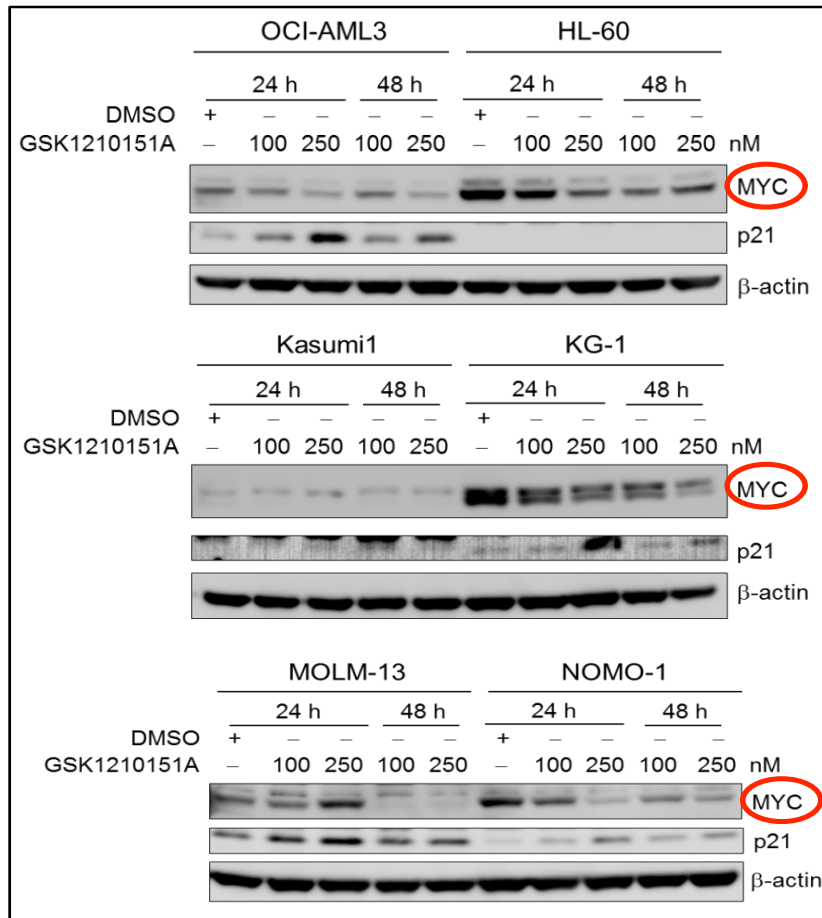
Figure 10. Western blot analyses of c-MYC expression after 24 and 48 h of treatment with BET inhibitor GSK1215101A on AML cell lines. β-actin was used for loading control.
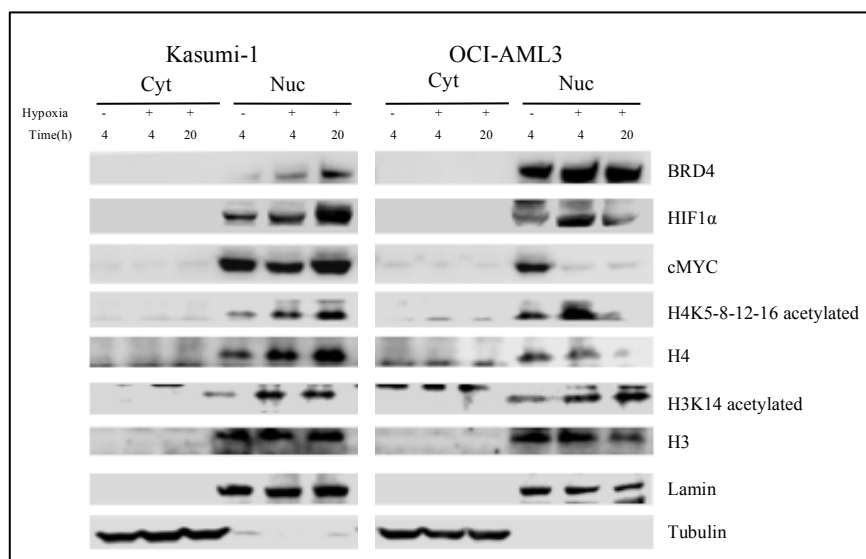
Figure 11. Western blot analyses of BRD4, HIF1α and acetylated histones expression in two representative AML cell lines after 4 and 20 h of culture under hypoxic conditions (Cyt: cytosol; Nuc: nucleus). Laminin and Tubulin were used for loading control of nuclear and cytosolic fractions, respectively.

To assess the effects of hypoxia on BRD4 inhibition, AML cell lines were treated with the bromodomain inhibitor GSK1215101A at two different concentrations, 250 and 500 μM, for 48h under normoxic and hypoxic conditions. GSK1215101A reduced cell viability in a dose-dependent manner in all the cell lines, except for HL-60 (Fig. 12A). We observed a reduction of viability of about 15%-35% at 250 μM and 25%-65% at 500 μM, with Kasumi-1 being the most sensitive model. We then assessed the induction of apoptosis after 48h of treatment with the high GSK1215101A dose (500 nM). A significant increase of AnnexinV$^+$ apoptotic cells was detected in all cell lines excepted for HL-60, with the higher levels in OCI-AML3 and Kasumi-1 cells, followed by NOMO-1, KG-1 and MOLM-13.

Since BRD4 inhibition was shown to induce cell cycle arrest in G_0/G_1 phase, we performed cell cycle analysis. OCI-AML3, Kasumi-1 and MOLM-13 showed a marked decrease in cell proliferation both, under normoxic and hypoxic conditions, with reduction of the percentage of cells in S phase and arrest into G_0/G_1 phase; whereas NOMO-1 and KG-1 showed G_0/G_1 arrest only in normoxia (Fig. 12B-C).
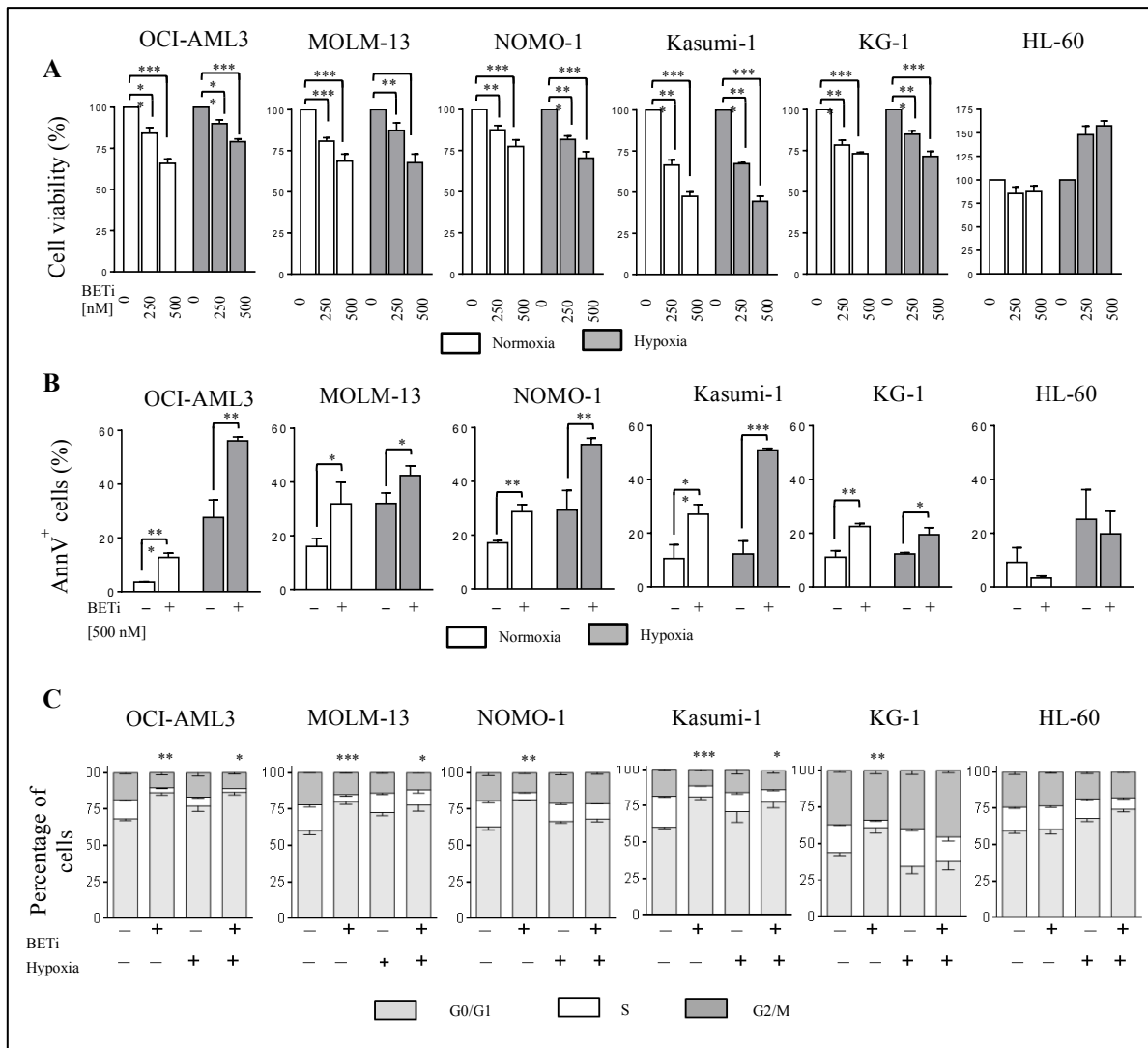
Figure 12. Analyses of the effect of GSK1215101A on AML cell lines after 48h of treatments under normoxic and hypoxic conditions. A) Cell viability mesured by RealTime-Glo. B) Percentage of apoptotic (Annexin V+) cells obtained after incubation with 500 nM of inhibitor. C) Cell cycle analysis after PI staining, P is relative to fraction of cells in G_0/G_1 phase (*$p<0.05$; **$p<0.01$; ***$p<0.001$).

BRD4 inhibition alters the translational profile of AML cell lines

To get further insights into the transcriptional role of BRD4, we performed GEP analysis on three AML cell lines, after 16h of treatment with BET inhibitor GSK1215101A, under normoxic and hypoxic conditions. We selected Kasumi-1 and OCI-AML3 as sensitive models and HL-60 as resistant cells. The timing of drug exposure was decided in order to evaluate the immediate changes in gene expression profiling and to avoid alterations related to apoptotic cells. Western blot analysis showed that GSK1215101A reduces cMYC protein levels after 20 hours of treatment under hypoxic conditions, mainly in the OCI-AML3 cell line (Fig. 13).

To better understand the transcriptional and translational effects of GSK1215101A, we performed GEP on both, total mRNA and polysomal mRNA isolated by polysome profilling. Figure 14 shows the graphic differences of polysomal profiling obtained after separation on sucrose gradient of treated cell lines. Kasumi-1 and OCI-AML3 showed a different translational profile, the latter being more active under steady state conditions. Hypoxia and BETi reduced the translational rate of both lines, as determined by a decrease of disome-polysome peaks height (Fig. 14). This result was associated with BETi-mediated downregulation of a ribosome pathway signature ($p<0.001$).

The two models shared a core translational program of 86 differentially expressed genes. Additional 881 and 168 genes were altered at translational level in Kasumi-1 and OCI-AML3 cells, respectively. Interestingly, GSK1215101A enforced hypoxia-induced c-MYC downregulation in all the cell lines and induced HIF-1α upregulation, specifically in drug-sensitive cells at translational level. Furthermore, we observed a reduced protein synthesis of the antiapoptitic gene BCL-2, and an increase of metabolic enzymes GLUT1 and LDHA (Fig. 15A).

On the contrary, when we compared the polysomal fraction with total mRNA of treated cell lines, we observed an opposite trend, which can reflect a compensatory machanism adopted by cells to bypass the drug effect on mRNA production. In particular, we observed a significant increase of c-MYC mRNA translation and a reduction of HIF-1α, GLUT1 and LDHA (Fig. 15B). Only Kasumi-1 showed a reduction of the oncogene c-KIT synthesis.

**BRD4 inhibition induces the up-regulation of genes involved in NRF2 pathway**

Depite the increased polysomal mRNA/total mRNA ratio in treated cells, GSEA of GEP data, confirmed that inhibition of BRD4 under hypoxic condition was associated with a significant down-regulation of a c-MYC signature at translational levels in both lines (Fig. 16A). By looking at the differentially expressed genes, we observed that GSK1215101A induces an activation of NRF2 pathway through the up-regulation of the regulator *ARNT* (p=0.02) in both cell lines, which activate the transcription of *NRF2*, and in parallel through the reduction of *NRF2* repressor, *KEAP1* at mRNA and protein levels, specifically at 1% O_2 (*p*=0.01) in Kasumi-1 cell line. Moreover, the activation of NRF2 pathway is also confirmed by the significant increased expression of several NRF2 targets including *CAT*, *EPHX1*, *FTH1*, *GSTM1*, *MGST1*, *PRDX1* (*p*<0.05) under normoxia and/or hypoxia (Fig. 16 B). NRF2 is a transcription factor involved in response mechanism to xenobiotic and oxidative stress[201], and it was recently associated with AML, hwever its role still remain controversial.
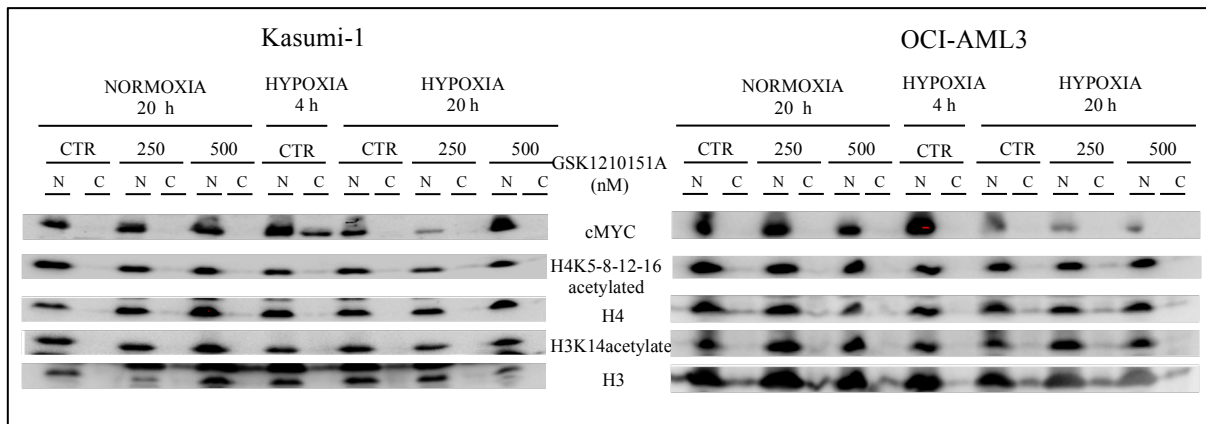
Figure 13. Western blot of two representative cell lines, Kasumi-1 and OCI-AML3, after 20h of treatment with GSK1215101A under normoxic and hypoxic conditions (CTR: control with DMSO; C: cytosol; N: nucleus).
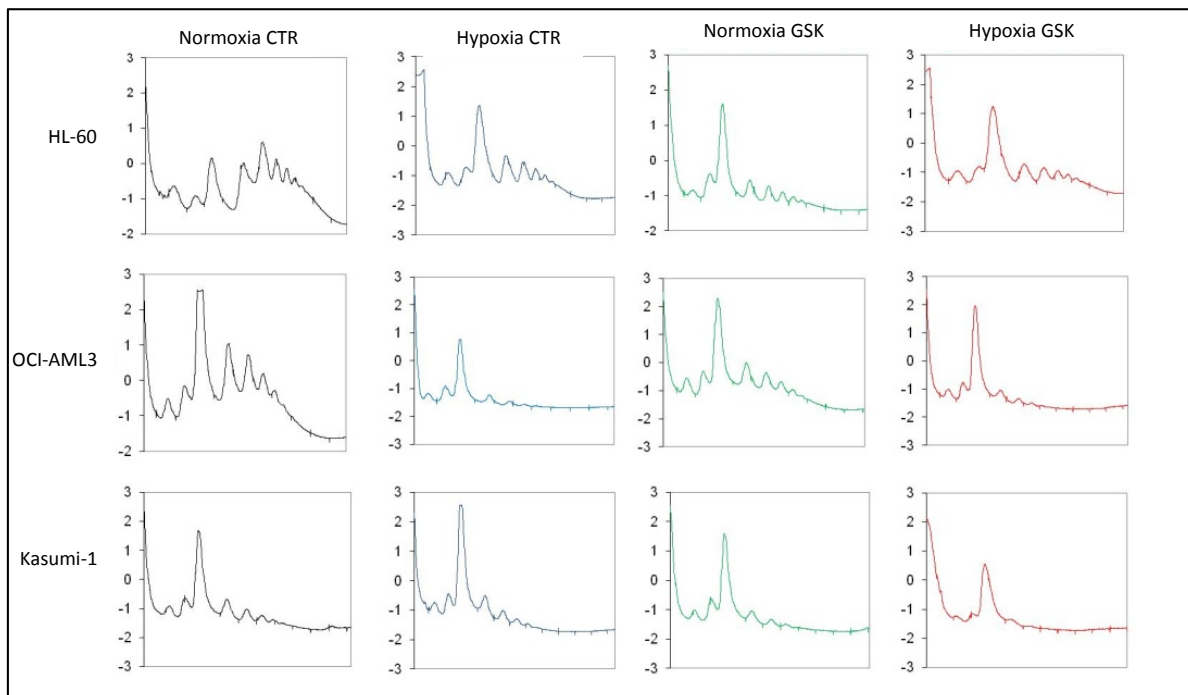
Figure 14. Polysomal profiling of AML cell lines treated with 250μM of GSK1215101A for 4+16h The first three peaks are relative to ribosomes subunits, 40s, 60s and 80s respectively. The others are relative to mRNAs actively translated, that are associated with ribosomes. (CTR: control; GSK: iBET)
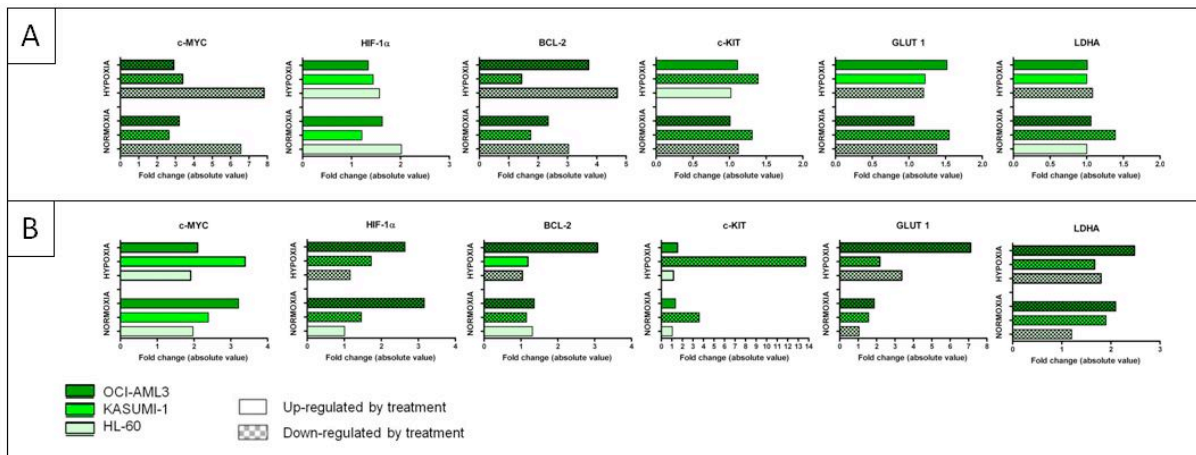
Figure 15. GEP analysis after 4+16 h of treatment with 250μM of GSK1215101A under normoxic and hypoxic conditions. A) Analysis of actively translated mRNAs isolated from disomal-polysomal fractions of treated *versus* control cell lines. Fold change is the ratio between disomal-polysomal RNA of treated cell lines compared with control ones. B) Analysis of actively translated mRNAs isolated from disomal-polysomal fraction and normalized to total mRNA of treated cell lines. Fold change is the ratio between di-polysomal mRNA and total mRNA of treated cell lines.
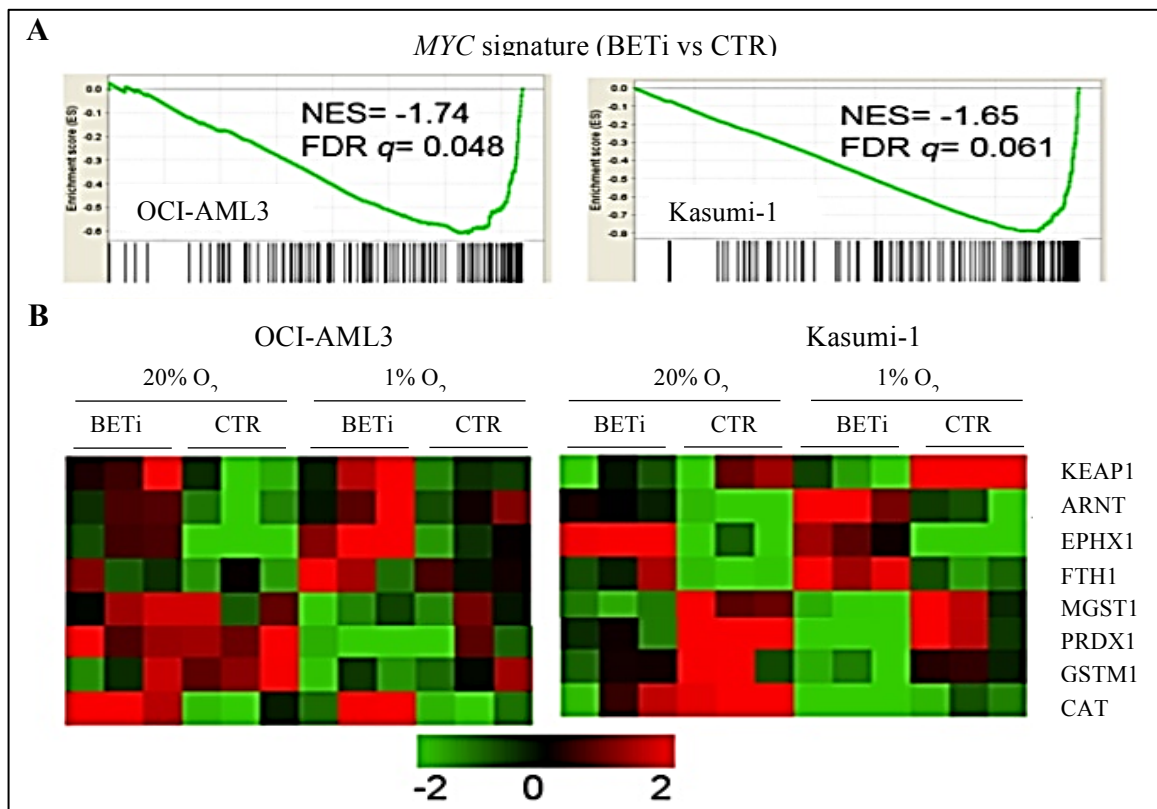

Figure 16. Analysis of GEP data obtained after 4+16 h of treatment with 250 μM of GSK1215101A under normoxic and hypoxic conditions. A) GSEA of down-regulation of a *MYC* signature under hypoxia. B) Deregulation of NRF2-related genes at translational level under hypoxia and normoxia (CTR: control).

BRD4 inhibition and hypoxia induce metabolic alterations in a cell line-specific manner

Since numerous studies have described the role of HIF-1α and c-MYC in regulation of cancer cell metabolism, we analyzed the effect of BET inhibitor on AML metabolism. To this aim, we analyzed the metabolic changes induced by GSK1215101A by Ultrahigh Performance Liquid Chromatography-Tandem Mass Spectroscopy under the same conditions used for GEP studies. Changes in metabolite levels are consistent with alterations in energy metabolism and cell component biosynthesis, with marked differences between the OCI-AML3 and Kasumi-1 models (Fig. 17). In particular, in normoxic condition treatment induced marked metabolic change in Kasumi-1 cell line with an increase of metabolites involved in amino acid (fold change≥1.5) peptide (fold change>1.5), and pyrimidine metabolism (fold change>1.3) ($p \leq 0.05$), together with a general increase of lipids (fold change>1.3 $p \leq 0.05$), and a moderated reduction of intermediates of TCA cycle, such as citrate, α-ketoglutarate, succinate, fumarate (fold change>0.5, $p \leq 0.05$). In OCI-AML3, GSK1215101A induced just an increase of metabolite involved in fatty acids chain (fold change>2), and a tiny reduction of those related to phospholipids metabolism (fold change>0.5) ($p \leq 0.05$). Interestingly, when the two cell lines were cultured under hypoxic condition we observed a completely different metabolic profiling after GSK1215101A treatment, with OCI-AM3 being the mostly altered cell line. Kasumi-1 cell line showed a general reduction in metabolites drugged in amino acid and lipide metabolism (fold change>0.5, $p \leq 0.05$). Moreover reduced lactate levels upon treatment, which may be due to a drug-dependent decrease in lactate dehydrogenase activity and decreased asparagine levels, along with down-regulation of a gene signature of alanine, aspartate and glutamate metabolism ($p < 0.001$), including asparagine synthetase (1.5-fold change, $p < 0.01$). On the contrary, OCI-AML3 showed an extended increase of

metabolites involved in amino acid (fold change>1.5), lipid (fold change>1.2) and nucleotide (fold change>1.4) metabolism ($p \leq 0.05$). In particular, OCI-AML3 showed a significant increase of both the reduced (3.9-fold) and oxidized (2.6-fold) forms of glutathione, which plays an important role in antioxidant defense, redox-homeostasis and protein folding (Fig.17). Consistently, the translational profile of OCI-AML3 cells showed enrichment of deregulated genes involved in superoxide metabolic process and response to oxidative stress, included NCF1/2, ADNP2, XBP1, HSPA1A/B.
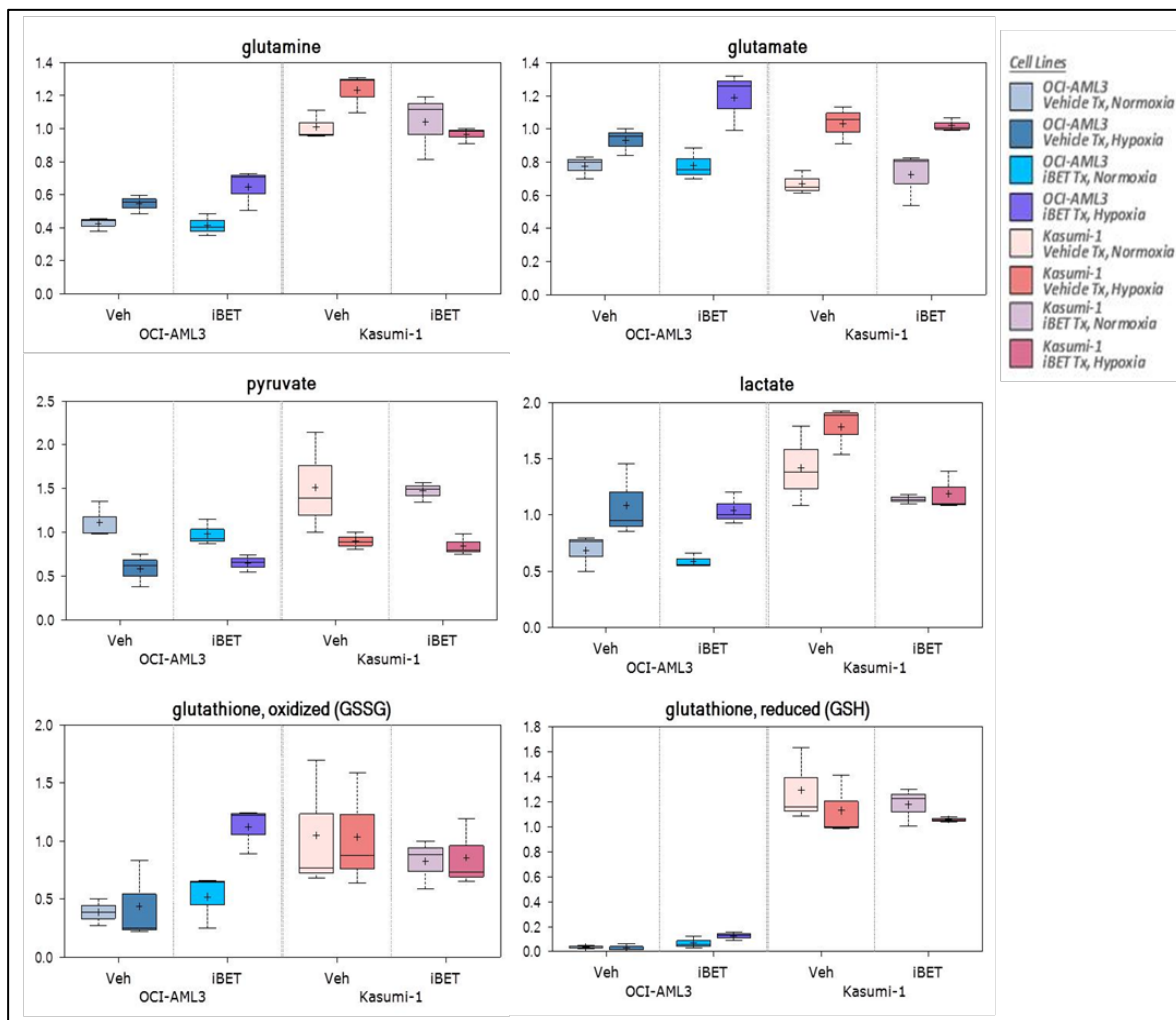

Figure 17. Levels of cellular metabolites after 4+16 h of treatment with 250μM of GSK1215101A under normoxic and hypoxic conditions. (Veh: vehicle, DMSO).

58

Omaveloxolone potentiates the anti-leukemic activity of BET inhibition against AML cells

As described in the previous section, the treatment with BET inhibitor induces an up regulation of NRF2 pathway, which play a role in the antioxidant response. Moreover the metabolic analysis performed after treatment confirmed that GSK1215101A induces alteration of glutathione metabolism in OCI-AML3, which is positively regulated by NRF2 in condition inducing oxidative stress. Therefore we wondered whether the antioxidant gene expression mediated by NRF2 was a defense response adopted by cells under BETi pressure. However, pharmacological inhibition of NRF2 or glutathione biosynthesis failed to potentiate the anti-leukemic effects of GSK1215101A and to induce oxidative stress (data not shown). Conversely, activation of the NRF2 pathway is required for myeloid cell differentiation, a feature associated with BET inhibition[43].

Therefore, we decided to test the combination of GSK1215101A and omaveloxolone (RTA-408), a drug used in phase 1 clinical trials in advanced solid tumors (NCT02029729), which combines NRF2 activation and NF-κB inhibition and has never been tested before in AML models. As shown in figure 18, treatment of AML cell lines with RTA-408 as single agent showed a dose-dependent decrease of cell viability, with the following IC50 values: 269.1 nM in KG-1, 271.7 nM in MOLM-13, 311.5 nM in NOMO-1, 492.6 nM in Kasumi-1 and 579.8 nM in OCI-AML3 (Fig. 18A).

When combined with GSK1215101A, RTA-408 treatment induced a significant decrease of cell viability in all tested cell lines in normoxia and hypoxia, compared with single agent effects (Fig. 18B). In agreement with survival results, the combination treatment resulted also in a significant increase of AnnexinV$^+$ apoptotic cells (Fig. 18C).
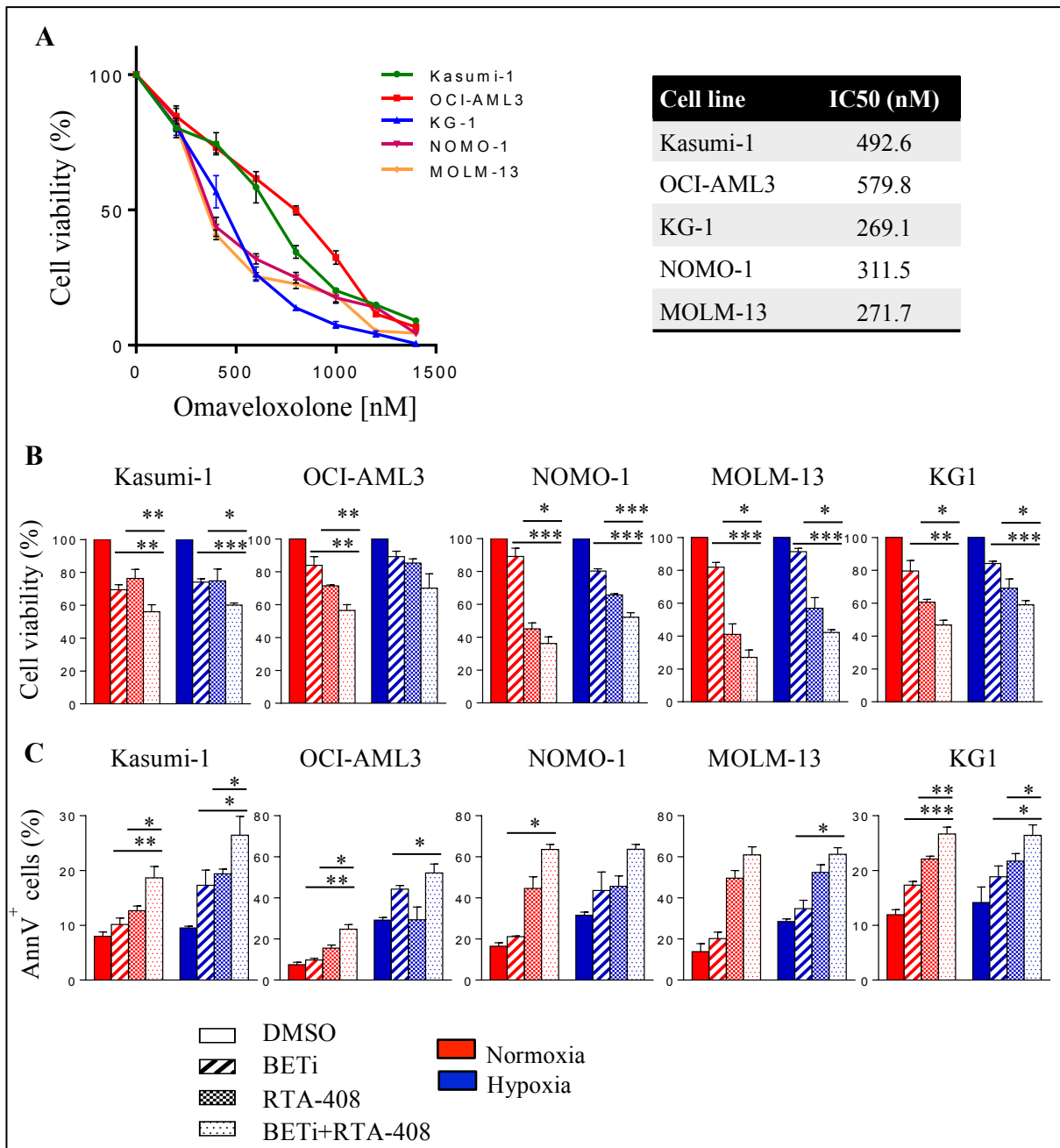
Figure 18. Combination of GSK1215101A and omaveloxolone treatment in AML cell lines. A) Cell viability mesured by RealTime-Glo after 48h of treatment with increasing doses of omaveloxolone (from 0 to 1500 nM). B) Cell viability mesured by RealTime-Glo after 48h of treatment with GSK1215101A (250 nM) and omaveloxolone (500 nM) as single agents and in combination. C) Percentage of apoptotic (Annexin V+) cells after 48h of treatment with GSK1215101A (250 nM) and omaveloxolone (500 nM) as single agents and in combination. Significativity was referred to percentage of apoptotic cells of combination treatment *versus* GSK1215101A. $*p<0.05$; $**p<0.01$; $***p<0.001$.

The combination of Omaveloxolone and GSK1215101A impairs the clonogenic capacity of CD34+ AML cells under normoxia and hypoxia

To investigate whether combinatorial BET inhibitor and NRF2 activator could impair colony-forming ability more that those of individual compound, CD34+ leukemia stem progenitor cells (LSPCs), isolated from BM of AML patients at diagnosis, were treated with increasing doses of both drugs (0.5 and 1 μM for GSK1215101A; 0.6 and 1.2 μM for Omaveloxolone), as single agent and in combination. The analysis performed after 48 h of treatment showed that combination treatment reduces the growth of CD34+ primary cells in a significant way, with a reduction of cellular viability ranging from 30% to 60%, both under hypoxia and normoxia ($p \leq 0.05$) (Fig. 19A). The absence of toxic effects in normal primary peripheral blood mononuclear cells (PBMCs) confirmed the LSC target-specificity of combination treatment (Fig. 19B). Moreover, colony-forming assay revealed that in LSPCs, high dose of GSK1215101A and both doses of Omaveloxolone alone induced a reduction in cell clonogenicity capacity of about 50% in normoxia, and 30% in hypoxia. Furthermore when we combined the two drugs the clonogenic potential of normoxic and hypoxic LPSPCs was reduced in a dose-dependent manner reaching a complete inhibition of colony formation at higher doses (Fig. 20).
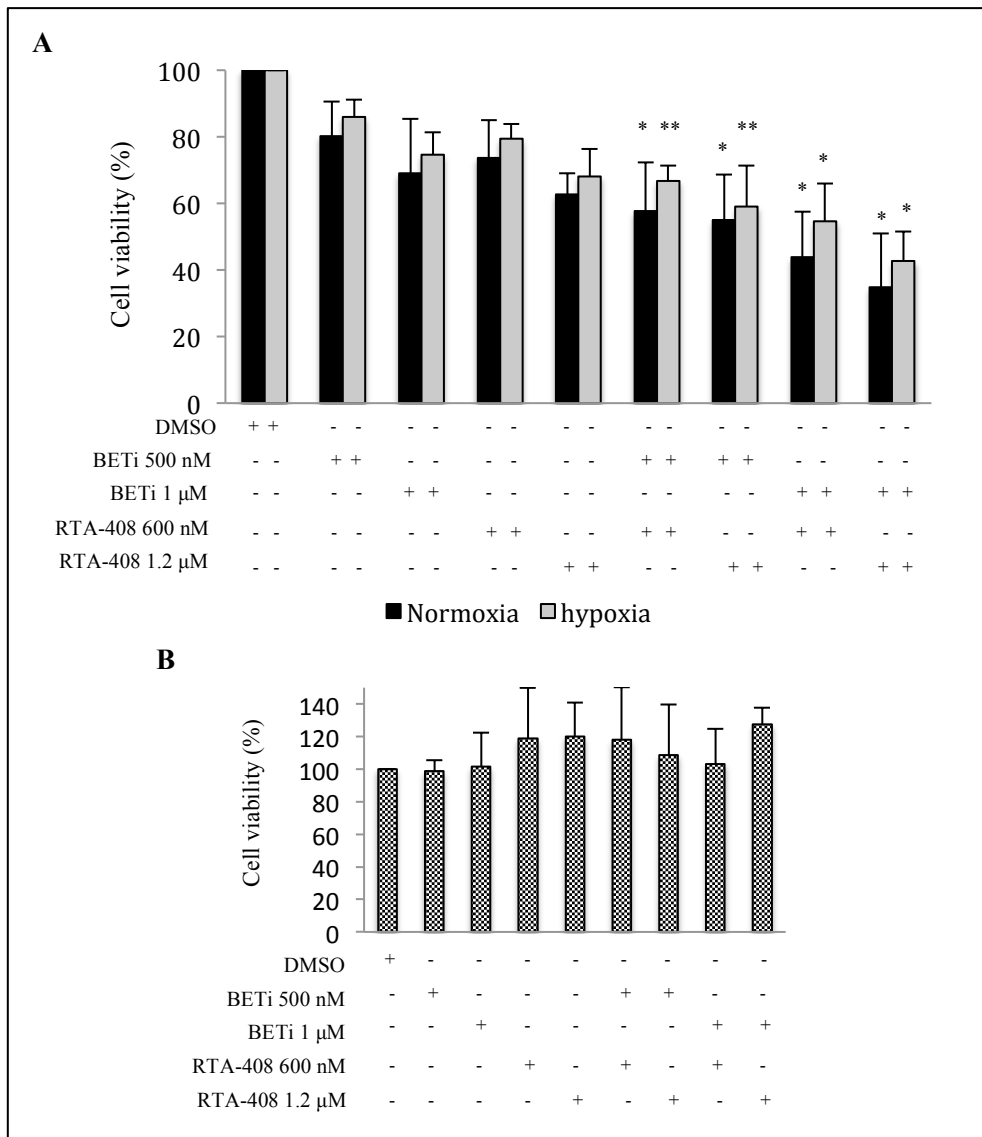
Figure 19. Cell viability of primary BM cells. A) Viability of primary LSPCs treated for 48h with two doses of GSK1215101A (0.5 and 1 μM) and Omaveloxolone (0.6 and 1.2 μM), as single agent and in combination. Experiment was performed under normoxia and hypoxia. *P* was relative to percentage of viable cells in combination treatment *versus* GSK1215101A. B) Cell viability on normal PBMCs treated with the same concentration of two drugs in normoxia. DMSO was used as negative control. *$p<0.05$; **$p<0.01$; ***$p<0.001$.
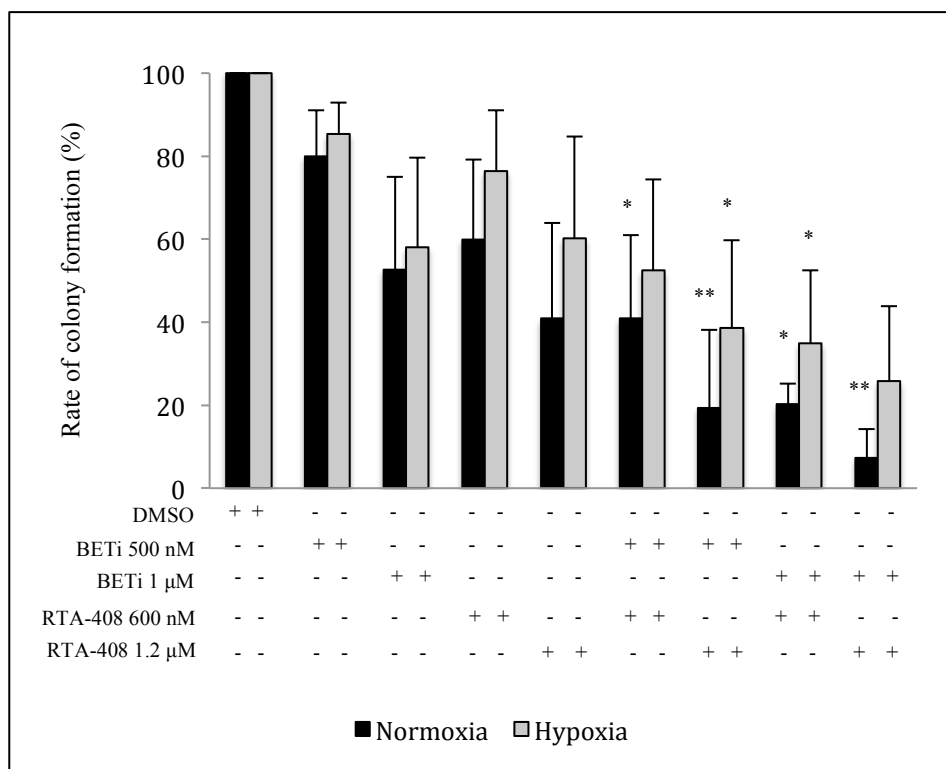
**Figure 20.** Colony-forming assays performed on primary LSPCs treated for 10 days with GSK1215101A (0.5 and 1 μM) and Omaveloxolone (0.6 and 1.2 μM), as single agent and in combination. Experiment was performed under normoxia and hypoxia. *P* was relative to rate of colony formation in combination treatment *versus* GSK1215101A. DMSO was used as negative control. *$p < 0.05$; **$p < 0.01$; ***$p < 0.001$.

The combination of Omaveloxolone and GSK1215101A altered expression of many cell cycle genes and correlated with enrichment of cell differentiation pathway.

To understand the biological processes altered by the drug combination in AML, we performed gene expression profile analysis of OCI-AML3 and Kasumi-1 cells after 24h of treatment with Omaveloxolone and GSK1215101A as single agent and in combination, both under normoxic and hypoxic conditions. In Kasumi-1 cells, 1900 and 1505 genes were deregulated after combined treatment in normoxia and hypoxia, respectively. Of them, 1176 and 737 genes were specifically altered by the drug combination, while they did not show a significant difference in single agent treatments. The treatment also affected OCI-AML3 cells, with 471 and 487 genes differentially expressed between combined drug administration compared with vehicle in normoxia and hypoxia, respectively. In particular, 241 and 193 genes were specifically altered by the drug combination. In line with the cell cycle analysis, the transcripts specifically altered by the drug combinations under both conditions were enriched for genes involved in cell cycle, DNA replication, G1/S transition, G2/M checkpoints pathways. Several genes involved in cell cycle progression and G1/S transition were down-regulated in the selected models, including ANAPC1, MCM6 in OCI-AML3, CHEK1, MCM genes, CCND2 in Kasumi-1 cells. Moreover, MYC down-regulation was enforced by the drug combination in Kasumi-1 cells and OCI-AML3, under normoxia showed activation of markers of apoptosis as CASP6 and CASP8. Of note, GSEA analysis revealed a specific enrichment of signatures related to autophagy, cell-fate determination and cell maturation/differentiation, together with enrichment of negative regulation of WNT e/o Smoothened signaling in cells treated with Omaveloxolone and GSK1215101A under normoxia and hypoxia (Fig. 21). Moreover, the combination induced an hypoxia-specific enrichment of oxidative

stress response pathway in OCI-AML3 and the positive regulation of energy homeostasis in Kasumi-1. These signatures were not enriched in single agent treatments, suggesting that the combination is able to hamper the stem cell capacity of leukemic cells, in line with the decreased colony forming ability observed in vitro in primary cells.
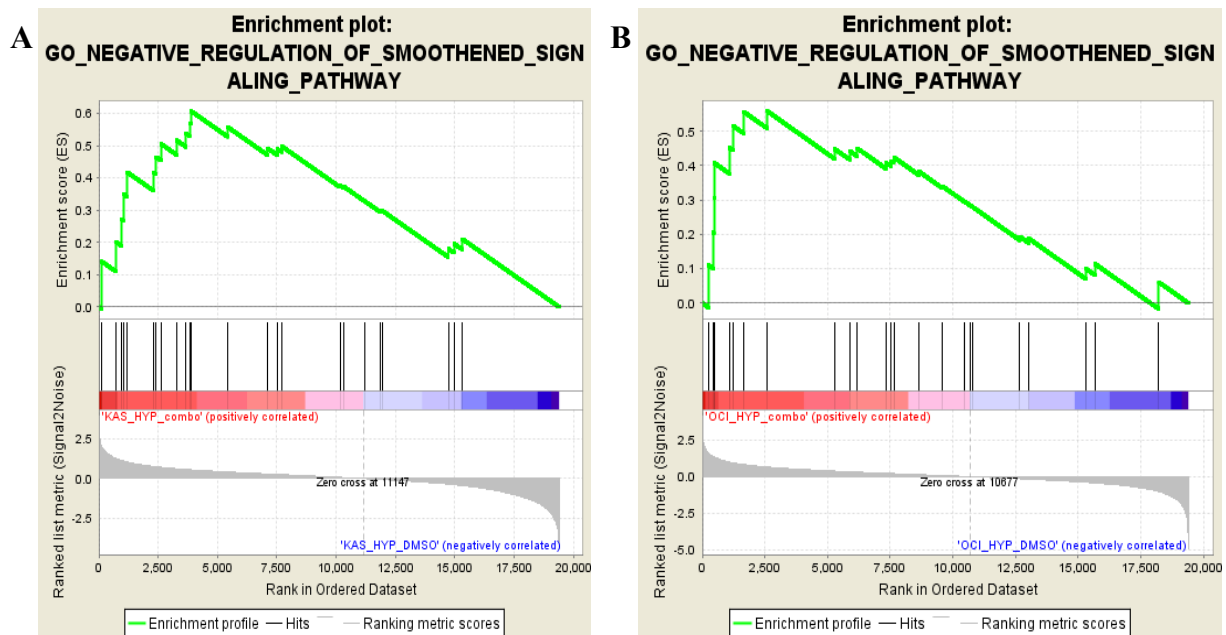

Figure 21. Representative enplots from GSEA of Kasumi-1 (A, normalized enrichment score, NES=1.85, *p*=0.003) and OCI-AML3 (B, NES=1.72, *p*= 0.007) cells treated with the drug combination under hypoxia.

4.2 CDC20 is a novel potential therapeutic target in AML

Pharmacological inhibition of the APC/C^{CDC20} with Apcin or proTAME results in a metaphase arrest and reduced viability of AML cells

To assess if APC/C^{CDC20} could be a potential therapeutic target in AML, we used two different small molecule inhibitor, Apcin and proTAME. AML cell lines exposed to increasing doses of Apcin (from 1 up to 1000 μM) and proTAME (from 1.8 up to 32 μM) (Fig 22) showed IC50 values in the range of microM at 24, 48 and 72h of treatment. We observed mild differences in sensitivity among the tested cell lines, with KG-1 cells resulting the most sensitive one to both drug (IC50 37.6 μM for Apcin and 5.16 μM for proTAME after 48h of treatment), followed by NOMO-1, Kasumi-1, and MOLM-13 (IC50 102.3-116.5-117.1 μM for Apcin and 7.46-10.6-8.7 μM for proTAME, respectively). MV-4-11, HT-93, HL-60, OCI-AML-3 and ME-1 were more resistant to treatments sowing higher IC50 values (IC50 > 180 μM for Apcin and > 10 μM for proTAME) (Tab 6). Based on these data, we selected two different doses of Apcin (50-100 μM) and proTAME (5-10 μM) in order to evaluate the effect of CDC20 inhibition on cellular viability. After 48h of drug exposure we observed a dose-dependent increase of AnnexinV^{+} apoptotic cells in KG-1, NOMO-1 and MV-4-11 cell lines, with KG-1 being the most sensitive model (Fig. 23A). Since APC/C^{CDC20} is involved in metaphase-to-anaphase transition during mitosis, we investigated whether CDC20 inhibition could lead a cell cycle arrest. PI staining showed that in KG-1 cells both drugs are able to induce a significant increase of percentage of cells in G2/M phase. Moreover, the same effect was observed in HT-93A cell lines exposed at highest concentration of Apcin (Fig. 23B). These results suggest that both cytotoxicity and cell cycle perturbation cooperate to Apcin-dependent sensitivity.
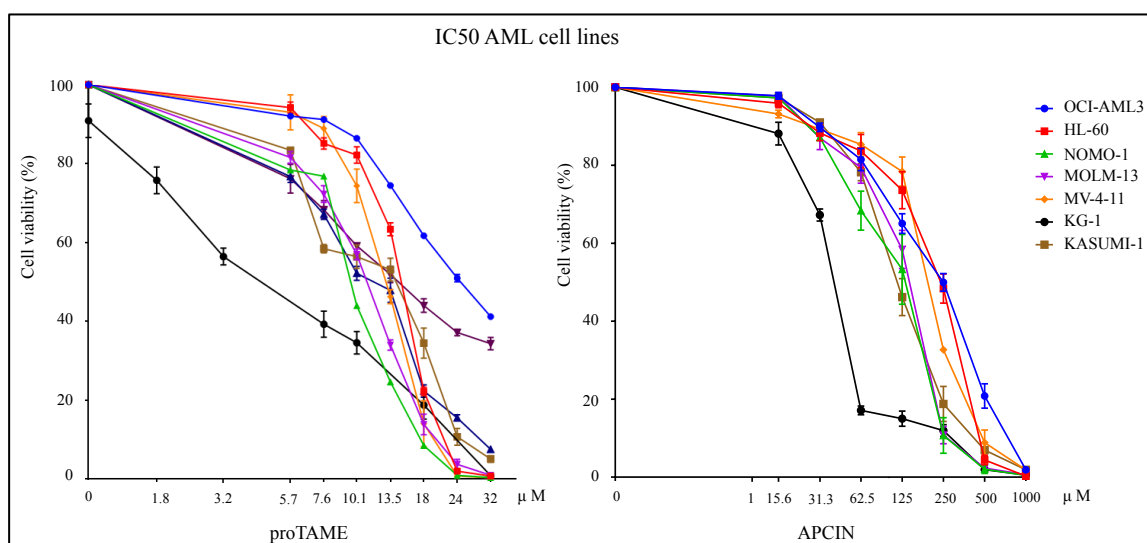
Figure 22. Dose-response curves of AML cell lines viability. Data were obtained after 48 h of treatment with increasing doses of APCIN (from 0 to 100 μM) and proTAME (from 0 to 32 μM) as single agents.

AML cell lines	Apcin (μM)			proTAME (μM)		
	24h	48h	72h	24h	48h	72h
OCI-AM3	334.1	201.9	141	67.63	33.19	22.03
HL60	226.4	189	112.7	12.46	13.75	10.25
NOMO-1	174.5	102.3	60.45	8.39	7.46	4.79
MOLM-13	230.3	117.1	85.77	15.74	8.73	7.11
MV-4-11	281.1	180.1	117.8	9.07	11.66	8.73
KG-1	154.4	37.63	23.4	12.55	5.16	6.55
KASUMI-1	213.6	116.5	104.8	15.54	10.58	9.76
HT-93	181.2	181.2	71.2	11.55	9.84	8.21
ME-1	203.6	203.6	75.92	18.31	15.43	20.65

Table 6. IC50 values of AML cell lines. The results were obtained from cell viability measurements performed by RealTime-Glo after 24, 48, and 72h of treatment with increasing doses of APCIN (from 0 to 100 μM) and proTAME (from 0 to 32 μM) as single agent.
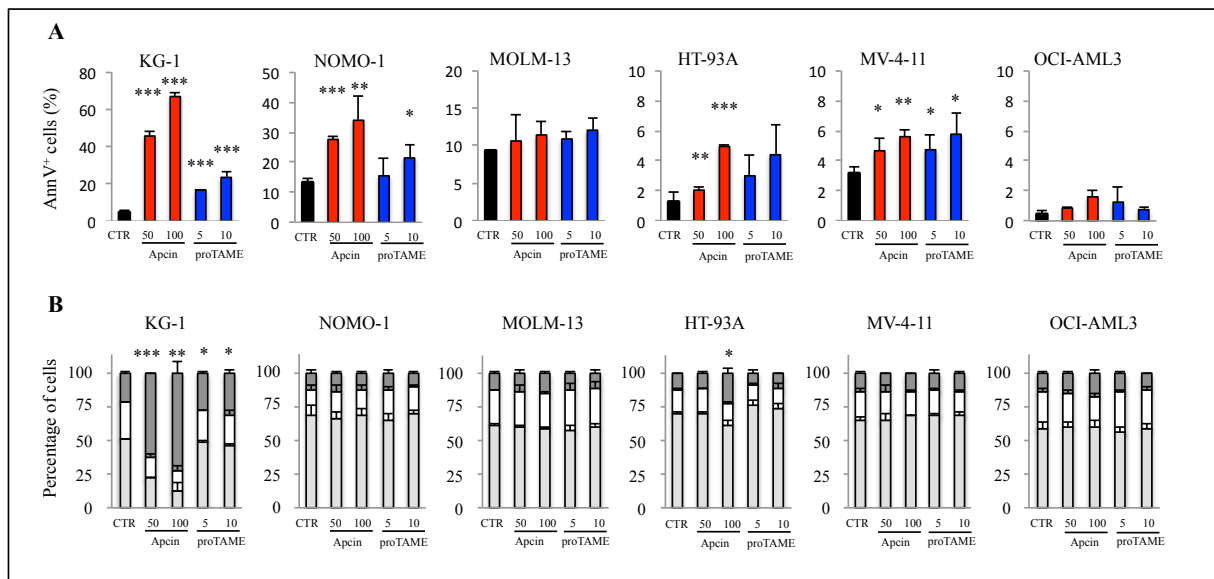
Figure 23. Consequences of Apcin and proTAME treatment in AML cell lines. Cells were analyzed after 48h of treatments with Apcin (50 and 100 µM) or proTAME (5 and 10 µM). A) Percentage of apoptotic (Annexin V+) cells. B) Cell cycle analysis using PI staining, P is relative to cells in G_2/M phase. $*p<0.05$; $**p<0.01$; $***p<0.001$.

CDC20 inhibition induces the stabilization of Cyclin B1 and Securin in AML cell lines

In order to confirm the alteration associated with CDC20 inhibition described in other tumor models we performed western blot analysis on three AML cell lines, MV-4-11, KG-1 and NOMO-1. Figure 24 show that both molecules induced a little down-regulation of CDC20 protein levels, associated with higher levels of Cyclin B1 in KG-1 and NOMO-1, and Securin in MV-4-11. Interestingly we observed also that in KG-1 and NOMO-1 cell lines CDH1 levels were reduced not only after proTAME treatment, as expected by its ability to block the interaction of APC/C with both activators CDC20 and CDH1, but either after incubation with Apcin.

CDC20 protein expression is related to cell cycle phases in AML cell lines, but is expressed across all stages of differentiation in primary cells

To better clarify the role of APC/C^{CDC20} during cell cycle, we synchronized KG-1, NOMO-1 and MV-4-11 cell lines in G_0/G_1, S and G_2/M phases using respectively serum starvation (72h), double thymidine block (3 mM) and inhibition of microtubules formation (thymidine 1 mM followed by nocodazole 50 ng/mL). Cell cycle analysis confirmed the achievement of cell synchronization across all condition (Fig. 25 A). As expected, we detected the highest amount of CDC20 protein in cells synchronized in the G_2/M phase. Low amounts of CDC20 protein were observed also in the other phases of cell cycle (Fig. 25B). The presence of CDC20 in all the phases of cell cycle supports the evidence that this protein could play several biological function in addition to those related with metaphase-to-anaphase transition during mitosis.

The results obtained in AML cell lines did not reproduce our previous observations from AML patients. Indeed, we observed increased levels of CDC20 expression in aneuploid AML, which show a reduced percentage of proliferating (Ki-67+) cells. We therefore analyzed CDC20 expression in a panel of primary AML samples (Fig. 26). First, we confirmed that CDC20 expression is higher in BM blasts compared with normal BM cells. Intracellular flow cytometric analysis of AML blast markers (CD34, CD38) in combination with CDC20 and Ki-67 in 23 samples revealed the highest CDC20 expression in the CD34+CD38+ population and the lowest expression in CD34-CD38+ cells. In addition, CDC20 levels across AML subpopulations do not correlate with the levels of Ki67+ (median % of Ki-67+/high cells: CD34+CD38+: 30.4%, CD34-CD38+: 35.9%).
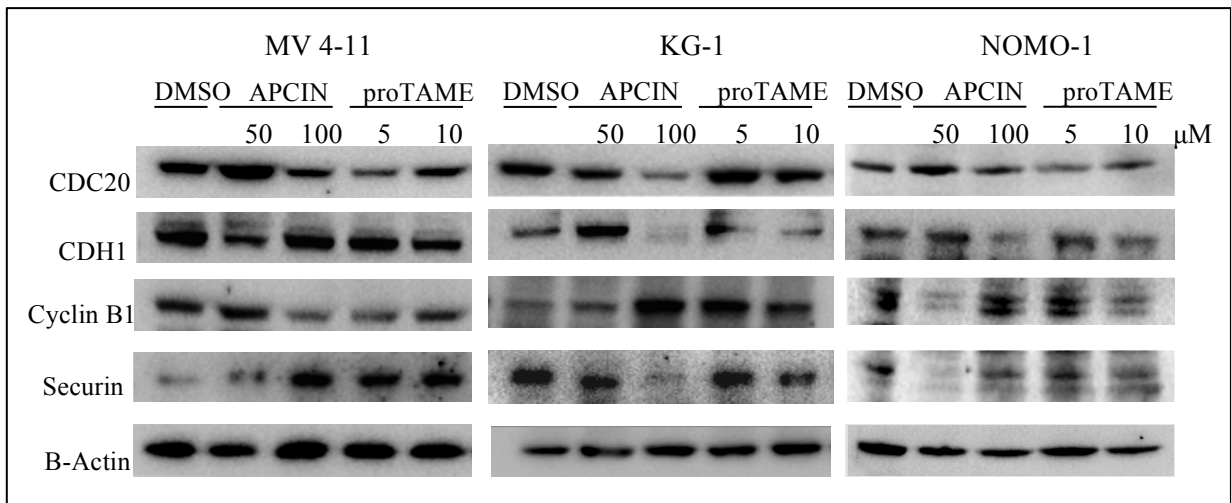
Figure 24. Western Blot analysis of AML cells lines. Protein levels of CDC20, its target Cyclin B1 and Securin, and CDH1 were analyzed after 48 h of treatment with two different doses of Apcin and proTAME. B-Actin was used for loading control.
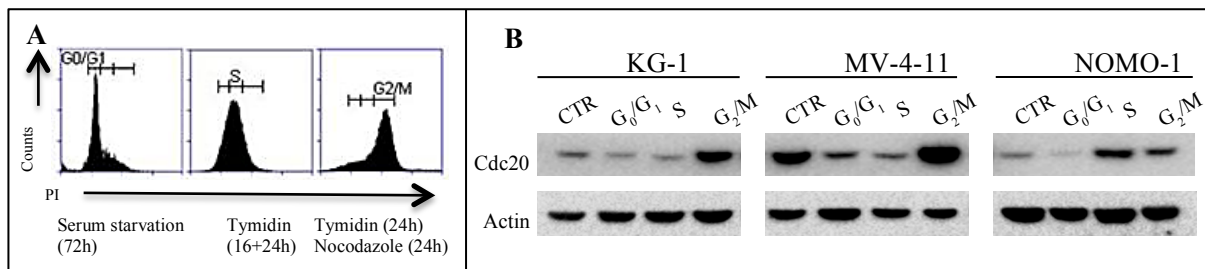
Figure 25. Analysis of synchronized cell lines. A) Cell cycle results obtained after PI staining. B) Western blot of KG-1 and MV-4-11 cell lines synchronized in the three phases of cell cycle (CTR: control). β-actin was used for loading control.
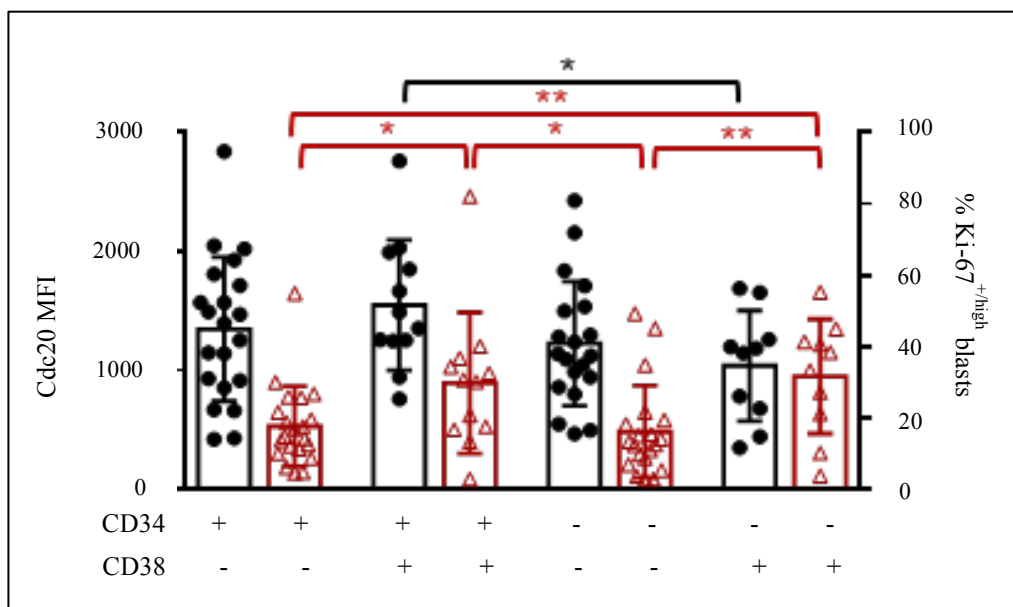
Figure 26. Immunophenotypic analysis of primary BM cells from AML patients at diagnosis. Cells were stained with anti-CD34, anti-CD38, anti-CDC20 (black symbols and bars) and anti-Ki-67 (red symbol and bars). MFI: mean fluorescence intensity.

Apcin treatment kills AML primary cells and inhibits their clonogenic potential

To understand whether LSPCs are sensitive to Apcin treatment, we treated CD34+ AML BM cells with increasing Apcin doses (50, 100, and 250 µM). The analysis performed after 48 h of treatment showed that Apcin reduces the growth of CD34+ primary cells in a significant way, with a reduction of cellular viability around 40% at of 50 and 100 µM (*p*= 0.0018 and 0.019, respectively) and 60% at the higher dose (p=0.00014) (Fig. 27 A-B).

To study the role of CDC20 in the maintenance of the clonogenic potential of AML cells, we performed colony-forming assays with LSPCs. Treatment with 10 and 50 µM of Apcin showed that inhibition of APC/C^{CDC20} induces a marked decrease of clonogenicity potential of primary cells, reaching a complete inhibition of colony formation at higher doses of Apcin (Fig. 27C).
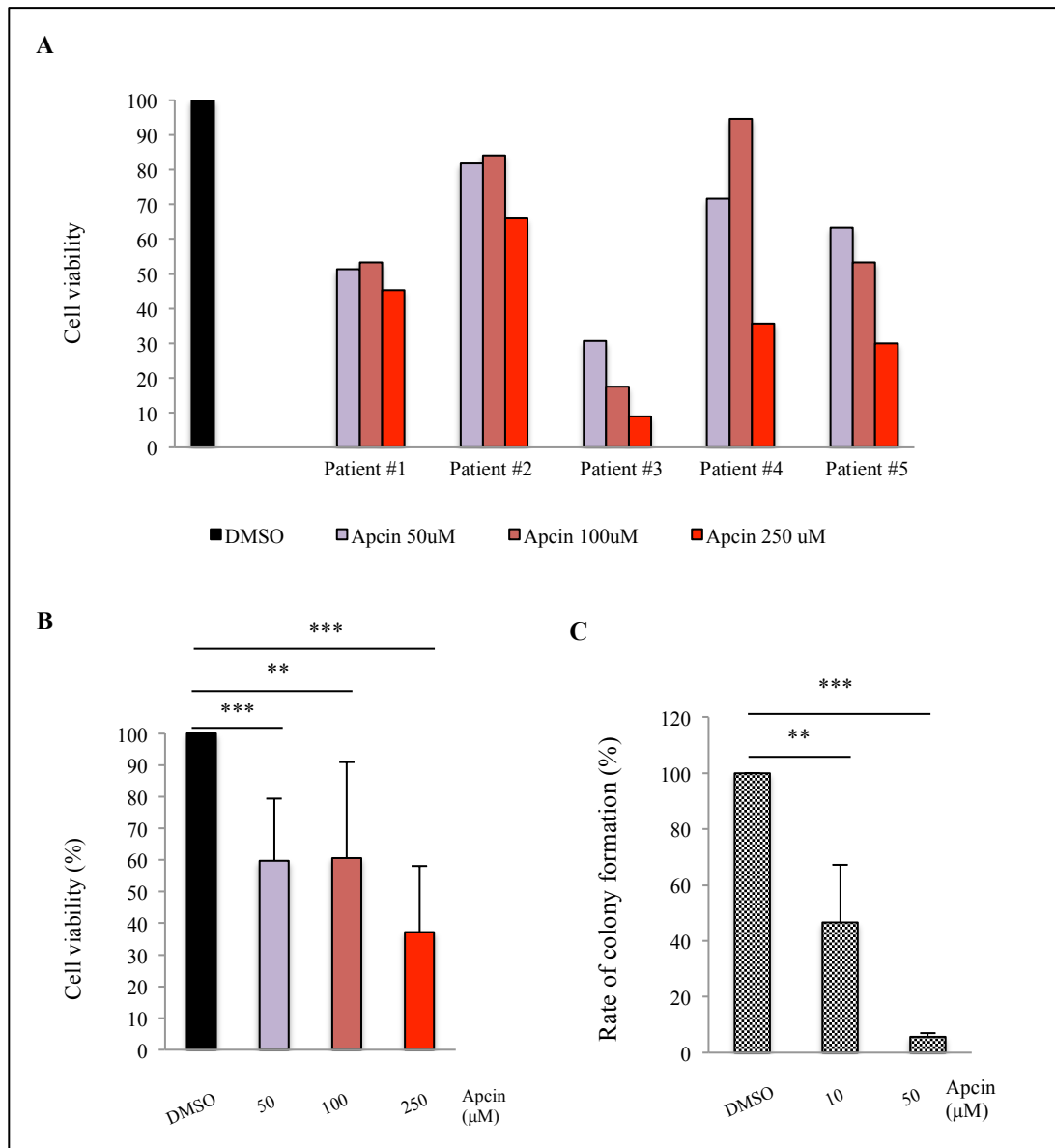
Figure 27. Effects of Apcin treatment on primary LSPCs. A) Cell viability mesurament obtained from blasts cells isolated from five AML patients after 48h of treatment with increased doses of Apcin (50, 100 and 250 µM). B) Mean value of cell viabilty. C) Colony-forming assays obtained from three AML patients treated for 10 days with Apcin (10 and 50 µM). DMSO was used as negative control. *$p<0.05$; **$p<0.01$; ***$p<0.001$.

Cdc20 knockdown results in a decreased proliferation and induced apoptosis in MV-4-11

Apcin binds to the WD40 domain of CDC20, thus inhibiting the APC/C-related activities, however WD40 domain-independent functions may be preserved. To understand whether CDC20 plays WD40 domain-independent activities relevant to AML cell, we knocked-down CDC20 in AML models.

Before starting experiments on AML cell lines we selected the CDC20-shRNA that silenced the expression of target gene with major efficacy. FACS analysis performed on 293T transformed cells showed that, although RFP signal was similar between the three CDC20-shRNA tested (Fig. 28A) the highest knock down (KD) efficiency on protein levels was obtained with CDC20-sh#1 (Fig. 28 B). Then, MV-4-11 and NOMO-1 cells were infected with lentivirus carrying the scrambled or CDC20-sh#1 constructs and were maintained under puromycin selection. RFP signal measured by FACS analysis confirmed that, upon 72 hours of Doxycycline treatment, the percentage of MV4-11 cells expressing the construct was 99.1% and 90% in cells infected with scrambled and CDC20-sh#1 lentiviral particles, respectively. In NOMO-1 the percentage of cells stably expressing the construct was slightly lower, with RFP signal in 87.2% and 78% for scrambled and CDC20-sh#1 (Fig. 29A). The following analysis were performed at different time points during the 9 days, following 72h of induction, in order to monitor RFP expression and CDC20 KD, and to evaluate the effect of CDC20 deletion on survival and proliferation capacity of AML cell lines. The obtained data showed that, RFP signal was ranging from 80% to 99% and was associated with down-regulation of CDC20 protein levels in both cell lines (Fig. 29A-B). Moreover, CDC20 KD was able to reduce the proliferation of MV-4-11 compared to the scrambled vector (Fig. 29C). Apoptosis analysis revealed that CDC20 KD increased significantly the percentage of AnnexinV$^+$ cells in MV-4-11 cell line (Fig. 29D).
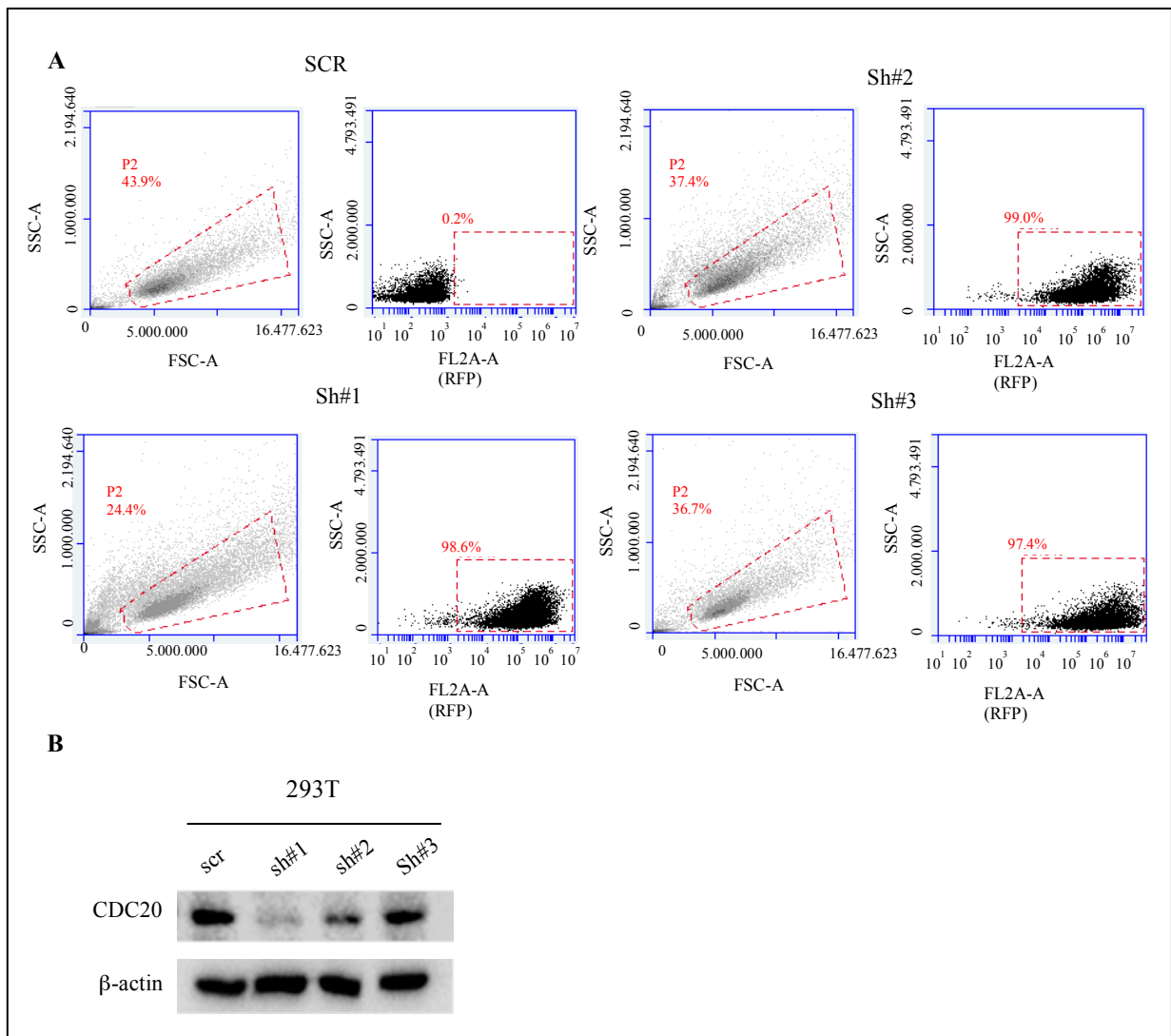
Figure 28. Evaluations of CDC20 KD efficiency. A) Percentage of cells expressing RFP in 293T transduced with sh#1, sh#2 or sh#3, obtained by FACS analysis. B) Western blot of CDC20 levels in transduced 293T cells. β-actin was used for loading control. (CTRL: control, without doxycycline induction; SCR: scrambled, used as negative control; sh#1, sh#2 and sh#3: CDC20-ShRNAs).
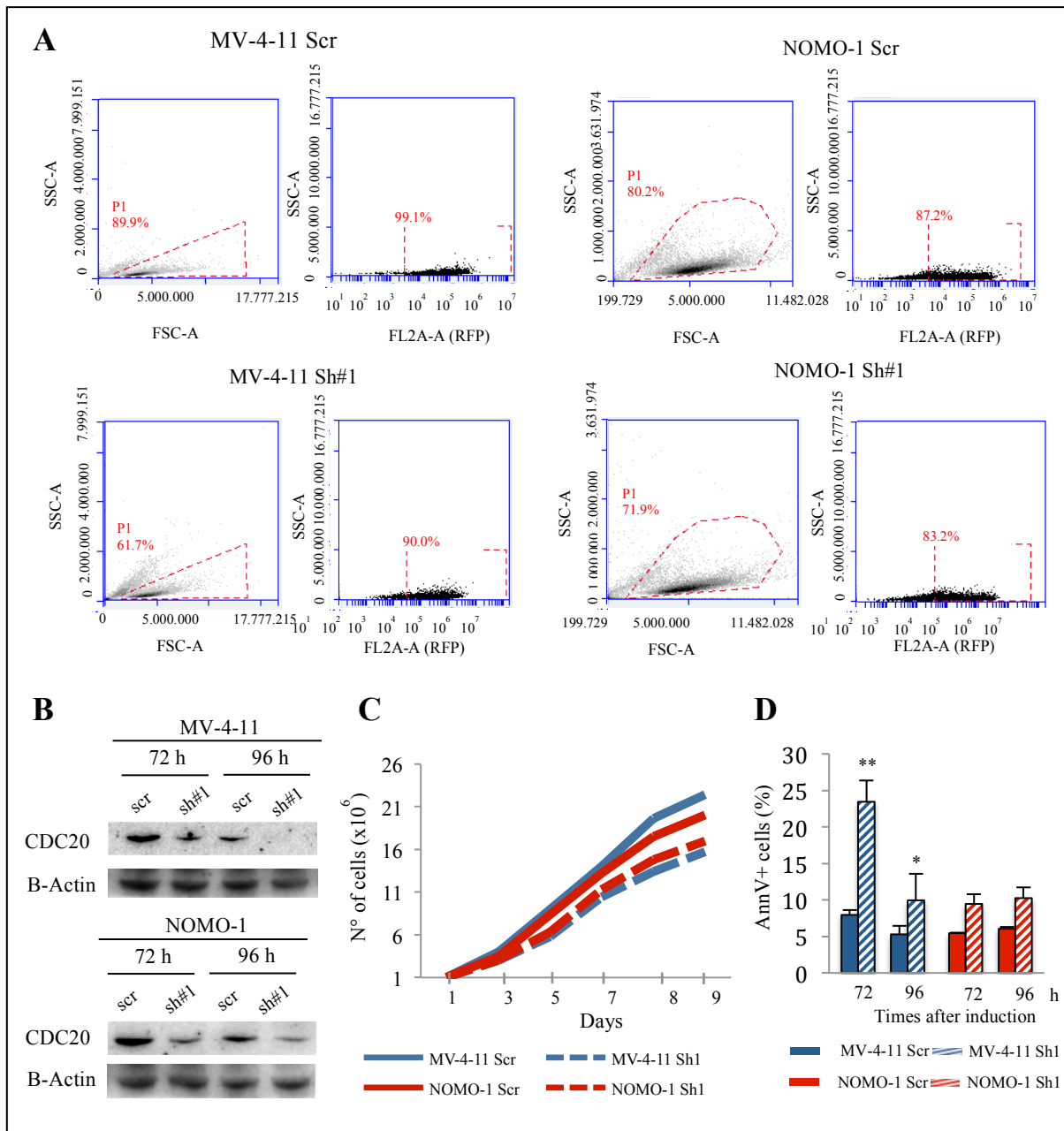
Figure 29. Evaluations of CDC20 knockdown efficiency on AML cell lines. A) FACS analysis of percentage of cells expressing RFP in MV-4-11 and NOMO-1 transduced with scrambled or sh#1, obtained after 72 hours of induction. B) Western blot of CDC20 levels in MV-4-11 and NOMO-1 after 72 and 96 h of induction. β-actin was used for loading control. (SCR: scrambled, used as negative control; sh#1: CDC20-ShRNA). C) Effect of CDC20 KD on cellular proliferation, evaluated by counting for nine days after induction. D) Percentage of apoptotic (Annexin V+) cells after 72 and 96 h of induction (*$p<0.05$).

5. Discussion

The identification of new target gene, relevant for LSC survival, is an important goal to improve treatment of AML patients. The development of NGS techniques during the last years allowed a deep characterization of AML pathogenesis, according with cytogenetic and genetic alterations of leukemic blasts. The genetic landscape of AML demonstrated that the disease is characterized by high levels of heterogeneity; indeed, patients typically carry more than one driver mutations, which are the basis of disease clonal evolution[4,202]. In particular, it is widely accepted that AML relapse is related to the selective pressure of chemotherapeutic treatments, which from one side allow the eradication of the dominant clone, but from the other side are responsible for the positive selection of therapy resistant clones. For this reason, the identification of new-targeted approaches able to eradicate LSCs represents an attractive challenge to cure AML. In this study we elucidated the effects induced by inhibition of two different potential targets for AML treatment, which are related to progression through the cell cycle.

I) The first part of the thesis was focused on the transcriptomic and metabolomic changes related to BRD4 inhibition and the impact of hypoxia in drug-response mechanisms. Several studies previously reported the efficacy of BRD4 inhibition in different AML subtype in terms of apoptosis induction and arrest of cell cycle in G_0/G_1 phase. These effects are related to the role of BRD4 in regulation of gene expression of oncogene *MYC*, and others early G_1 genes. Moreover, AML blasts reside and proliferate in the BM, where cellular growth and survival of LSC is supported by hypoxic BM microenvironment. Based on these observations, with the present study we aimed to elucidate the impact of the hypoxic microenvironment on drug-response. Our results showed that GSK1215101A is effective under hypoxia, with a reduction of cell viability in

all tested cell lines excepted for HL-60 cells that were resistant to treatment. Cell cycle analysis confirmed the induction of G_0/G_1 arrests after BET inhibition, although this effect was modest when AML cell lines were cultured under hypoxic condition. Since BRD4 is a transcription factor, we performed gene expression analysis in order to identify the most altered genes. The obtained data showed that as expected, the down-regulation of MYC expression, induced by GSK1215101A, is increased by hypoxic microenvironment, together with some genes involved in glycolysis, such as *GLUT1* and *LDHA*. The analysis of polysomal mRNA showed that both, BETi and hypoxia reduce the translational rate of AML cell lines. In particular, we observed a compensatory mechanism at translational level to balance the transcription changes induced by GSK1215101A and hypoxia. Furthermore, as already demonstrated by other groups, treatment induced the down-regulation of *c-KIT* in Kasumi-1 cells at translational and transcriptional levels. Interestingly, enrichment analysis showed that BET inhibition induces the activation of *NRF2* pathway, by affecting the expression of two important up-stream regulators, *KEAP1* and *ARNT* (*HIF-1 β*), in addition to up-regulation of several NRF2 down-stream genes. The enrichment of NRF2 pathway was observed both under hypoxic and normoxic conditions. Additionally, metabolomic profiling of AML cell lines showed that GSK1215101A induced marked metabolic changes, which differ between OCI-AML3 and Kasumi-1 cell lines, with OCI-AML3 showing an increase of reduced and oxidized glutathione, in agreement with NRF2 activation. Despite the differences between the two cell lines, we found that hypoxia enhanced a common increase of metabolites involved in energy production, which suggest the induction of a metabolic switch to support glycolysis in order to reduce energy production from OXPHOS. Taken together, our data suggest that BDR4 inhibition mediates the antioxidant response in AML via NRF2/KEAP1 axis. This reponse mechanism may be an attempt to restore normal levels of intracellular reactive oxygen species (ROS). This

hypothesis is supported by a recent study, which demonstrated that BRD4 is responsible for the induction of redox imbalance through increased production of ROS, and that its inhibition restore the redox homeostasis in myofibroblast[203]. This could represent an important finding considering that the alteration of redox signaling is a hallmark of cancer cells that usually show increased levels of ROS production. Based on these observation, we decided to explore whether the activation of NRF2 pathway influence the response to GSK1215101A in AML. Combination treatments showed that neither, NRF2 or glutathione inhibition, potentiates the effect of GSK1215101A, confirming that the activation of antioxidant response did not represents a defensive mechanism adopted by cells. In line with that, we did not detect any difference in intracellular ROS levels. NRF2 activation is also required for myeloid cell differentiation[204,205]. We therefore tested omaveloxolone, a drug inducing NRF2 activation and NF-κB inhibition. The combination with omaveloxolone potentiated GSK1215101A under normoxic and hypoxic condition. To deeply understand the role of NRF2 activation we analyzed the alterations of gene expression after combination treatment. GSEA showed a combination-specific enrichment of pathways related to autophagy, cell-fate determination and cell maturation/differentiation, together with enrichment of WNT regulation pathway in both cell lines. Interestingly pathway associated with oxidative stress response resulted enriched only in hypoxic OCI-AML3, whereas the pathway of positive regulation of energy homeostasis was found in hypoxic Kasumi-1. These results suggest that in AML the activation of NRF2 pathway observed after BRD4 inhibition could restore redox balance. Furthermore, the negative regulation of WNT pathway induced by GSK1215101A and Omaveloxolone combination demonstrated that the combination could represent a strategy to improve the effect of BRD4 inhibition. This conclusion is supported by an elegant study that investigated the drug resistance mechanisms induced by BETi in MLL-AF9 mouse model. The study demonstrated that

BETi-resistant LSCs showed an activation of WNT/β-catenin pathway, which in turn restored *MYC* expression[116], representing the most relevant resistance mechanisms known, so far. In conclusion, our study clarified the mechanism of action of BET inhibition and provided the rationale to examine in depth with *in vitro* study the efficacy of BET inhibitor treatment in association with Omaveloxolone.

II) The second part of the project focused on the investigation the role of CDC20 in AML. During the last years CDC20 was classified as oncogene, based on experimental evidence, which suggest its role as a prognostic and/or therapeutic target in several cancers. As described, CD20 plays different cellular functions, not only in cell cycle progression, but also in DNA damage repair, regulation of apoptosis and activation of Wnt/β-catenin pathway. We previously reported that CDC20 was up-regulated in AML patients, specifically in those carrying aneuploidy[10]. Starting from this observation, we speculated that the up-regulation of CDC20 could represent one mechanism adopted by leukemia progenitor cells to prevent mitotic arrest and apoptosis. To test this hypothesis we treated different AML cell lines with two inhibitors of APC/C^{CDC20} activity, Apcin and proTAME. A dose-dependent decrease in viability was observed with both drugs. Consistent with previous studies conducted in other cancer models, we found that CDC20 inhibition induced a significant increase of apoptotic cells and cell cycle arrest in G2/M phase in sensitive models. Western blot analysis confirmed the up-regulation of Cyclin B1 and Securin after treatment with proTAME and higher dose of Apcin; additionally, in the same condition, we observed a down-regulation of CDH1 protein levels in NOMO-1 and KG-1 cells. The efficacy of CDC20 functional inhibition was tested also in primary AML blasts, isolated from newly diagnosed patients, by treatment with increasing doses of Apcin. We observed that treatment induced dose-dependent reduction of cell viability and colony formation capacity of primary leukemic

blasts. In addition, all primary samples examined from newly diagnosed AML patients were found to express CDC20 in more than 50% of cells, and the expression of CDC20 resulted increased in the population of stem- and progenitor- cells CD34+CD38+, without any correlation with Ki67+ levels, used as marker for proliferation. This data provide new evidence regarding engagement of CDC20 in other functions independent from transition through mitosis. As described, the mechanism of action of both drugs is mediated by destruction of the interactions between CDC20 and APC/C, therefore the two inhibitors presumably acts only in the context of CDC20 functions related to APC/C activation. Therefore, to deep clarify the alternative roles of CDC20, we knocked-down CDC20 in MV4-11 and NOMO-1 cell lines. Lentiviral shRNA was able to reduce CDC20 at protein levels, although we reached a complete abrogation of protein only in MV4-11. Unexpectedly, CDC20-KD cell lines were able to survive, with increased levels of apoptosis only in MV-4-11 cell lines. Furthermore, we observed a reduction in the proliferation rate of both cell lines, despite the fact that cell cycle analysis did not revealed any significant alterations. This may be related to the mitotic slippage capacity of AML cell lines[206]. Morevoer, these controversial finding open new questions about the functions of CDC20 in AML. Indeed, our data showed for the first time that pharmacological inhibition of APC/C^{CDC20} seems to be a new potential approach to reduces the survival and proliferation advantage of AML cells. However, KD experiments demonstrated that, silencing of CDC20 had lower effects on apoptosis induction and it is not sufficient to induce the mitotic arrest. This data suggests that there should be an alternative mechanism to compensate the absence of CDC20. Interestingly, the major effect on cell cycle arrest and protein stabilization, observed after treatment with Apcin and proTAME, coincided with CDH1 down-regulation at protein levels in addition to CDC20 inhibition. Based on this observation we speculated that the efficacy of these two drugs could be related to their ability to act on both protein. This

interpretation requires new studies to elucidate the role of CDH1 in absence of CDC20. Indeed, it is known that the two proteins, bind sequentially the complex APC/C, during the last phases of mitosis, in order to confer target specificity to the E3 ubiquitin ligase activity. Our hypothesis is that CDH1 might prematurely bind the APC/C complex and might lack its target specificity action when CDC20 is abrogated. This might implicate when the ubiquitination of both APC/C^{CDC20} and APC/C^{CDH1} target proteins, or at least of the essential ones for the chromosomes segregation. As consequence, the effects related to CDC20 silencingwould be reduced by CDH1 function , at least in the context of APC/C activation.

Overall, these data suggest novel therapeutic approaches to target AML LSCs and progenitor cells.

6. Bibliography

1. Deschler, B. & Lübbert, M. Acute myeloid leukemia: epidemiology and etiology. *Cancer* **107**, 2099–107 (2006).
2. Döhner, H., Weisdorf, D. J. & Bloomfield, C. D. Acute Myeloid Leukemia. *N. Engl. J. Med.* **373**, 1136–52 (2015).
3. Tyner, J. W. *et al.* Functional genomic landscape of acute myeloid leukaemia. *Nature* **562**, 526–531 (2018).
4. Cancer Genome Atlas Research Network *et al.* Genomic and epigenomic landscapes of adult de novo acute myeloid leukemia. *N. Engl. J. Med.* **368**, 2059–74 (2013).
5. Moarii, M. & Papaemmanuil, E. Classification and risk assessment in AML: integrating cytogenetics and molecular profiling. *Hematol. Am. Soc. Hematol. Educ. Progr.* **2017**, 37–44 (2017).
6. Döhner, H. *et al.* Diagnosis and management of AML in adults: 2017 ELN recommendations from an international expert panel. *Blood* **129**, 424–447 (2017).
7. Papaemmanuil, E. *et al.* Genomic Classification and Prognosis in Acute Myeloid Leukemia. *N. Engl. J. Med.* **374**, 2209–2221 (2016).
8. Barbacid, M. *et al.* Cell cycle and cancer: genetic analysis of the role of cyclin-dependent kinases. *Cold Spring Harb. Symp. Quant. Biol.* **70**, 233–40 (2005).
9. Otto, T. & Sicinski, P. Cell cycle proteins as promising targets in cancer therapy. *Nat. Rev. Cancer* **17**, 93–115 (2017).
10. Simonetti, G. *et al.* Aneuploid acute myeloid leukemia exhibits a signature of genomic alterations in the cell cycle and protein degradation machinery. *Cancer* **125**, 712–725 (2019).
11. Dey, A., Nishiyama, A., Karpova, T., McNally, J. & Ozato, K. Brd4 marks select genes on mitotic chromatin and directs postmitotic transcription. *Mol. Biol. Cell* **20**, 4899–909 (2009).
12. Mochizuki, K. *et al.* The bromodomain protein Brd4 stimulates G1 gene transcription and promotes progression to S phase. *J. Biol. Chem.* **283**, 9040–8 (2008).
13. Maruyama, T. *et al.* A Mammalian bromodomain protein, brd4, interacts with replication factor C and inhibits progression to S phase. *Mol. Cell. Biol.* **22**, 6509–20 (2002).
14. Tasdemir, N. *et al.* BRD4 Connects Enhancer Remodeling to Senescence Immune Surveillance. *Cancer Discov.* **6**, 612–29 (2016).
15. Yang, Z., He, N. & Zhou, Q. Brd4 recruits P-TEFb to chromosomes at late mitosis to promote G1 gene expression and cell cycle progression. *Mol. Cell. Biol.* **28**, 967–76 (2008).

16. You, J. *et al.* Regulation of aurora B expression by the bromodomain protein Brd4. *Mol. Cell. Biol.* **29**, 5094–103 (2009).

17. Farina, A. *et al.* Bromodomain protein Brd4 binds to GTPase-activating SPA-1, modulating its activity and subcellular localization. *Mol. Cell. Biol.* **24**, 9059–69 (2004).

18. Simonetti, G., Bruno, S., Padella, A., Tenti, E. & Martinelli, G. Aneuploidy: Cancer strength or vulnerability? *Int. J. cancer* **144**, 8–25 (2019).

19. Florence, B. & Faller, D. V. You bet-cha: a novel family of transcriptional regulators. *Front. Biosci.* **6**, D1008-18 (2001).

20. Filippakopoulos, P. *et al.* Histone recognition and large-scale structural analysis of the human bromodomain family. *Cell* **149**, 214–31 (2012).

21. Wu, S.-Y. & Chiang, C.-M. The double bromodomain-containing chromatin adaptor Brd4 and transcriptional regulation. *J. Biol. Chem.* **282**, 13141–5 (2007).

22. Larue, R. C. *et al.* Bimodal high-affinity association of Brd4 with murine leukemia virus integrase and mononucleosomes. *Nucleic Acids Res.* **42**, 4868–81 (2014).

23. Wu, S.-Y., Lee, A.-Y., Lai, H.-T., Zhang, H. & Chiang, C.-M. Phospho switch triggers Brd4 chromatin binding and activator recruitment for gene-specific targeting. *Mol. Cell* **49**, 843–57 (2013).

24. Crowe, B. L. *et al.* Structure of the Brd4 ET domain bound to a C-terminal motif from γ-retroviral integrases reveals a conserved mechanism of interaction. *Proc. Natl. Acad. Sci. U. S. A.* **113**, 2086–91 (2016).

25. Bisgrove, D. A., Mahmoudi, T., Henklein, P. & Verdin, E. Conserved P-TEFb-interacting domain of BRD4 inhibits HIV transcription. *Proc. Natl. Acad. Sci. U. S. A.* **104**, 13690–5 (2007).

26. Shi, J. & Vakoc, C. R. The mechanisms behind the therapeutic activity of BET bromodomain inhibition. *Mol. Cell* **54**, 728–36 (2014).

27. Devaiah, B. N. *et al.* BRD4 is an atypical kinase that phosphorylates serine2 of the RNA polymerase II carboxy-terminal domain. *Proc. Natl. Acad. Sci. U. S. A.* **109**, 6927–32 (2012).

28. Baranello, L. *et al.* RNA Polymerase II Regulates Topoisomerase 1 Activity to Favor Efficient Transcription. *Cell* **165**, 357–71 (2016).

29. Zhang, W. *et al.* Bromodomain-containing protein 4 (BRD4) regulates RNA polymerase II serine 2 phosphorylation in human CD4+ T cells. *J. Biol. Chem.* **287**, 43137–55 (2012).

30. Lovén, J. *et al.* Selective inhibition of tumor oncogenes by disruption of super-enhancers. *Cell* **153**, 320–34 (2013).

31. Ferri, E., Petosa, C. & McKenna, C. E. Bromodomains: Structure, function and pharmacology of inhibition. *Biochem. Pharmacol.* **106**, 1–18 (2016).

32. Devaiah, B. N. *et al.* BRD4 is a histone acetyltransferase that evicts

nucleosomes from chromatin. *Nat. Struct. Mol. Biol.* **23**, 540–8 (2016).

33. Floyd, S. R. *et al.* The bromodomain protein Brd4 insulates chromatin from DNA damage signalling. *Nature* **498**, 246–50 (2013).

34. Houzelstein, D. *et al.* Growth and early postimplantation defects in mice deficient for the bromodomain-containing protein Brd4. *Mol. Cell. Biol.* **22**, 3794–802 (2002).

35. Bolden, J. E. *et al.* Inducible in vivo silencing of Brd4 identifies potential toxicities of sustained BET protein inhibition. *Cell Rep.* **8**, 1919–1929 (2014).

36. Rodriguez, R. M. *et al.* Role of BRD4 in hematopoietic differentiation of embryonic stem cells. *Epigenetics* **9**, 566–78 (2014).

37. Whyte, W. A. *et al.* Master transcription factors and mediator establish super-enhancers at key cell identity genes. *Cell* **153**, 307–19 (2013).

38. Brown, J. D. *et al.* NF-κB directs dynamic super enhancer formation in inflammation and atherogenesis. *Mol. Cell* **56**, 219–231 (2014).

39. Deshpande, A. J., Bradner, J. & Armstrong, S. A. Chromatin modifications as therapeutic targets in MLL-rearranged leukemia. *Trends Immunol.* **33**, 563–70 (2012).

40. Chapuy, B. *et al.* Discovery and characterization of super-enhancer-associated dependencies in diffuse large B cell lymphoma. *Cancer Cell* **24**, 777–90 (2013).

41. Hogg, S. J. *et al.* BET Inhibition Induces Apoptosis in Aggressive B-Cell Lymphoma via Epigenetic Regulation of BCL-2 Family Members. *Mol. Cancer Ther.* **15**, 2030–41 (2016).

42. Roe, J.-S., Mercan, F., Rivera, K., Pappin, D. J. & Vakoc, C. R. BET Bromodomain Inhibition Suppresses the Function of Hematopoietic Transcription Factors in Acute Myeloid Leukemia. *Mol. Cell* **58**, 1028–39 (2015).

43. Zuber, J. *et al.* RNAi screen identifies Brd4 as a therapeutic target in acute myeloid leukaemia. *Nature* **478**, 524–8 (2011).

44. Chen, C. *et al.* Cancer-associated IDH2 mutants drive an acute myeloid leukemia that is susceptible to Brd4 inhibition. *Genes Dev.* **27**, 1974–85 (2013).

45. Dawson, M. A. *et al.* Recurrent mutations, including NPM1c, activate a BRD4-dependent core transcriptional program in acute myeloid leukemia. *Leukemia* **28**, 311–20 (2014).

46. Dawson, M. A. *et al.* Inhibition of BET recruitment to chromatin as an effective treatment for MLL-fusion leukaemia. *Nature* **478**, 529–33 (2011).

47. Coudé, M.-M. *et al.* BET inhibitor OTX015 targets BRD2 and BRD4 and decreases c-MYC in acute leukemia cells. *Oncotarget* **6**, 17698–712 (2015).

48. Eilers, M. & Eisenman, R. N. Myc's broad reach. *Genes Dev.* **22**, 2755–66

(2008).

49. Paulsson, K. & Johansson, B. Trisomy 8 as the sole chromosomal aberration in acute myeloid leukemia and myelodysplastic syndromes. *Pathol. Biol. (Paris).* **55**, 37–48 (2007).

50. Stine, Z. E., Walton, Z. E., Altman, B. J., Hsieh, A. L. & Dang, C. V. MYC, Metabolism, and Cancer. *Cancer Discov.* **5**, 1024–39 (2015).

51. Levens, D. 'You Don't Muck with MYC'. *Genes Cancer* **1**, 547–554 (2010).

52. Wolf, E., Lin, C. Y., Eilers, M. & Levens, D. L. Taming of the beast: shaping Myc-dependent amplification. *Trends Cell Biol.* **25**, 241–8 (2015).

53. Rahl, P. B. *et al.* c-Myc regulates transcriptional pause release. *Cell* **141**, 432–45 (2010).

54. Lin, C. Y. *et al.* Transcriptional amplification in tumor cells with elevated c-Myc. *Cell* **151**, 56–67 (2012).

55. Shim, H. *et al.* c-Myc transactivation of LDH-A: implications for tumor metabolism and growth. *Proc. Natl. Acad. Sci. U. S. A.* **94**, 6658–63 (1997).

56. Gao, P. *et al.* c-Myc suppression of miR-23a/b enhances mitochondrial glutaminase expression and glutamine metabolism. *Nature* **458**, 762–5 (2009).

57. Osthus, R. C. *et al.* Deregulation of glucose transporter 1 and glycolytic gene expression by c-Myc. *J. Biol. Chem.* **275**, 21797–800 (2000).

58. Yuneva, M., Zamboni, N., Oefner, P., Sachidanandam, R. & Lazebnik, Y. Deficiency in glutamine but not glucose induces MYC-dependent apoptosis in human cells. *J. Cell Biol.* **178**, 93–105 (2007).

59. Wise, D. R. *et al.* Myc regulates a transcriptional program that stimulates mitochondrial glutaminolysis and leads to glutamine addiction. *Proc. Natl. Acad. Sci. U. S. A.* **105**, 18782–7 (2008).

60. Dang, C. V, Le, A. & Gao, P. MYC-induced cancer cell energy metabolism and therapeutic opportunities. *Clin. Cancer Res.* **15**, 6479–83 (2009).

61. Shroff, E. H. *et al.* MYC oncogene overexpression drives renal cell carcinoma in a mouse model through glutamine metabolism. *Proc. Natl. Acad. Sci. U. S. A.* **112**, 6539–44 (2015).

62. Xiang, Y. *et al.* Targeted inhibition of tumor-specific glutaminase diminishes cell-autonomous tumorigenesis. *J. Clin. Invest.* **125**, 2293–306 (2015).

63. Gordan, J. D., Thompson, C. B. & Simon, M. C. HIF and c-Myc: sibling rivals for control of cancer cell metabolism and proliferation. *Cancer Cell* **12**, 108–13 (2007).

64. Corn, P. G. *et al.* Mxi1 is induced by hypoxia in a HIF-1-dependent manner and protects cells from c-Myc-induced apoptosis. *Cancer Biol.*

Ther. **4**, 1285–94 (2005).

65. Dang, C. V, Kim, J., Gao, P. & Yustein, J. The interplay between MYC and HIF in cancer. *Nat. Rev. Cancer* **8**, 51–6 (2008).
66. Calvi, L. M. *et al.* Osteoblastic cells regulate the haematopoietic stem cell niche. *Nature* **425**, 841–6 (2003).
67. Kiel, M. J. *et al.* SLAM family receptors distinguish hematopoietic stem and progenitor cells and reveal endothelial niches for stem cells. *Cell* **121**, 1109–21 (2005).
68. Ding, L., Saunders, T. L., Enikolopov, G. & Morrison, S. J. Endothelial and perivascular cells maintain haematopoietic stem cells. *Nature* **481**, 457–62 (2012).
69. Nwajei, F. & Konopleva, M. The bone marrow microenvironment as niche retreats for hematopoietic and leukemic stem cells. *Adv. Hematol.* **2013**, 953982 (2013).
70. Zhang, J. *et al.* Identification of the haematopoietic stem cell niche and control of the niche size. *Nature* **425**, 836–41 (2003).
71. Lo Celso, C. *et al.* Live-animal tracking of individual haematopoietic stem/progenitor cells in their niche. *Nature* **457**, 92–6 (2009).
72. Xie, Y. *et al.* Detection of functional haematopoietic stem cell niche using real-time imaging. *Nature* **457**, 97–101 (2009).
73. Fujisaki, J. *et al.* In vivo imaging of Treg cells providing immune privilege to the haematopoietic stem-cell niche. *Nature* **474**, 216–9 (2011).
74. Cardier, J. E. & Barberá-Guillem, E. Extramedullary hematopoiesis in the adult mouse liver is associated with specific hepatic sinusoidal endothelial cells. *Hepatology* **26**, 165–75 (1997).
75. Li, W., Johnson, S. A., Shelley, W. C. & Yoder, M. C. Hematopoietic stem cell repopulating ability can be maintained in vitro by some primary endothelial cells. *Exp. Hematol.* **32**, 1226–37 (2004).
76. Ohneda, O. *et al.* Hematopoietic stem cell maintenance and differentiation are supported by embryonic aorta-gonad-mesonephros region-derived endothelium. *Blood* **92**, 908–19 (1998).
77. Eliasson, P. & Jönsson, J.-I. The hematopoietic stem cell niche: low in oxygen but a nice place to be. *J. Cell. Physiol.* **222**, 17–22 (2010).
78. Nombela-Arrieta, C. & Silberstein, L. E. The science behind the hypoxic niche of hematopoietic stem and progenitors. *Hematol. Am. Soc. Hematol. Educ. Progr.* **2014**, 542–7 (2014).
79. Kubota, Y., Takubo, K. & Suda, T. Bone marrow long label-retaining cells reside in the sinusoidal hypoxic niche. *Biochem. Biophys. Res. Commun.* **366**, 335–9 (2008).
80. Lo Celso, C., Wu, J. W. & Lin, C. P. In vivo imaging of hematopoietic stem cells and their microenvironment. *J. Biophotonics* **2**, 619–31 (2009).
81. Parmar, K., Mauch, P., Vergilio, J.-A., Sackstein, R. & Down, J. D. Distribution of hematopoietic stem cells in the bone marrow according to

regional hypoxia. *Proc. Natl. Acad. Sci. U. S. A.* **104**, 5431–6 (2007).

82. Zheng, J. *et al.* Ex vivo expanded hematopoietic stem cells overcome the MHC barrier in allogeneic transplantation. *Cell Stem Cell* **9**, 119–30 (2011).

83. Arai, F. *et al.* Tie2/angiopoietin-1 signaling regulates hematopoietic stem cell quiescence in the bone marrow niche. *Cell* **118**, 149–61 (2004).

84. Bradley, T. R., Hodgson, G. S. & Rosendaal, M. The effect of oxygen tension on haemopoietic and fibroblast cell proliferation in vitro. *J. Cell. Physiol.* **97**, 517–22 (1978).

85. Katahira, J. & Mizoguchi, H. Improvement of culture conditions for human megakaryocytic and pluripotent progenitor cells by low oxygen tension. *Int. J. Cell Cloning* **5**, 412–20 (1987).

86. Koller, M. R., Bender, J. G., Miller, W. M. & Papoutsakis, E. T. Reduced oxygen tension increases hematopoiesis in long-term culture of human stem and progenitor cells from cord blood and bone marrow. *Exp. Hematol.* **20**, 264–70 (1992).

87. LaIuppa, J. A., Papoutsakis, E. T. & Miller, W. M. Oxygen tension alters the effects of cytokines on the megakaryocyte, erythrocyte, and granulocyte lineages. *Exp. Hematol.* **26**, 835–43 (1998).

88. Wood, S. M., Gleadle, J. M., Pugh, C. W., Hankinson, O. & Ratcliffe, P. J. The role of the aryl hydrocarbon receptor nuclear translocator (ARNT) in hypoxic induction of gene expression. Studies in ARNT-deficient cells. *J. Biol. Chem.* **271**, 15117–23 (1996).

89. Ke, Q. & Costa, M. Hypoxia-inducible factor-1 (HIF-1). *Mol. Pharmacol.* **70**, 1469–80 (2006).

90. Lee, J.-W., Bae, S.-H., Jeong, J.-W., Kim, S.-H. & Kim, K.-W. Hypoxia-inducible factor (HIF-1)alpha: its protein stability and biological functions. *Exp. Mol. Med.* **36**, 1–12 (2004).

91. Mazure, N. M. & Pouysségur, J. Hypoxia-induced autophagy: cell death or cell survival? *Curr. Opin. Cell Biol.* **22**, 177–80 (2010).

92. Takubo, K. *et al.* Regulation of the HIF-1alpha level is essential for hematopoietic stem cells. *Cell Stem Cell* **7**, 391–402 (2010).

93. Zhang, H. *et al.* HIF-1-dependent expression of angiopoietin-like 4 and L1CAM mediates vascular metastasis of hypoxic breast cancer cells to the lungs. *Oncogene* **31**, 1757–70 (2012).

94. Iyer, N. V *et al.* Cellular and developmental control of O2 homeostasis by hypoxia-inducible factor 1 alpha. *Genes Dev.* **12**, 149–62 (1998).

95. Seagroves, T. N. *et al.* Transcription factor HIF-1 is a necessary mediator of the pasteur effect in mammalian cells. *Mol. Cell. Biol.* **21**, 3436–44 (2001).

96. Simsek, T. *et al.* The distinct metabolic profile of hematopoietic stem cells reflects their location in a hypoxic niche. *Cell Stem Cell* **7**, 380–90 (2010).

97. Kocabas, F. *et al.* Meis1 regulates the metabolic phenotype and oxidant

defense of hematopoietic stem cells. *Blood* **120**, 4963–72 (2012).

98. Nilsson, S. K. *et al.* Osteopontin, a key component of the hematopoietic stem cell niche and regulator of primitive hematopoietic progenitor cells. *Blood* **106**, 1232–9 (2005).

99. Naveiras, O. & Daley, G. Q. Stem cells and their niche: a matter of fate. *Cell. Mol. Life Sci.* **63**, 760–6 (2006).

100. Colmone, A. *et al.* Leukemic cells create bone marrow niches that disrupt the behavior of normal hematopoietic progenitor cells. *Science* **322**, 1861–5 (2008).

101. Kode, A. *et al.* FoxO1-dependent induction of acute myeloid leukemia by osteoblasts in mice. *Leukemia* **30**, 1–13 (2016).

102. Kode, A. *et al.* Leukaemogenesis induced by an activating β-catenin mutation in osteoblasts. *Nature* **506**, 240–4 (2014).

103. Wei, J. *et al.* Microenvironment determines lineage fate in a human model of MLL-AF9 leukemia. *Cancer Cell* **13**, 483–95 (2008).

104. Wang, Y., Liu, Y., Malek, S. N., Zheng, P. & Liu, Y. Targeting HIF1α eliminates cancer stem cells in hematological malignancies. *Cell Stem Cell* **8**, 399–411 (2011).

105. Kuett, A. *et al.* IL-8 as mediator in the microenvironment-leukaemia network in acute myeloid leukaemia. *Sci. Rep.* **5**, 18411 (2015).

106. Lodi, A. *et al.* Hypoxia triggers major metabolic changes in AML cells without altering indomethacin-induced TCA cycle deregulation. *ACS Chem. Biol.* **6**, 169–75 (2011).

107. Zhou, H.-S., Carter, B. Z. & Andreeff, M. Bone marrow niche-mediated survival of leukemia stem cells in acute myeloid leukemia: Yin and Yang. *Cancer Biol. Med.* **13**, 248–59 (2016).

108. Wang, C.-Y. & Filippakopoulos, P. Beating the odds: BETs in disease. *Trends Biochem. Sci.* **40**, 468–79 (2015).

109. Herrmann, H. *et al.* Small-molecule inhibition of BRD4 as a new potent approach to eliminate leukemic stem- and progenitor cells in acute myeloid leukemia AML. *Oncotarget* **3**, 1588–99 (2012).

110. Gröschel, S. *et al.* A single oncogenic enhancer rearrangement causes concomitant EVI1 and GATA2 deregulation in leukemia. *Cell* **157**, 369–381 (2014).

111. Zhao, Y. *et al.* High-Resolution Mapping of RNA Polymerases Identifies Mechanisms of Sensitivity and Resistance to BET Inhibitors in t(8;21) AML. *Cell Rep.* **16**, 2003–16 (2016).

112. Chen, C. *et al.* MLL3 is a haploinsufficient 7q tumor suppressor in acute myeloid leukemia. *Cancer Cell* **25**, 652–65 (2014).

113. Delmore, J. E. *et al.* BET bromodomain inhibition as a therapeutic strategy to target c-Myc. *Cell* **146**, 904–17 (2011).

114. Berthon, C. *et al.* Bromodomain inhibitor OTX015 in patients with acute leukaemia: a dose-escalation, phase 1 study. *Lancet. Haematol.* **3**, e186-95

(2016).

115. Rathert, P. *et al.* Transcriptional plasticity promotes primary and acquired resistance to BET inhibition. *Nature* **525**, 543–547 (2015).

116. Fong, C. Y. *et al.* BET inhibitor resistance emerges from leukaemia stem cells. *Nature* **525**, 538–42 (2015).

117. Transcriptional Reprogramming Underlies BET Inhibitor Resistance. *Cancer Discov.* **5**, 1120.1-1120 (2015).

118. Maresca, T. J. & Salmon, E. D. Welcome to a new kind of tension: translating kinetochore mechanics into a wait-anaphase signal. *J. Cell Sci.* **123**, 825–35 (2010).

119. Liu, D., Vader, G., Vromans, M. J. M., Lampson, M. A. & Lens, S. M. A. Sensing chromosome bi-orientation by spatial separation of aurora B kinase from kinetochore substrates. *Science* **323**, 1350–3 (2009).

120. Welburn, J. P. I. *et al.* Aurora B phosphorylates spatially distinct targets to differentially regulate the kinetochore-microtubule interface. *Mol. Cell* **38**, 383–92 (2010).

121. Stucke, V. M., Baumann, C. & Nigg, E. A. Kinetochore localization and microtubule interaction of the human spindle checkpoint kinase Mps1. *Chromosoma* **113**, 1–15 (2004).

122. Nijenhuis, W. *et al.* A TPR domain-containing N-terminal module of MPS1 is required for its kinetochore localization by Aurora B. *J. Cell Biol.* **201**, 217–31 (2013).

123. Shepperd, L. A. *et al.* Phosphodependent recruitment of Bub1 and Bub3 to Spc7/KNL1 by Mph1 kinase maintains the spindle checkpoint. *Curr. Biol.* **22**, 891–9 (2012).

124. London, N., Ceto, S., Ranish, J. A. & Biggins, S. Phosphoregulation of Spc105 by Mps1 and PP1 regulates Bub1 localization to kinetochores. *Curr. Biol.* **22**, 900–6 (2012).

125. Vleugel, M. *et al.* Arrayed BUB recruitment modules in the kinetochore scaffold KNL1 promote accurate chromosome segregation. *J. Cell Biol.* **203**, 943–55 (2013).

126. Yamagishi, Y., Yang, C.-H., Tanno, Y. & Watanabe, Y. MPS1/Mph1 phosphorylates the kinetochore protein KNL1/Spc7 to recruit SAC components. *Nat. Cell Biol.* **14**, 746–52 (2012).

127. Primorac, I. *et al.* Bub3 reads phosphorylated MELT repeats to promote spindle assembly checkpoint signaling. *Elife* **2**, e01030 (2013).

128. Larsen, N. A., Al-Bassam, J., Wei, R. R. & Harrison, S. C. Structural analysis of Bub3 interactions in the mitotic spindle checkpoint. *Proc. Natl. Acad. Sci. U. S. A.* **104**, 1201–6 (2007).

129. Mora-Santos, M. D. M. *et al.* Bub3-Bub1 Binding to Spc7/KNL1 Toggles the Spindle Checkpoint Switch by Licensing the Interaction of Bub1 with Mad1-Mad2. *Curr. Biol.* **26**, 2642–2650 (2016).

130. Mapelli, M., Massimiliano, L., Santaguida, S. & Musacchio, A. The Mad2

conformational dimer: structure and implications for the spindle assembly checkpoint. *Cell* **131**, 730–43 (2007).

131. Tipton, A. R. *et al.* Monopolar spindle 1 (MPS1) kinase promotes production of closed MAD2 (C-MAD2) conformer and assembly of the mitotic checkpoint complex. *J. Biol. Chem.* **288**, 35149–58 (2013).

132. Hewitt, L. *et al.* Sustained Mps1 activity is required in mitosis to recruit O-Mad2 to the Mad1-C-Mad2 core complex. *J. Cell Biol.* **190**, 25–34 (2010).

133. Jia, L., Li, B. & Yu, H. The Bub1-Plk1 kinase complex promotes spindle checkpoint signalling through Cdc20 phosphorylation. *Nat. Commun.* **7**, 10818 (2016).

134. O'Connor, A. *et al.* Requirement for PLK1 kinase activity in the maintenance of a robust spindle assembly checkpoint. *Biol. Open* **5**, 11–9 (2015).

135. Di Fiore, B. *et al.* The ABBA motif binds APC/C activators and is shared by APC/C substrates and regulators. *Dev. Cell* **32**, 358–372 (2015).

136. Rosenberg, J. S., Cross, F. R. & Funabiki, H. KNL1/Spc105 recruits PP1 to silence the spindle assembly checkpoint. *Curr. Biol.* **21**, 942–7 (2011).

137. Liu, D. *et al.* Regulated targeting of protein phosphatase 1 to the outer kinetochore by KNL1 opposes Aurora B kinase. *J. Cell Biol.* **188**, 809–20 (2010).

138. Clute, P. & Pines, J. Temporal and spatial control of cyclin B1 destruction in metaphase. *Nat. Cell Biol.* **1**, 82–7 (1999).

139. Nasmyth, K. Disseminating the genome: joining, resolving, and separating sister chromatids during mitosis and meiosis. *Annu. Rev. Genet.* **35**, 673–745 (2001).

140. Jin, L., Williamson, A., Banerjee, S., Philipp, I. & Rape, M. Mechanism of ubiquitin-chain formation by the human anaphase-promoting complex. *Cell* **133**, 653–65 (2008).

141. Hartwell, L. H., Culotti, J. & Reid, B. Genetic control of the cell-division cycle in yeast. I. Detection of mutants. *Proc. Natl. Acad. Sci. U. S. A.* **66**, 352–9 (1970).

142. Zur, A. & Brandeis, M. Securin degradation is mediated by fzy and fzr, and is required for complete chromatid separation but not for cytokinesis. *EMBO J.* **20**, 792–801 (2001).

143. Shirayama, M., Tóth, A., Gálová, M. & Nasmyth, K. APC(Cdc20) promotes exit from mitosis by destroying the anaphase inhibitor Pds1 and cyclin Clb5. *Nature* **402**, 203–7 (1999).

144. Geley, S. *et al.* Anaphase-promoting complex/cyclosome-dependent proteolysis of human cyclin A starts at the beginning of mitosis and is not subject to the spindle assembly checkpoint. *J. Cell Biol.* **153**, 137–48 (2001).

145. Hames, R. S. APC/C-mediated destruction of the centrosomal kinase

Nek2A occurs in early mitosis and depends upon a cyclin A-type D-box. *EMBO J.* **20**, 7117–7127 (2001).

146. Gurden, M. D. J. *et al.* Cdc20 is required for the post-anaphase, KEN-dependent degradation of centromere protein F. *J. Cell Sci.* **123**, 321–30 (2010).

147. Amador, V., Ge, S., Santamaría, P. G., Guardavaccaro, D. & Pagano, M. APC/CCdc20 Controls the Ubiquitin-Mediated Degradation of p21 in Prometaphase. *Mol. Cell* **27**, 462–473 (2007).

148. Li, M., York, J. P. & Zhang, P. Loss of Cdc20 Causes a Securin-Dependent Metaphase Arrest in Two-Cell Mouse Embryos. *Mol. Cell. Biol.* **27**, 3481–3488 (2007).

149. Li, M., Fang, X., Wei, Z., York, J. P. & Zhang, P. Loss of spindle assembly checkpoint-mediated inhibition of Cdc20 promotes tumorigenesis in mice. *J. Cell Biol.* **185**, 983–94 (2009).

150. Malureanu, L. *et al.* Cdc20 hypomorphic mice fail to counteract de novo synthesis of cyclin B1 in mitosis. *J. Cell Biol.* **191**, 313–29 (2010).

151. Wang, W., Wu, T. & Kirschner, M. W. The master cell cycle regulator APC-Cdc20 regulates ciliary length and disassembly of the primary cilium. *Elife* **3**, (2014).

152. Yang, Y. *et al.* A Cdc20-APC ubiquitin signaling pathway regulates presynaptic differentiation. *Science* **326**, 575–8 (2009).

153. Chun, A. C.-S., Kok, K.-H. & Jin, D.-Y. REV7 is required for anaphase-promoting complex-dependent ubiquitination and degradation of translesion DNA polymerase REV1. *Cell Cycle* **12**, 365–78 (2013).

154. Kuang, C. *et al.* A novel fizzy/Cdc20-dependent mechanism suppresses necrosis in neural stem cells. *Development* **141**, 1453–64 (2014).

155. Hadjihannas, M. V, Bernkopf, D. B., Brückner, M. & Behrens, J. Cell cycle control of Wnt/β-catenin signalling by conductin/axin2 through CDC20. *EMBO Rep.* **13**, 347–54 (2012).

156. Quek, L. S., Grasset, N., Jasmen, J. B., Robinson, K. S. & Bellanger, S. Dual Role of the Anaphase Promoting Complex/Cyclosome in Regulating Stemness and Differentiation in Human Primary Keratinocytes. *J. Invest. Dermatol.* **138**, 1851–1861 (2018).

157. Mao, D. D. *et al.* A CDC20-APC/SOX2 Signaling Axis Regulates Human Glioblastoma Stem-like Cells. *Cell Rep.* **11**, 1809–21 (2015).

158. Harley, M. E., Allan, L. A., Sanderson, H. S. & Clarke, P. R. Phosphorylation of Mcl-1 by CDK1-cyclin B1 initiates its Cdc20-dependent destruction during mitotic arrest. *EMBO J.* **29**, 2407–20 (2010).

159. Wan, L. *et al.* APC(Cdc20) suppresses apoptosis through targeting Bim for ubiquitination and destruction. *Dev. Cell* **29**, 377–91 (2014).

160. Manchado, E. *et al.* Targeting mitotic exit leads to tumor regression in vivo: Modulation by Cdk1, Mastl, and the PP2A/B55α,δ phosphatase. *Cancer Cell* **18**, 641–54 (2010).

161. Cragg, M. S., Harris, C., Strasser, A. & Scott, C. L. Unleashing the power of inhibitors of oncogenic kinases through BH3 mimetics. *Nat. Rev. Cancer* **9**, 321–6 (2009).

162. Cory, S. & Adams, J. M. The Bcl2 family: regulators of the cellular life-or-death switch. *Nat. Rev. Cancer* **2**, 647–56 (2002).

163. Chen, Z. *et al.* Functional roles of PC-PLC and Cdc20 in the cell cycle, proliferation, and apoptosis. *Cell Biochem. Funct.* **28**, 249–57 (2010).

164. Reimann, J. D. R. Emi1 regulates the anaphase-promoting complex by a different mechanism than Mad2 proteins. *Genes Dev.* **15**, 3278–3285 (2001).

165. Reimann, J. D. *et al.* Emi1 is a mitotic regulator that interacts with Cdc20 and inhibits the anaphase promoting complex. *Cell* **105**, 645–55 (2001).

166. Stegmeier, F. *et al.* Anaphase initiation is regulated by antagonistic ubiquitination and deubiquitination activities. *Nature* **446**, 876–81 (2007).

167. Song, M. S. *et al.* The tumour suppressor RASSF1A regulates mitosis by inhibiting the APC-Cdc20 complex. *Nat. Cell Biol.* **6**, 129–37 (2004).

168. Kidokoro, T. *et al.* CDC20, a potential cancer therapeutic target, is negatively regulated by p53. *Oncogene* **27**, 1562–71 (2008).

169. Banerjee, T., Nath, S. & Roychoudhury, S. DNA damage induced p53 downregulates Cdc20 by direct binding to its promoter causing chromatin remodeling. *Nucleic Acids Res.* **37**, 2688–98 (2009).

170. Lizé, M., Herr, C., Klimke, A., Bals, R. & Dobbelstein, M. MicroRNA-449a levels increase by several orders of magnitude during mucociliary differentiation of airway epithelia. *Cell Cycle* **9**, 4579–83 (2010).

171. Yamanaka, S. *et al.* Coordinated effects of microRNA-494 induce G_2/M arrest in human cholangiocarcinoma. *Cell Cycle* **11**, 2729–2738 (2012).

172. Li, D. *et al.* Overexpression of oncogenic STK15/BTAK/Aurora A kinase in human pancreatic cancer. *Clin. Cancer Res.* **9**, 991–7 (2003).

173. Chang, D. Z. *et al.* Increased CDC20 expression is associated with pancreatic ductal adenocarcinoma differentiation and progression. *J. Hematol. Oncol.* **5**, 15 (2012).

174. Yuan, B. *et al.* Increased expression of mitotic checkpoint genes in breast cancer cells with chromosomal instability. *Clin. Cancer Res.* **12**, 405–10 (2006).

175. Karra, H. *et al.* Cdc20 and securin overexpression predict short-term breast cancer survival. *Br. J. Cancer* **110**, 2905–13 (2014).

176. Kwan, P. S. *et al.* Daxx regulates mitotic progression and prostate cancer predisposition. *Carcinogenesis* **34**, 750–9 (2013).

177. Wang, Q. *et al.* Targeting amino acid transport in metastatic castration-resistant prostate cancer: effects on cell cycle, cell growth, and tumor development. *J. Natl. Cancer Inst.* **105**, 1463–73 (2013).

178. Bieniek, J., Childress, C., Swatski, M. D. & Yang, W. COX-2 inhibitors

arrest prostate cancer cell cycle progression by down-regulation of kinetochore/centromere proteins. *Prostate* **74**, 999–1011 (2014).

179. Wu, W. *et al.* CDC20 overexpression predicts a poor prognosis for patients with colorectal cancer. *J. Transl. Med.* **11**, 142 (2013).

180. LI, J., GAO, J.-Z., DU, J.-L., HUANG, Z.-X. & WEI, L.-X. Increased CDC20 expression is associated with development and progression of hepatocellular carcinoma. *Int. J. Oncol.* **45**, 1547–1555 (2014).

181. Ding, Z.-Y., Wu, H.-R., Zhang, J.-M., Huang, G.-R. & Ji, D.-D. Expression characteristics of CDC20 in gastric cancer and its correlation with poor prognosis. *Int. J. Clin. Exp. Pathol.* **7**, 722–7 (2014).

182. Marucci, G. *et al.* Gene expression profiling in glioblastoma and immunohistochemical evaluation of IGFBP-2 and CDC20. *Virchows Arch.* **453**, 599–609 (2008).

183. Choi, J.-W., Kim, Y., Lee, J.-H. & Kim, Y.-S. High expression of spindle assembly checkpoint proteins CDC20 and MAD2 is associated with poor prognosis in urothelial bladder cancer. *Virchows Arch.* **463**, 681–7 (2013).

184. Mondal, G. *et al.* Overexpression of Cdc20 leads to impairment of the spindle assembly checkpoint and aneuploidization in oral cancer. *Carcinogenesis* **28**, 81–92 (2007).

185. Kim, Y., Choi, J.-W., Lee, J.-H. & Kim, Y.-S. MAD2 and CDC20 are upregulated in high-grade squamous intraepithelial lesions and squamous cell carcinomas of the uterine cervix. *Int. J. Gynecol. Pathol.* **33**, 517–23 (2014).

186. Thirthagiri, E. *et al.* Spindle assembly checkpoint and centrosome abnormalities in oral cancer. *Cancer Lett.* **258**, 276–85 (2007).

187. Yang, Y., Gu, C., Luo, C., Li, F. & Wang, M. BUB1B promotes multiple myeloma cell proliferation through CDC20/CCNB axis. *Med. Oncol.* **32**, 81 (2015).

188. Lub, S. *et al.* Inhibiting the anaphase promoting complex/cyclosome induces a metaphase arrest and cell death in multiple myeloma cells. *Oncotarget* **7**, 4062–76 (2016).

189. Crawford, L. J., Anderson, G., Johnston, C. K. & Irvine, A. E. Identification of the APC/C co-factor FZR1 as a novel therapeutic target for multiple myeloma. *Oncotarget* **7**, 70481–70493 (2016).

190. Genga, K. R. *et al.* Proteins of the mitotic checkpoint and spindle are related to chromosomal instability and unfavourable prognosis in patients with myelodysplastic syndrome. *J. Clin. Pathol.* **68**, 381–7 (2015).

191. Borges, D. de P. *et al.* Prognostic importance of Aurora Kinases and mitotic spindle genes transcript levels in Myelodysplastic syndrome. *Leuk. Res.* **64**, 61–70 (2018).

192. Liu, X. *et al.* PPM1K Regulates Hematopoiesis and Leukemogenesis through CDC20-Mediated Ubiquitination of MEIS1 and p21. *Cell Rep.* **23**, 1461–1475 (2018).

193. Sun, C. *et al.* Gene expression profiles analysis identifies a novel two-gene signature to predict overall survival in diffuse large B-cell lymphoma. *Biosci. Rep.* **39**, BSR20181293 (2019).

194. Liu, B. *et al.* Human T-Lymphotropic Virus Type 1 Oncoprotein Tax Promotes Unscheduled Degradation of Pds1p/Securin and Clb2p/Cyclin B1 and Causes Chromosomal Instability. *Mol. Cell. Biol.* **23**, 5269–5281 (2003).

195. Liu, B., Hong, S., Tang, Z., Yu, H. & Giam, C.-Z. HTLV-I Tax directly binds the Cdc20-associated anaphase-promoting complex and activates it ahead of schedule. *Proc. Natl. Acad. Sci.* **102**, 63–68 (2005).

196. Wang, L. *et al.* Targeting Cdc20 as a novel cancer therapeutic strategy. *Pharmacol. Ther.* **151**, 141–51 (2015).

197. Kapanidou, M., Curtis, N. L. & Bolanos-Garcia, V. M. Cdc20: At the Crossroads between Chromosome Segregation and Mitotic Exit. *Trends Biochem. Sci.* **42**, 193–205 (2017).

198. Wang, Z. *et al.* Cdc20: a potential novel therapeutic target for cancer treatment. *Curr. Pharm. Des.* **19**, 3210–4 (2013).

199. Sackton, K. L. *et al.* Synergistic blockade of mitotic exit by two chemical inhibitors of the APC/C. *Nature* **514**, 646–9 (2014).

200. Zeng, X. *et al.* Pharmacologic inhibition of the anaphase-promoting complex induces a spindle checkpoint-dependent mitotic arrest in the absence of spindle damage. *Cancer Cell* **18**, 382–95 (2010).

201. Tonelli, C., Chio, I. I. C. & Tuveson, D. A. Transcriptional Regulation by Nrf2. *Antioxid. Redox Signal.* **29**, 1727–1745 (2018).

202. Welch, J. S. *et al.* The origin and evolution of mutations in acute myeloid leukemia. *Cell* **150**, 264–78 (2012).

203. Stock, C. J. W. *et al.* Bromodomain and Extraterminal (BET) Protein Inhibition Restores Redox Balance and Inhibits Myofibroblast Activation. *Biomed Res. Int.* **2019**, 1484736 (2019).

204. Merchant, A. A., Singh, A., Matsui, W. & Biswal, S. The redox-sensitive transcription factor Nrf2 regulates murine hematopoietic stem cell survival independently of ROS levels. *Blood* **118**, 6572–9 (2011).

205. Bobilev, I. *et al.* The Nrf2 transcription factor is a positive regulator of myeloid differentiation of acute myeloid leukemia cells. *Cancer Biol. Ther.* **11**, 317–29 (2011).

206. Schnerch, D. *et al.* Proteasome inhibition enhances the efficacy of volasertib-induced mitotic arrest in AML in vitro and prolongs survival in vivo. *Oncotarget* **8**, 21153–21166 (2017).